Production and optimization of cell-specific and brain-targeted recombinant adeno-associated virus tools for target validation in Parkinson's disease models

Master thesis
University of Turku
Department of Life Technologies
Molecular Systems Biology
May 2022

Soroush Abyari

“The originality of this thesis has been checked in accordance with the University of Turku quality assurance system using the Turnitin OriginalityCheck service”.

UNIVERSITY OF TURKU
Department of Life Technologies
ABYARI, SOROUSH
Production and optimization of cell-specific and brain-targeted recombinant adeno-associated virus tools for target validation in Parkinson's disease models
Master's thesis, 80 p.
May 2022
Molecular Systems Biology
"The originality of this thesis has been checked in accordance with the University of Turku quality assurance system using the Turnitin OriginalityCheck service"

Parkinson's disease (PD) is a heterogeneous disorder associated with the progressive loss of dopaminergic neurons in specific brain regions. The underlying molecular events in PD result from the complicated interplay of genetics and the environment. Currently, there is no disease-modifying therapy for PD and developing novel therapeutics requires a deeper understanding of the early neuropathological mechanisms of the disease. The first aim of this project was to generate recombinant adeno-associated virus (rAAV) vectors to deliver transgenes in a cell-type-specific manner. The transgenes transfer phosphomutants of three target proteins implicated in PD pathogenesis for further studies. The second aim of this project was to optimize the produced rAAVs to achieve the most efficient integration into target dopaminergic cells.

The rAAVs were generated using a special capsid, enabling them to systematically infect specific cells. Following production, rAAVs transduction efficiency was optimized by cell transduction assays and visualized by immunofluorescence staining.

In total, 11 high titer rAAVs were generated with titer ranging from 0.2 - 5.6 x 10^{13} vg/ml. All rAAVs were functionally working with different transduction efficiency. The best labeling titer and infection incubation time were optimized. The results show that our rAAVs were reliably transducing target cells and can be used for *in vitro* and *in vivo* experiments. The follow-up experiments will assess the effects of phosphomutants delivered by rAAVs on cellular mechanisms of PD to validate new target proteins as potentially involved in the early stages of the disease and pave the way for further studies.

Keywords: Parkinson's disease, recombinant adeno-associated virus, viral transduction, dopaminergic neurons, midbrain.

Contents

Abbreviations 3

1 INTRODUCTION 4

1.1 Parkinson's disease: clinical characteristics, diagnosis, and therapy 4

1.2 Pathogenesis of Parkinson's disease 8

1.3 Etiology of Parkinson's disease 10

1.3.1 Idiopathic Parkinson's disease 10

1.3.2 Familial Parkinson's disease 11

1.4 Neuropathology of Parkinson's disease 12

1.5 Clathrin-mediated endocytosis 14

1.6 LRRK2 in Parkinson's disease 15

1.7 Vector tools for neurological disorders 18

1.8 Adeno-associated virus 19

1.9 Adeno-associated virus life cycle 21

1.10 Recombinant adeno-associated virus 23

1.10.1 Routes of administration 23

1.10.2 Cell-type specific promoters and tetracycline expression system 24

1.10.3 Adeno-associated virus serotypes 26

1.11 Study aims 30

2 MATERIALS AND METHODS 31

2.1 Study design 32

2.2 Ethical statement 32

2.3 Antibodies 32

2.4 Cell transformation with pUCmini-iCAP-PHP and pHelper 32

2.5 Maintenance of HEK 293FT cell line 34

2.6 AAV vector production 35

2.7 AAV purification and concentration 37

2.8 Quantitative real-time polymerase chain reaction 39
2.9 Midbrain cell culture 40
2.10 In vitro viral transduction 41
2.10.1 Titer optimization 41
2.10.2 Optimization of the co-transduction ratio of TRE:tTA viruses 42
2.10.3 Target 1 and 2 transduction 42
2.11 Immunofluorescence staining 42
2.12 Widefield Imaging 43

3 RESULTS 44

3.1 Cell transformation with pHelper and pUCmini-iCAP-PHP.eB 44
3.2 Generation, purification, and stock titer of rAAV viruses 45
3.3 Functional titer optimization 46
3.4 The TRE:tTA ratio optimization 48
3.5 Testing HA tag for targets 1 and 2 50

4 DISCUSSION 52

4.1 Generation of rAAV constructs 52
4.2 Important considerations and criteria when generating AAVs 55
4.3 Transduction efficiency and optimization of labeling titer 55
4.4 Optimization of the co-transduction ratio of TRE:tTA viruses 57
4.5 Validation of rAAVs with target proteins 1 and 2 57
4.6 Future prospect 58

5 CONCLUSION 59

References **60**

Abbreviations

AAV: Adeno-associated virus

ALP: Autophagy-Lysosomal Pathway

BBB: Blood-brain-barrier

CME: Clathrin-mediated endocytosis

CNS: Central nervous system

COR: C-terminal-of-Roc

DA: Dopamine

GWAS: Genome-wide association studies

ITR: Inverted terminal repeats

LBs: Lewy bodies

LNs: Lewy neurites

LRRK2: Leucine-rich repeat kinase 2

MDS: Movement disorder society

MQW: Milli-Q water

MPTP: 1-methyl-4-phenyl-1,2,3,6-tetrahydropyridine

PD: Parkinson's disease

rAAV: Recombinant adeno-associated virus

ROC: Ras-of-Complex

SNpc: Substantia nigra pars compacta

tetO: tetracycline-resistance operator

TRE: Tet-responsive elements

tTA: tetracycline-controlled transactivator

UPS: Ubiquitin-proteasome system

wtAAV: Wild-type adeno-associated virus

1 Introduction

1.1 Parkinson's disease: clinical characteristics, diagnosis, and therapy

Parkinson's disease (PD) is a heterogenous neurological disorder associated with motor dysfunction and non-motor symptoms. It is the second in prevalence after Alzheimer's disease among neurodegenerative disorders (Kalia & Lang, 2015). In 1817, the term "Parkinson's disease" was described by Dr. James Parkinson, and in the following two centuries, it became known as a common neurological disorder (Dorsey et al., 2018). According to recent studies, it is considered as one of the fastest-growing disorders worldwide (Feigin et al., 2017). The reason behind this increase has not yet been known, but aging is considered the most important player, consistent with increased longevity and decreased smoking rate (Bloem et al., 2021; Dorsey et al., 2018). PD affects 1% of the population over the age of 60 (Kouli et al., 2018). Between 1990 and 2019, the global prevalence of PD elevated by 155.50 %. On the regional scale, East Asia had the highest prevalence rate in 2019, while Oceania had the lowest (Ou et al., 2021).

PD occurs mainly with the selective loss of dopaminergic neurons in specific brain regions responsible for body movement control and coordination (Kouli et al., 2018). The clinical features of PD are categorized into two phases, with non-motor and motor symptoms. However, symptoms are widely separated through an extended period, from the onset of non-motor traits to the development of motor dysfunction. PD is currently diagnosed after the motor symptoms manifest, while non-motor symptoms preceded several years before the movement disability (Kalia & Lang, 2015). It is reported that approximately 50% to 60% of dopaminergic neurons have already been lost when patients develop motor impairments (Gibb WR & Lees AJ, 1991).

The premotor symptoms of the disease might occur 10 to 20 years before the motor impairment become symptomatic (Antonina Kouli et al., 2018; Kalia & Lang, 2015) (Figure1). In the prodromal stage of PD, the extent and the variety of non-motor symptoms differ from patient to patient; some characteristics of non-motor symptoms are the disturbance in autonomic functions, sleeping disorders, cognitive impairment and depression, and sensory symptoms deficit (Sveinbjornsdottir, 2016). Both the central nervous system (CNS) and peripheral nervous systems might be involved in autonomic dysfunction (Sveinbjornsdottir, 2016). Some examples of autonomic dysfunction are

gastrointestinal issues such as abnormal increases in sweating, decreased salivary secretion, and slowness of mobility in the large intestine, which together lead to slow transit constipation, the most frequent symptom of autonomic dysfunction among PD patients (Jost, 2010).

On the other hand, at the advanced level of the disease progression, motor function impairment starts manifesting, and it consists of rigidity, tremor, and bradykinesia as three main characteristics, with postural instability at the later stage (Antonina Kouli et al., 2018) (Figure 1). These movement symptoms usually appear asymmetrically, meaning that only one part of the body is involved (Berardelli et al., 2013). The term bradykinesia has various distinct definitions and can be related to several movement disorders. In PD, the term bradykinesia is used synonymously with akinesia and hypokinesia and is defined as the slowness in the execution of voluntary movements or prolongation of movement initiation (Berardelli et al., 2001). As a form of hypertonia, rigidity restricts upper body motor neuron functions regardless of movements' direction. The effects of muscle rigidity on the axial and limb segments are not uniform. Tremor in PD patients appears as involuntary, repetitive, and oscillatory movements of different body parts that can occur alone or in conjunction with other PD symptoms (Lenka & Jankovic, 2021). Rigidity affects axial and limbs segments on one side of the body with stiffness in muscles (Rinalduzzi et al., 2015). Tremor is classified based on its etiology, such as PD tremor and tremors linked with neuropathies (Bhatia et al., 2018). Rigidity is commonly accompanied by postural instability that results in flexed neck and trunk posture; however, it appears in the later stages of the disease (Jankovic, 2008).

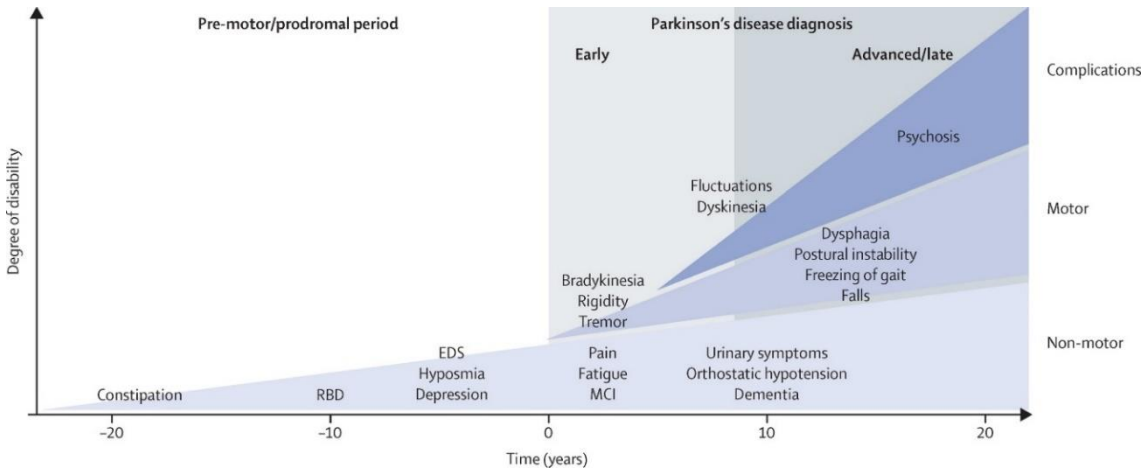

Figure 1. Clinical symptoms and time course of PD development (From Kalia & Lang, 2015 with permission).

PD is particularly a heterogenous disorder because of its broad pathology, making it challenging to diagnose, as of yet, no definitive diagnostic test is available (Antonina Kouli et al., 2018). Currently, diagnosis of PD relies primarily on movement features that have become symptomatic. A variety of diseases exhibit a set of neurological conditions that cause movement abnormalities and exhibit partly or entirely main clinical symptoms of PD (Dickson, 2017); these conditions are referred to as "parkinsonism." Many disorders are implicated by parkinsonism named "parkinsonian disorders," with PD hosting the majority of those disorders (Dickson, 2017). The first step in diagnosis is to determine whether the patient has “parkinsonism.” (Greenland & Barker, 2018). Once the patient's parkinsonism has been established, an accurate diagnosis needs to rule out other probable causes of this syndrome (Greenland & Barker, 2018). There are three conditions conducted by movement disorder society (MDS), which allow for excluding PD from other parkinsonism causes (Postuma et al., 2015). In addition, The Unified Parkinson’s Disease Rating Scale (UPDRS) is the most widely used and internationally accepted scale for assessing PD severity which was established in 1987, revised by MDS in 2008, and updated to MDS-UPDRS (Goetz et al., 2008). This scaling system aims to provide a comprehensive measurement to assess and monitor PD-related criteria. The UPDRS is divided into four sections, with each assessed by a clinician and focuses on motor features examination, the patient's ability to conduct daily activities, non-motor symptoms examination, and complications in treatments (Hendricks & Khasawneh, 2021). It should be noted that although clinical symptoms can help diagnose the disorder, a conclusive diagnosis needs histological examination, including the presence of Lewy bodies (LBs) or Lewy neurite (LNs) (Antonina Kouli et al., 2018).

The certainty in diagnosing PD improves follow-up treatments; because of that, a comprehensive history of the patients can assist in distinguishing various Parkinsonism conditions. Other 20% of cases of parkinsonism can stem from neurological causes such as dementia with LBs, multiple system atrophy, corticobasal syndrome, or secondary causes like toxins, drugs, and vascular conditions (Greenland & Barker, 2018).

At the moment, there is no cure or disease-modifying treatment for PD; with treatment strategies relying solely on symptomatic relief. Such drugs can help control and ease motor symptoms. Despite their effectiveness in improving motor symptoms, these medications commonly cause adverse side effects, particularly as the disease advances and with prolonged treatment (Zahoor et al., 2018). The underlying pathophysiology of PD includes several cellular processes; therefore, a single medication might not be

impactful against the wide range of disturbed pathways (AlDakheel et al., 2014). However, since these pathways mainly lead to the loss of dopaminergic neurons in the midbrain, restoring dopamine (DA) activity in those areas with dopaminergic drugs appears as a viable therapy. These drugs are intended to imitate the role of precursor molecules for DA biosynthesis or modulate the DA metabolism pathway (Zahoor et al., 2018).

Levodopa-based drugs are the centerpiece of current PD therapy and serve as DA precursors. Levodopa, unlike dopamine, can cross the blood-brain barrier (BBB) and then convert to DA by Aromatic L-amino acid decarboxylase. Levodopa normally acts quickly and has a long-lasting effect on motor symptoms, but its effects usually fade as the disease progresses. The side effects of levodopa, on the other hand, can drastically worsen the motor symptoms experienced by the patient in the final stages of the disease. This might be due to Levodopa being converted to DA outside of the brain. In addition to levodopa, other therapeutics are available in the market for PD, such as monoamine oxidase B inhibitors, DA agonists, and catechol-o-methyl transferase inhibitors which are described in Table 1.

Table 1. Some of the current PD medications based on dopamine (DA) metabolism (Adopted from Zahoor et al., 2018**)**

Treatment	Mechanism of action	Prescription	Benefits	Side effects
DA agonists (Pergolide, Bromocriptine, Cabergoline)	Binds to dopaminergic receptors and stimulates the DA system's activity.	As an initial therapy for PD for the delay in the levodopa administration.	Minimizes the impact of motor complications and is helpful in patients unable to tolerate levodopa	Patients develop compulsive and impulsive behavioral problems with symptoms including hypersexuality, binge eating, and gambling.
Monoamine Oxidase B inhibitors (selegiline, rasagiline)	Blocks the enzymes involved in DA metabolism and preserves endogenous DA levels.	As an initial therapy for PD for the delay in the levodopa administration.	Control the symptoms in early disease.	Gastrointestinal problems (mainly), depression, fatigue, and dry mouth.
Catechol-O-methyl transferase inhibitors (entacapone, tolcapone, opicapone)	Reduces endogenous DA breakdown by inhibiting the catechol-o-methyl transferase enzyme responsible for DA degradation.	As an adjunctive treatment to levodopa.	Prolongs Levodopa duration of action.	Cause levodopa-induced side effects, such as dyskinesias.
Anticholinergics	Increase dopaminergic activity in the striatum.	In the early stages of PD, in combination with levodopa.	Improves rigidity and tremor and helps to relieve mild movement symptoms.	Dry mouth, constipation, drowsiness, urinating problems, cognitive impairment, dizziness.

1.2 Pathogenesis of Parkinson's disease

The neuropathology of PD is characterized by the accumulation of misfolded α-synuclein proteins in the form of LBs or LNs cytoplasmic inclusions, resulting in the selective death of dopamine-producing neurons in the substantia nigra pars compacta (SNpc) area of the midbrain (Deng et al., 2018; Kouli et al., 2018). This neuronal loss is generally limited to the neuromelanin-containing ventrolateral cell groups, such as cells in the nigrostriatal pathway, while other neuronal and glial cell types are substantially preserved (Dickson, 2017; Kouli et al., 2018). Propagation of misfolded α-synuclein proteins subsequently spreads and infects other healthy cells, probably explaining the progressive developmental loss of cells in this region (Dickson, 2017).

Morphometric data of postmortem PD brain tissues approximate 30% loss of dopaminergic neurons in the SNpc by the disease onset. This loss exceeds more than 60% when motor symptoms start to manifest and correlates directly with the severity of symptoms. The dopaminergic cell degeneration can project to the basal ganglia, specifically the striatum, and induce cellular and synaptic dysfunction (Mallet et al., 2019). In addition Kalia et al. reported in 2013 that nondopaminergic neurotransmitter systems such as GABAergic, noradrenergic, and glutamatergic are also implicated in the pathogenesis of PD. Degeneration of these systems is reported to involve some of the non-motor symptoms of PD that do not respond efficiently to DA replacement therapies such as levodopa (Chaudhuri et al., 2006).

As mentioned before, the development of aberrant cytoplasmic deposits known as LBs or LNs are considered the hallmarks of PD. The morphology of LBs varies depending on their location in the brain (Shahmoradian et al., 2019). For instance, cortical LBs have a rounded structure without a halo, whereas LBs in the brainstem are spherical with a peripheral halo (Choong & Mochizuki, 2022) (Figure 2A). The biochemical properties and proteomic compositions of LBs are very complex. According to proteomics analysis of postmortem data, LBs contain 300 proteins, over 90 of which have been verified and are mainly related to α-synuclein and molecular chaperones (Wakabayashi et al., 2012). The LNs morphology resembles that of α-synuclein aggregation but only in the neurites (Wakabayashi et al., 2012) (Figure 2B).

Results from electron microscopy images represent LBs containing 10 nm diameter filaments (Duffy & Tennyson, 1965), with α-synuclein as the major constituent of these

filaments (Kanazawa et al., 2008). α-synuclein is abundant throughout different brain regions, predominantly in presynaptic terminals (Choong & Mochizuki, 2022). Those brain regions include the hippocampus, thalamus, nucleus accumbens, amygdala, olfactory bulb, and dentate gyrus (Iwai et al., 1995). α-synuclein exists physiologically in a dynamic between unfolded monomeric cytosolic and membrane-bound states (Burré et al., 2014). Under PD-related pathogenic conditions, the native monomeric form of α-synuclein undergoes structural modifications into oligomeric and protofibril intermediates followed by β-sheet rich amyloid fibrils and polymers that are prone to accumulation (Lashuel et al., 2002; Wood et al., 1999) (Figure 2C). Oligomers can sort into toxic pathways, which are considered to be the primary source of α-synuclein neurotoxicity (Lorenzen et al., 2014). These toxic oligomers can cause cellular lesions by permeabilizing cell membranes (Winner et al., 2011). Fibril forms, on the other hand, are reported to cause toxicity even to a greater extent (Pieri et al., 2012). In fact, while oligomers are linked to neuronal dysfunction, fibrils can spread from one cell to another and drive the disease's progression (Choong & Mochizuki, 2022).

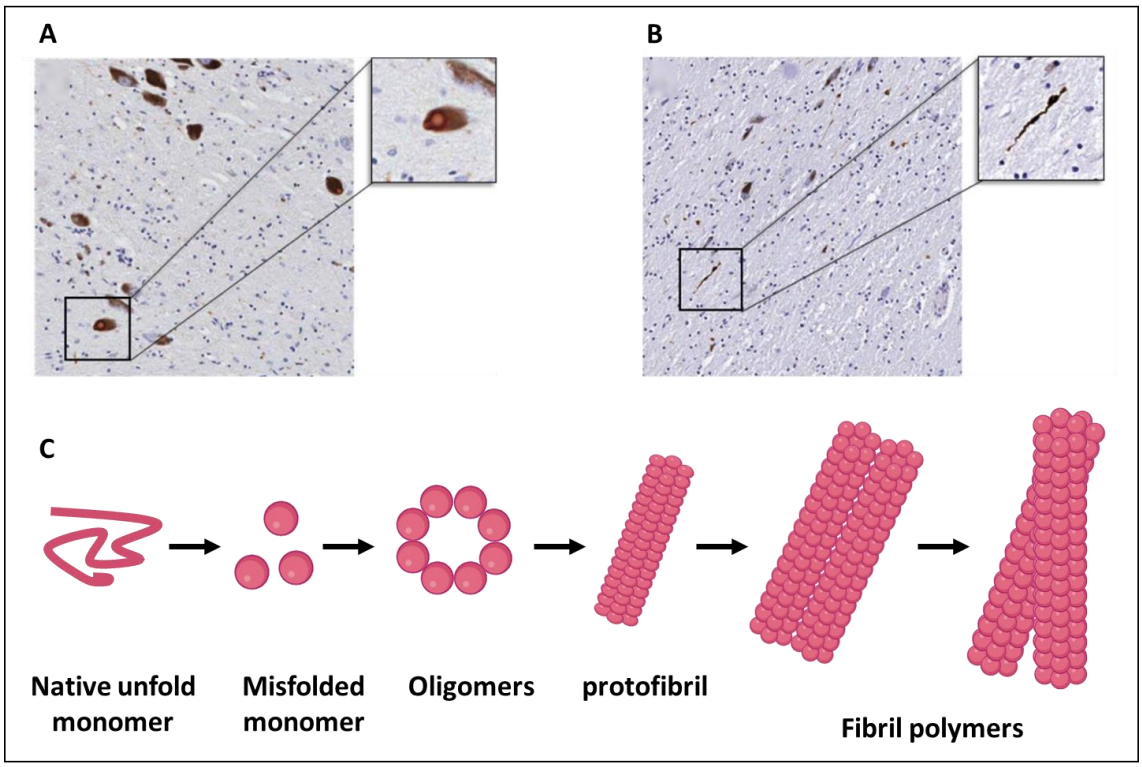

Figure 2. Examples of Lewy-pathology in dopaminergic cells of SNpc of PD patients, and schematic of α-synuclein fibril formation pathway. **A-B)** Typical Lewy body surrounded by a halo and dystrophic Lewy neurites, visualized by α-synuclein immunohistochemistry (adopted from Kouli et al., 2018). **C)** Misfolded α-synuclein can form oligomeric intermediates, and eventually, amyloid fibrils, which can exhibit in different polymer forms (Adopted from Choong & Mochizuki, 2022, created by Biorender).

1.3 Etiology of Parkinson's disease

Several PD-related genes have uncovered valuable information about the molecular and cellular pathways underlying the disease. However, due to the lack of a robust genetic footprint in the majority of PD patients, scientists have begun to focus on the significance of environmental factors or genetic and environmental interplay as the etiology of PD (Freire & Koifman, 2012). Nevertheless, age appears to be the most critical risk factor. It is reported that the incidence of PD rises sharply with age, from 17.4 per 100,000 people aged 50 to 59 to 93.1 per 100,000 people aged 70 to 79 (Lees et al., 2009).

1.3.1 Idiopathic Parkinson's disease

The link between PD and 1-methyl-4-phenyl-1,2,3,6-tetrahydropyridine (MPTP) was identified in 1983 when many people exposed to drugs tainted with MPTP developed chronic PD symptoms (Freire & Koifman, 2012; Kouli et al., 2018). MPTP is a molecule with a structure similar to the herbicide paraquat, which can damage mitochondrial complex I in the human body, inhibiting cell respiration or disturbing cytoskeletal proteins and destabilizing microtubules (Betarbet et al., 2000; Cartelli et al., 2013). MPTP is an efficient substrate for the DA transporter, which accumulates predominantly in dopaminergic cells, thereby leading to dopaminergic cell loss (Betarbet et al., 2000). Environmental exposure to paraquat and toxic pesticides, such as rotenone, is strongly associated with PD. Pesticides may lead to neurotoxic processes via oxidative stress, which can be defined as the imbalance between the production of free radicals and the body's antioxidant defense (Abdollahi et al., 2004) that can lead to the degeneration of dopaminergic neurons. Rotenone is a natural chemical with similar mechanisms of action to MPTP; however, to enter the cells, it is not dependent on the DA transporter and is widely used to produce animal models of PD (Betarbet et al., 2000; Wrangel et al., 2015). In addition, overexposure to essential metals such as manganese (Mn) and iron (Fe), as well as non-essential metals such as aluminum (Al) and mercury (Hg), may play a part in pathological disorders such as PD (Ullah et al., 2021).

As another environmental factor, the effects of smoking cigarettes on PD have been examined extensively, with fairly consistent results showing an inverted correlation between smoking and PD (Kouli et al., 2018). The mechanisms of this effect have not yet been fully understood. Still, the neuroprotective effects of nicotine in cigarette on dopaminergic neurons via activating nicotine acetylcholine receptor is reported to play a

role in PD models (Bordia et al., 2015; Hernán et al., 2002). The same trend has been reported for coffee consumers as caffeine is an antagonist to the adenosine A2A receptor, with neuroprotective benefits by preventing neuroinflammation and neurotoxicity due to excessive calcium release in the neuronal cells (Hong et al., 2020; Kolahdouzan & Hamadeh, 2017). However, caffeine tablets had no effects on the course of the disease when administrated to PD patients (Postuma et al., 2012).

1.3.2 Familial Parkinson's disease

PD is primary an idiopathic disease; however, a minority (10-15%) of cases indicate a family history, and around 5% of patients follow Mendelian inheritance (Deng et al., 2018). According to meta-analysis research, having a family history of PD is the strongest risk factor for subsequent PD diagnosis (Noyce et al., 2012). Genetic variation accounts for about 25% of the total risk of developing PD (Day & Mullin, 2021). The incidence and risk of developing PD are different for genetic variations linked to it (Day & Mullin, 2021). On one side, only a few rare monogenic variants of genes are individually sufficient to trigger PD. These monogenic variations were discovered through linkage analysis of involved families in PD (Day & Mullin, 2021). On the other side, there are several genetic variants, each of which can contribute to PD development as risk factors with only minimal effects (Day & Mullin, 2021). These genetic variants were identified in genome-wide association studies (GWAS) and are recognized as mostly the genetic contributors to sporadic PD.

More than 80 loci and 24 disease-causing genes have been linked to Parkinson's disease thus far (Aasly, 2020; Blauwendraat et al., 2019). The 24 monogenic variants that are involved in PD development are designated as "PARK" in the order they were discovered (Kouli et al., 2018) (Table 2). It should be noted that the role of some PARK genes is still unclear. The designated genes show both autosomal or dominant inheritance. In one GWAS study, Blauwendraat et al., 2019 discovered that not all PD risk loci impact the age at onset in one GWAS research. Aside from the PARK-designated genes, glucocerebrosidase mutation careers have been linked to the development of Parkinson's disease (Aasly, 2020). This mutation does not show a Mendelian inheritance pattern (Day & Mullin, 2021). The loss of function mutation in its protein may compromise lysosomal function, resulting in the buildup of α-synuclein protein, which raises the risk of Parkinson's disease (Deng et al., 2018).

Table 2. Lists of Park-designated genes (Adopted from Deng et al., 2018a)

Locus	Gene	Inheritance	Protein	Disease Onset
PARK1; PARK4	SNCA	AD	α-synuclein	EO - LO
PARK2	PRKN	AR	Parkin RBR E3 ubiquitin-protein ligase	EO
PARK5	UCHL1	AD	ubiquitin C-terminal hydrolase L1	EO – LO
PARK6	PINK1	AR	PTEN-induced putative kinase 1	EO
PARK7	DJ-1	AR	Parkinsonism-associated deglycase	EO
PARK8	LRRK2	AD	Leucine-rich repeat kinase 2	LO
PARK9	ATP13A2	AR	Cation-transporting ATPase 13A2	EO
PARK11	GIGYF2	AD	GRB10 interacting GYF protein 2	LO
PARK13	HTRA2	AD	HtrA serine peptidase 2	LO – EO
PARK14	PLA2G6	AR	Calcium-independent phospholipase A2 enzyme	EO
PARK15	FBX07	AR	F-box protein 7	EO
PARK17	VPS35	AD	Vacuolar protein sorting-associated protein 35	LO
PARK18	EIF4G1	AD	Eukaryotic translation initiation factor 4	LO
PARK19	DNAJC6	AR	HSP40 Auxilin	EO
PARK20	SYNJ1	AR	Synaptojanin 1	EO
PARK21	DNAJC13	AD	Receptor-mediated endocytosis 8	LO – EO
PARK22	*CHCHD2*	AD	coiled-coil-helix-coiled-coil-helix domain	LO – EO
PARK23	VPS13C	AR	Vacuolar protein sorting-associated protein 13C	LO - EO

AD: Autosomal dominant, AR: Autosomal recessive, EO: early-onset, LO: late-onset

1.4 Neuropathology of Parkinson's disease

In relation to α-synuclein aggregation, which plays a central role in the pathogenesis of PD, there are several other mechanisms, such as mitochondrial dysfunctioning and aberrant protein clearance systems that are implicated in PD pathogenesis.

Mitochondrial dysfunction in DA-producing neurons is reported to contribute as a critical factor in the pathogenesis of familial and idiopathic PD (Hattori & Mizuno, 2015). However, it remains unknown whether it is the cause or the consequence of PD pathology (Wright, 2022). Mitochondrial dysfunction occurs when reactive oxygen species are produced, which in turn leads to a decrease in mitochondrial complex I activity.

Consequently, mitochondrial protein cytochrome-c is released into the cytosol, enabling caspase-9 protein activation (Hattori & Mizuno, 2015). Caspase-9 can trigger cell apoptosis through a loop of reactions which eventually leads to cell loss (Ow et al., 2008). This cycle can result from the aggregation of monomeric forms of α-synuclein in mitochondrial membranes, increased oxidative stress, interference of toxic substances such as MPTP, and rotenone with mitochondrial complex I. In addition, the mutation in PD-related genes that are involved in the clearance of malfunctioned mitochondria, such as PARK1 and PARK 2, can also be involved in mitochondrial pathogenicity (Kouli et al., 2018).

As part of the protein quality control mechanisms, the protein degradation system removes non-essential, misfolded, or damaged proteins (Lehtonen et al., 2019). Autophagy-lysosomal pathway (ALP) and the ubiquitin-proteasome system (UPS) are two major protein degradation systems that are implicated in α-synuclein pathogenesis (Lehtonen et al., 2019). These routes are responsible for the degradation of α-synuclein, and failure in one or both can result in aggregation (Lindersson et al., 2004). UPS acts by tagging undesirable proteins with ubiquitin leading to degradation by proteasomes (Pickart, 2003). Studies suggest that reduced activity of catalytic units of proteasomes in specific brain regions such as SNpc leads to UPS malfunctioning. In addition, the two PARK5 and PARK2 genes encode for proteasome subunits which are downregulated in PD patients (McNaught et al., 2002). Similar to the UPS system, many ALP-related components are dysfunctional or differently expressed in PD. The ALP system is responsible for removing harmful organelles and intracellular elements, as well as recycling long-lasting proteins to ensure proteome renewal via the lysosomal compartment (Kouli et al., 2018; Lindersson et al., 2004). ALP is implicated with many genetic mutations linked to PD. For example, a mutation in the GBA gene can lead to lysosomal malfunction and result in autophagy disruption. Another autophagy-controlled mechanism known as mitophagy, which is responsible to degrade malfunctioned mitochondria, has shown to be related to multiple mutations in PARK2, PARK6, and PARK7 genes (Burchell et al., 2013; Gan-Or et al., 2015). The main mechanism of α-synuclein degradation is suggested to be lysosomal; and inhibition of ALP leads to the accumulation of overexpressed or mutant α-synuclein due to lysosomal disfunctioning (Webb et al., 2003).

1.5 Clathrin-mediated endocytosis

The synaptic vesicle cycle is an essential process in presynaptic terminals that modulates the neurotransmitter release into the synaptic cleft and is crucial for proper neuronal function. Nerve terminals are responsible for releasing different chemicals through exocytosis, followed by endocytosis, and refilling the vesicle for the next round of release (Südhof, 2004).

When vesicles are filled with neurotransmitters, they form clusters as a reserve pool of refilled vesicles, then they dock at the active zone of presynaptic terminals waiting for the action potential. Along with the arrival of an action potential, Ca^{2+} influx to the cell via fusion-pores leads to fusion of the synaptic vesicle with plasma membrane and release of neurotransmitters (Südhof, 2004). Following that, empty synaptic vesicles take different routes for endocytosis and recycling. Three alternative routes namely "kiss-and-stay," "Kiss-and-run," and "Clathrin-mediated endocytosis" (CME) are proposed for vesicle recycling according to previous studies (Barker et al., 1972; Ceccarelli et al., 1973; Heuser & Reese, 1973). Interestingly, CME is likely to be the main early target in PD. CME is the principal endocytosis route in eukaryotic cells and is regulated in a highly conserved manner by recruiting over 50 cytosolic proteins. These proteins assemble in a well-organized order to generate 60 to 120 nm cargo-loaded vesicles (Kaksonen & Roux, 2018). CME controls the availability of the transmembrane receptors and transporters between the interior and the surface of the cells so that internal parts of the cells can receive signals from external environments (Schechter & Sharon, 2021).

CME can be divided into four phases beginning with membrane bending and coating with clathrin lattice protein with the help of adaptor protein-2 (AP2) (Schechter & Sharon, 2021). The α-Synuclein and endophilin A proteins are involved in bending the membrane (Vidyadhara et al., 2019). Next, endophilin A recruits dynamin that triggers membrane fission, forming vesicles coated with clathrin protein. Auxilin, endophilin A, and synaptojanin 1 work together to uncoat clathrin, which is required for synaptic vesicle recycling. LRRK2 protein phosphorylation is required for activation of the mentioned proteins (Figure 3). Mutations in proteins involved in CME may contribute to the early/late onset of PD. Autosomal loss of function mutation in the PARK19 gene which encodes for Auxilin is responsible for juvenile-onset PD (Edvardson et al., 2012). Mutations in the Sac domain or phosphatase domain of Synaptojanin 1 have been linked to early- and late-onset parkinsonism respectively. LRRK2 plays a very critical role in

CME, studies in flies and mice have shown that silencing mutation in LRRK2 leads to aggregation of endocytic intermediates and decreased number of synaptic vesicle cycle (Arranz et al., 2015).

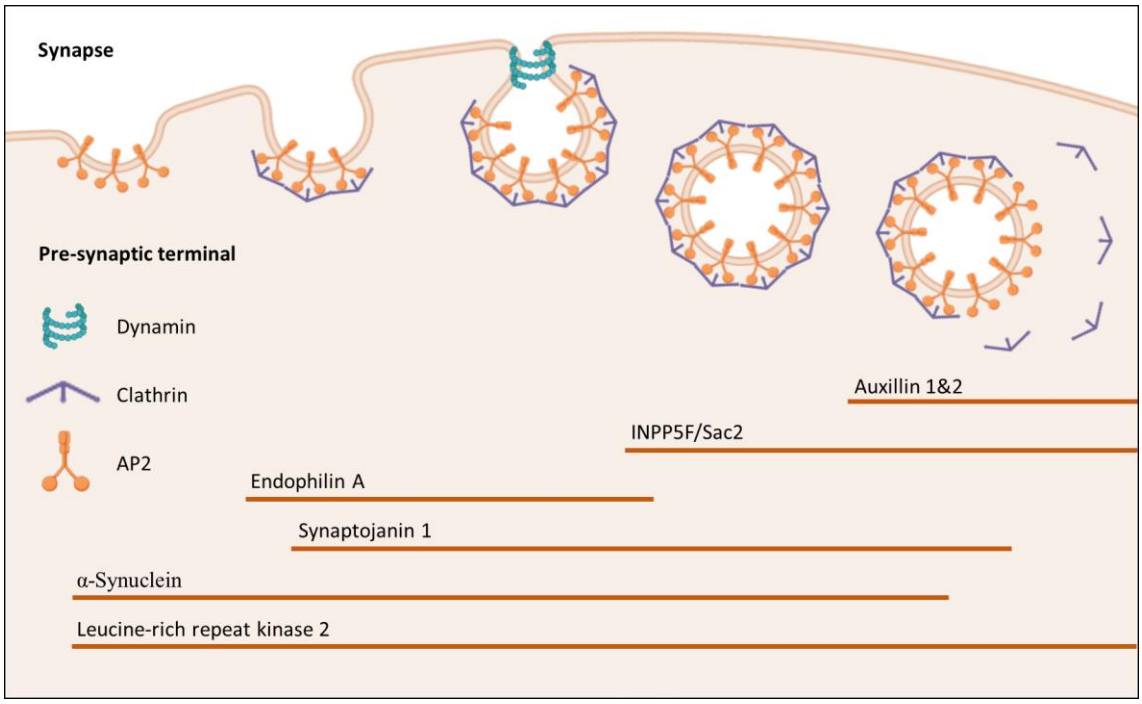

Figure 3. Simplified overview of the clathrin-mediated endocytosis with PD-associated proteins involved in this process. Mutation in each of these proteins can implicate in PD development (Adopted from Schechter & Sharon, 2021, created by Biorender).

1.6 LRRK2 in Parkinson's disease

Among a growing list of genes and loci that has been implicated in the neuropathology of PD, mutations in the leucine-rich repeat kinase 2 (LRKK2) gene contribute to 4% of familial and 1% of idiopathic PD cases (Albanese et al., 2022). LRRK2 is responsible for late-onset autosomal dominant mutation in 7% of familial PD cases (Mata et al., 2006). The clinical symptoms of familial PD triggered by LRRK2 mutations are symptomatically indistinguishable from idiopathic cases (Erb & Moore, 2020), making it a promising target that may provide insights into the underlying mechanisms of idiopathic PD, which accounts for the majority of patients.

The *LRRK2* gene is located on chromosome 12 with 51 exons and 21 alternative transcripts with expression in different human organs (Mata et al., 2006; Zimprich et al., 2004). It encodes for a relatively large multidomain protein LRRK2 (2527 amino acids). The N-terminal site of LRRK2 starts with armadillo repeats and ankyrin repeats, followed by a leucine-rich repeat domain (Erb & Moore, 2020). LRRK2 has three enzymatic

domains, including a Ras-of-Complex (ROC) GTPase, a C-terminal-of-Roc (COR), and a kinase domain; all three domains are located in the center of this protein. The protein ends with WD40 repeats on the C-terminal site (Erb & Moore, 2020) (Figure 4).

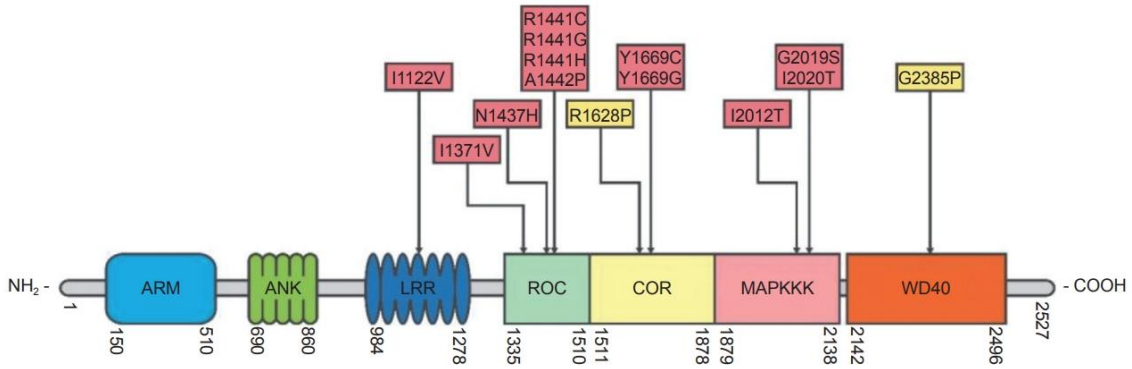

Figure 4. The structure of LRRK2 protein and its point mutations. LRRK2 is a multidomain protein with three enzymatic domains: ROC, COR, and Kinase. Disease-generating mutations (red) and risk variants (yellow) in different domains of LRRK2 are represented (From Aasly, 2020, can be reused under the CC BY license).

LRRK2 is a homodimer protein with dimerization occurring in its ROC-COR domain (Esteves et al., 2014). The ROC domain of LRRK2 is also responsible for its GTPase activity, which binds and hydrolyses GTP. The GTPase activity might also be modulated by LRRK2 dimerization or by the recruitment of other cellular proteins (Esteves et al., 2014). The kinase domain of LRRK2 shares similarities with mixed-lineage kinase proteins that are implicated in the control of neuronal apoptosis (Gallo & Johnson, 2002). Nevertheless, LRRK2 kinase activity is reported to be dependent on its functional GTPase activity. Moreover, LRRK2 has many autophosphorylation sites on its ROC and kinase domain, suggesting that LRRK2 is active through its kinase-GTPase interaction (Esteves et al., 2014). Several protein-protein interaction domains imply that, in addition to its expected protein kinase and GTPase functions, LRRK2 might operate as a major integrator in the assembly and modification of the downstream multiprotein signaling complex (Mata et al., 2006).

Among a list of genetic variants related to LRRK2, more than six polymorphisms can lead to the risk of developing PD (Esteves et al., 2014). LRRK2 mutations can be clustered according to their catalytic domains. R1441 position mutation to cysteine (R1441C), glycine (R1441G), or histidine (R1441H) in the ROC domain cause reduced GTPase activity (X. Li et al., 2007). Similarly, Y1699C mutation in the COR domain reduces GTP hydrolysis (Daniëls et al., 2011). Furthermore, I2020T and G2019S

mutations occur in the kinase domain of LRRK2. The G2019S mutation is the most frequent PD-associated mutation worldwide (Kelly et al., 2018). G2019S mutation increases the kinase activity of LRRK2 by facilitating substrate access and raising the catalytic rate of LRRK2 (Esteves et al., 2014). In contrast, the I2020T mutation has no effect on LRRK2 kinase activity. Autopsies of carriers of G2019S and I2020T mutations were reported to show LBs pathology (Poulopoulos et al., 2012).

Among the different organs, LRRK2 is expressed broadly in the brain, liver, and heart, and with high levels of expression are found in kidneys, lungs, and peripheral blood cells (Zimprich et al., 2004). Throughout the brain, LRRK2 is expressed in the cortex, olfactory bulb, hippocampus, and midbrain at higher levels when compared to its expression in the substantia nigra, and ventral tegmental area (Biskup et al., 2006; Higashi et al., 2007). However, because the overall expression of LRRK2 in various cells is low, different studies aimed to understand its role and interaction with different intracellular organelles, membranes, and vesicles in systems with overexpressed LRRK2 (Usmani et al., 2021), revealing that it functions predominantly in the cytoplasm bounding to organelles membrane or cytoskeleton (Berger et al., 2010). Such membrane bounds occur in different organelles like the Golgi complex, mitochondria, lysosome and endoplasmic reticulum (Cookson, 2010) (Figure 5).

LRRK2's kinase activity is reported to be increased when it forms membrane-associated dimers (Berger et al., 2010). In the brain, 14-3-3 adaptor proteins phosphorylation is mediated by cytoplasmic LRRK2; when this interaction is disturbed, LRRK2 aggregations form inclusion bodies, which may be associated with PD (Nichols et al., 2010) (Figure 5). The interaction of LRRK2 with the Rab GTPase family is an essential part of LRRK2 biology. Rab proteins control intracellular vesicle trafficking by cycling between GTP/GDP-bound forms (Xu et al., 2021). In one study in 2017, Steger et al. showed the association of LRRK2 phosphorylation activity with 14 members of the Rab family (Figure 5). In another study, an increased risk of PD due to the interaction of some LRRK2-polymorphisms and Rab29 function has been reported (MacLeod et al., 2013) (Figure 5). LRRK2 is also localized to vesicles, where it modulates the synaptic vesicle endocytosis by phosphorylation of proteins such as auxilin, synaptojanin, and endophilin A, which are all implicated in the clathrin-based pathway (Nguyen & Krainc, 2018). Shin et al. in 2008 reported that LRRK2, in collaboration with Rab5b, modulates synaptic vesicle endocytosis.

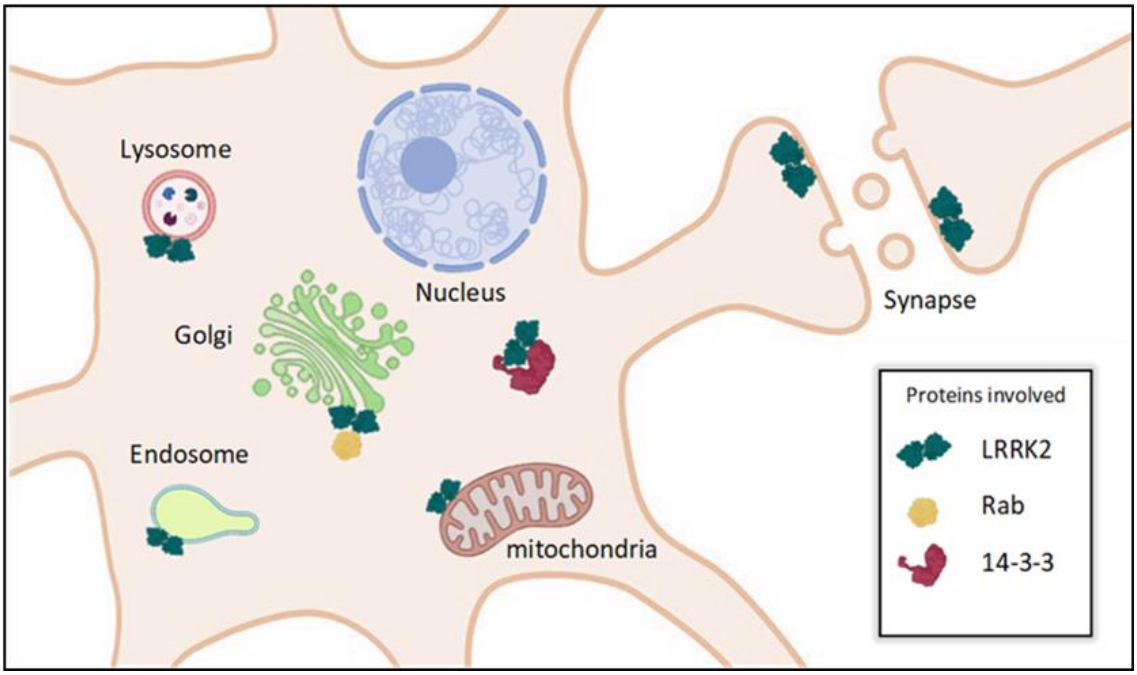

Figure 5. Subcellular localization of LRRK2 and its major interaction partners. LRRK2 is present in the cytoplasm, where it binds with 14-3-3 proteins through its kinase activity. The endolysosomal system and trans-Golgi network are particularly dependent on LRRK2 function. LRRK2 is widely associated with Rab family proteins for its phosphorylation activity and has a significant role in mitochondrial functioning (Adopted from Usmani et al., 2021, created by Biorender).

1.7 Vector tools for neurological disorders

Neuroscience is a very diversified field with an incredibly complicated nature moving forward to reach a comprehensive understanding of the nervous system and its function. In one way, this understanding can help answer the unsolved questions about neurological diseases with the eventual goal of developing novel treatments. However, due to the complexity of the nervous system and its circuits, achieving this goal is only feasible by studying the underlying mechanisms and contributors of different neurological disorders in subpopulations of neurons. Among several different approaches, one is to introduce transgenes that can manipulate the genetic information governing the disease state in a group of neuronal cells (Snyder et al., 2010). Another approach is to introduce a new protein that interferes with the target cell groups, then evaluate its impacts by comparing healthy and diseased cells. For many of these procedures, the first step is to develop tools that can transport genetic materials to the target cells, where they can be reproduced and expressed. Distinct strategies were devised for these tools, two widely used of which are viral and non-viral vector gene delivery systems (Y. Li et al., 2020).

Non-viral vectors are extensively studied for gene therapy and gene delivery. Due to their flexible construction, several types of these vectors are developed (Y. Li et al., 2020). They mainly comprise naked plasmid DNA combined with organic cationic materials (O'Connor & Boulis, 2015). However, a major limitation of this method is the inefficient transient expression which is not suitable for long-term expression if performed in dividing cells (Y. Li et al., 2020; O'Connor & Boulis, 2015). In addition, there are specific fundamental challenges in delivering non-viral vectors into the brain and then to particular brain cells; such challenges are BBB, appropriate targeting of specific neuronal populations, and inefficient cellular uptake (Y. Li et al., 2020).

On the other hand, viral vectors are exploited based on their inherent ability to invade, replicate, and live in cells. The efficiency of these vectors for transducing the target cells is generally high (Y. Li et al., 2020). Several studies and therapeutic approaches currently focus on modifying genetic abnormalities underlying neurodegenerative disorders such as Alzheimer's disease, Huntington's disease, other CNS-related disorders with genetic origins, and some idiopathic diseases such as PD (Marks et al., 2008) using viral vector gene therapy. Moreover, viral vehicles provoke low immunogenicity and genotoxicity (Kotterman et al., 2015). However, effective immune response against the viral vectors might reduce the ability of the virus to deliver transgene into the target cell and diminish the intensity and duration of transgene expression, resulting in transfection failure (Bessis et al., 2004). Current hurdles in employing viral tools are to find strategies for higher transduction efficiency, precise gene delivery to the target cell, and overcoming pre-existing immunity (Kotterman et al., 2015). Numerous viral vectors are currently available for gene delivery, such as adenovirus, retrovirus, herpes simplex virus, adeno-associated virus (AAV), and lentivirus. AAVs and Lentiviruses are the two most commonly used vectors for neurodegenerative disorders (O'Connor & Boulis, 2015). The focus of this project is on the AAV gene delivery tool.

1.8 Adeno-associated virus

The AAV was initially characterized in 1965 as a replication-defective non-pathogenic virus (Atchison et al., 1965) that belongs to the *Parvoviridae* family. It differs from other members of the *Parvoviridae* family since its replication is dependent on helper viruses, such as adenovirus or herpes virus (Berry & Asokan, 2017). So far, more than 100 AAV variants and multiple serotypes of AAVs have been identified from various animal species, presenting a diverse tissue-specific tropism of the virus (Wu et al., 2006). AAV-

derived vectors can encapsulate transgenes with a total genome size of less than ~5 kb and can transduce both dividing and non-dividing cells (Berry & Asokan, 2017; O'Connor & Boulis, 2015). Recombinant adeno-associated virus (rAAV) has a highly customizable cargo and provides distinctive features that are currently considered one of the most promising candidates for targeted gene delivery, with two marketing AAV-based gene therapy applications approved by the FDA (Bower et al., 2021).

In neuroscience, AAV vectors received much attention in research and clinical application because of their capacity to provide long-term and efficient transgene expression with low immune response in post-mitotic tissues (Gil-Farina & Schmidt, 2016; D. Liu et al., 2021). In one study in 2004, Burger et al. showed that different serotypes of AAVs followed different patterns of transduction in the hippocampus, striatum, SNpc, and spinal cord, making them suitable for targeting diverse tissues. In addition, AAVs are weakly immunogenic compared to other viral vectors (Bedbrook et al., 2018).

AAV genome has a small 4.7 kb single-stranded DNA, with two 145 base inverted terminal repeats (ITR) flanked on two sites of the DNA and three different promoters (P5, P19, and P40) that can drive expression (Berns & Linden, 1995). The AAV genome does not encode polymerases, and it is dependent on the host cell polymerase enzymes. At the 3′ end of the AAV genome, ITRs form hairpin structures that act as a primer for DNA synthesis by host cell DNA polymerase; thus, they are important elements for converting single-stranded AAVs' DNA into double-stranded DNA, which is required for proper transcription and replication (McCarty et al., 2004). The AAV has two main open reading frames (ORFs) for encoding different forms of Rep and Cap proteins (Figure 6). Non-structural Rep proteins (Rep78, Rep68, Rep52, Rep40) with overlapping amino acids are involved in AAV genome replication and packaging into the capsid (Berns & Linden, 1995). Rep78 and Rep 68 are large proteins responsible for site-specific integration of AAVs' DNA and endonucleolytic activity, and the smaller Rep proteins (52/40) control the helicase activity (Bower et al., 2021). Cap proteins (VP1, VP2, VP3) are the structural proteins of the virus capsid that are translated through alternative splicing of one mRNA combined with translation initiation from different regions (Becerra et al., 1988) (Figure 6). AAV genome also has a polyadenylation site for signaling (L. Wang et al., 2015). The AAV genome is embedded through a non-envelop icosahedral capsid structure approximately 250 Å in diameter (Rayaprolu et al., 2013), with VP1:VP2:VP3 proteins incorporation ratio of around 1:1:10 (Earley et al., 2017). The viral capsid is assembled

by sixty copies of these three proteins together with the help of assembly-activating protein (AAP), which is encoded through alternative splicing of the Cap gene (Earley et al., 2017; Kwon & Schaffer, 2008).

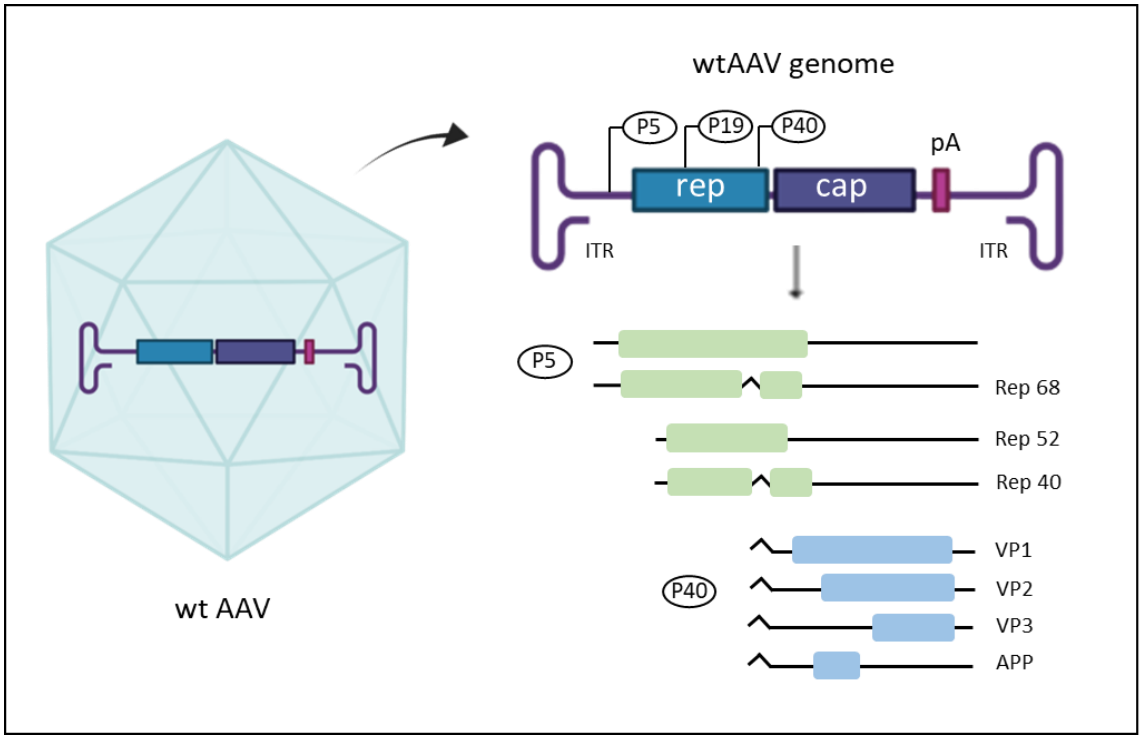

Figure 6. Wild-type adeno-associated virus genome structure. It contains two ORFs (rep and cap), with three promoters that encode eight different proteins through alternative start codon and splicing. It also contains a polyadenylation site (pA), and two flanked ITRs (Adopted from Saraiva et al., 2016, created by Biorender).

1.9 Adeno-associated virus life cycle

Like many viruses, wild-type adeno-associated virus (wtAAV) has two different cycles for reproduction, lysogenic (latent) and lythis or cycle (Chandler et al., 2017). AAV is a replication-defective virus, in the absence of a helper virus, the lysogenic infection pathway is pursued as the default infectious pathway for wtAAV. The virus integrates into a specific location in chromosome 19 of humans, termed AAV integration site 1 (AAVS1) through a non-homologous recombination mechanism (Gil-Farina & Schmidt, 2016). The interaction of viral Rep68/78 proteins with 16 nucleotides Rep-binding elements (REB) that exist in both AAVS1 and ITRs of the AAV vector mediates this mechanism (Bower et al., 2021; Howden et al., 2008). Helper viruses carry specific genes that mediate AAV replication. Once they integrate into cells infected with AAV, they help AAVs to proceed into the lytic cycle. On the other hand, the rAAVs used for transgene delivery represent different characteristics compared to wtAAV. rAAVs are

generated by transient transfection of HEK 293 cells with three different plasmids (Saraiva et al., 2016) (Figure 7). First, the ssDNA of rAAV is engineered, so that most of the wtAAV genome (consisting of Rep and Cap genes) except the two ITRs are replaced by exogenous sequences (including the promoters, transgenes, and a Poly A signal) (Chandler et al., 2017). The second plasmid provides the Rep and Cap genes *in trans*, as their presence is crucial for mediating genome replication and capsid assembly for the production of rAAVs (Chandler et al., 2017). The third plasmid is called the helper plasmid containing the adenoviral regions E1, E2, E3, and VA required for rAAV replication (Chandler et al., 2017) (Figure 7).

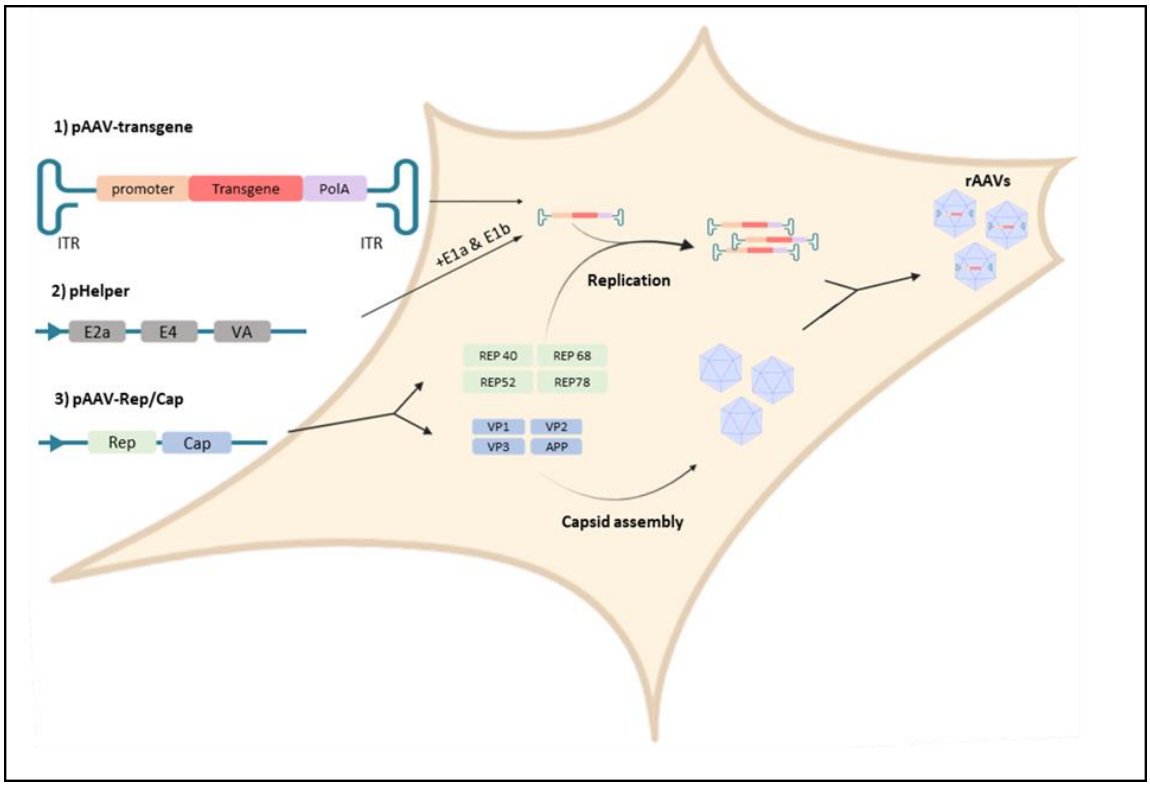

Figure 7. Recombinant AAV (rAAV) generation process by infecting HEK 293FT cells (Adopted from Saraiva et al., 2016, created by Biorender).

1.10 Recombinant adeno-associated virus

Numerous engineering studies have been conducted with AAVs' prominence as a gene delivery tool; especially in CNS-related research viral vectors are of immense value. Yet, regardless of how particular the experiment is, three crucial properties of rAAVs must be considered. The route of administration, transgene nature, and the most suitable capsid serotype (Bedbrook et al., 2018). In addition, the importance of experimental factors such as AAV physical titer (stock) and dosage or the infectious titer should not be neglected as an influential factor (Haery et al., 2019). The parameters outlined below can contribute to a variety of rAAV combinations, whether they are going to target specific populations of neurons or used to globally express in the brian (Bedbrook et al., 2018).

1.10.1 Routes of administration

One important aspect of *in vivo* transduction with viral vectors is the delivery route of rAAVs. Choosing the most appropriate route when transducing the CNS, is bound to the rAAV structure, transgene specificity, model organism, and host cell receptors. The proper administration route results in increased viral transduction within the intended region and effective expression of the target gene (Fajardo-Serrano et al., 2021). Direct delivery of the AAV vectors to the CNS has been the most widely used administration in research and clinical studies (Saraiva et al., 2016). It provides regional control of expression, does not require large amounts of AAV reagent, and provides low immunogenicity (Bedbrook et al., 2018; Cearley & Wolfe, 2007). Although this method circumvents the highly selective BBB, the transduction is poorly distributed, resulting in limited transgene expression at the injection site (Saraiva et al., 2016). Furthermore, it bears the drawbacks of being invasive. In one clinical study, the AAV2- neurturin vectors were delivered to PD patients' brains through frontal burr holes, reporting severe side effects from the surgical process (Marks Jr et al., 2010).

Remote delivery, on the other hand, refers to non or less-invasive approaches that allow for widespread vector distribution throughout the CNS. Infusion of AAV vectors via intraparenchymal, intra-cerebrospinal fluid (intra-CSF), intramuscular, or intravascular delivery are some instances of this delivery route (Fajardo-Serrano et al., 2021). However, BBB is a substantial barrier that poses challenges for intramuscular, or intravascular methods as the less invasive methods (Fajardo-Serrano et al., 2021). The BBB is a highly selective specialized system characterized by unique microvascular endothelial cells of the blood vessels in the vicinity of the brain, preventing toxic substances' penetration and

regulating the trafficking of ions, molecules, and cells into the brain (Daneman & Prat, 2015). Evidently, viral vectors are considered outsiders to the brain, limiting their ability to cross BBB. The brain is highly vascularized and an AAV that could efficiently cross the BBB have unparalleled access to the entire organ providing the opportunity for either broad or specific targeting gene delivery (Girouard & Munter, 2018). The discovery of AAV serotype 9 that can circumvent BBB opened a new avenue for systemic delivery of the target gene to the CNS (Duque et al., 2009). However, natural AAV serotypes require high doses, cross the BBB with weaker efficiency, and are mostly unable to transfect specific cells (Goertsen et al., 2021). Nevertheless, the highly customizable AAV capsid and cargo provide opportunities for scientists to alter AAV behavior and enhance its efficiency. Recent advances in AAV engineering resulted in the generation of a series of AAV variants, such as AAV-PHP.B, AAV-AS, and AAV-PHP.eB, that can effectively transduce mice CNS or peripheral nervous systems by systemic non-invasive administration (Chan et al., 2017; Choudhury et al., 2016; Deverman et al., 2016). AAV-PHP.eB is reported to transduce more than 50% of different neuronal populations (Chan et al., 2017).

1.10.2 Cell-type specific promoters and tetracycline expression system

To be able to investigate the activity and functions of a subpopulation of neurons within the nervous system, cell-type-specific expression of molecular tools is crucial. In a targeted modification strategy, scientists use the combination of traditional genetic techniques with various transcriptional or translational regulatory components (Bedbrook et al., 2018). With regards to AAVs, they can be utilized to precisely target specific groups of neurons when the understanding of the target neurons' intrinsic gene expression pathway and locations within the brain is available (Haery et al., 2019).

The selective expression of transgenes can benefit from using different promoters and enhancers. Typically, there are two types of promoters (Bedbrook et al., 2018); general/ubiquitous and cell-type-specific promoters (Haery et al., 2019) (Table 3). The former provides an overall expression of the transgene with high efficiency while the latter promotes expression in specific cells. The choices of different promoters are restricted due to the current challenge of the limited packaging capacity of AAVs (Bedbrook et al., 2018). Aside from promoter specificity, its strength also affects the transgene expression; some might not be able to tolerate high levels of expression, while

others require increased levels for sufficient activity. A strong promoter can sometimes lead to leaky fluorescent protein expression (Bedbrook et al., 2018).

Table 3. Some examples of cell-type-specific promoters (Adopted from Bedbrook et al., 2018).

Promoters' name	properties	References
CMV (cytomegalovirus early enhancer/promoter)	Ubiquitous, with high-level expression, strong in some types of cells (e.ge HEK 293T)	(Rodova et al., 2013)
CAG (CMV enhancer, chicken, β -actin gene, splice acceptor of the rabbit β-globin)	Ubiquitous, strong synthetic promoter in mammalian cells	(Miyazaki et al., 1989)
hSyn1 (Human synapsin 1 gene promoter)	Ubiquitous, only targeting neuronal populations, long-term expression	(Kügler et al., 2003)
mTH (mouse tyrosine hydroxylase promoter)	Cell-specific promoter, targeting dopaminergic neurons	(Chan et al., 2017)
rTH (Rat tyrosine hydroxylase promoter)	Cell-specific promoter, targeting dopaminergic neurons	(Oh et al., 2009)
mDlx (Mouse Distal-less homeobox enhancer)	Cell-specific promoter, targeting GABA-ergic neurons	(Dimidschstein et al., 2016)

Scientists developed a few regulatable strategies to achieve a more efficient expression of target cells, and overcome the constant unregulated over-expression of transgenes; one of these strategies is the binary expression system. This binary system exploits the expression of two genetic components; the first one is the transgene of interest (effector) packed in an rAAV vector which remains silent in the absence of the second construct (also packed in an rAAV) that induces transcription of the effector (Haery et al., 2019). One example of this system is the tetracycline-inducible system which was described by (Harding et al., 1998). The first component (effector) in this system consists of the transgene with a promoter harboring tet-responsive elements (TRE). TRE promoter is

made of seven repeats of the tetracycline-resistance operator (tetO) (Gallia & Khalili, 1998). The second component (inducer), is a gene with a cell-type-specific promoter that can express a tetracycline-controlled transactivator (tTA). tTA is created by fusing the VP16 domain of herpes virus to the tet repressor (Agha-Mohammadi et al., 2004). Both components can be packed into separate rAAVs. When rAAVs of the system co-administrate e.g. systematically in the brain, expression of tTA in target cells under the control target cell endogenous promoter induces TRE promoter to express the transgene (Figure 8).

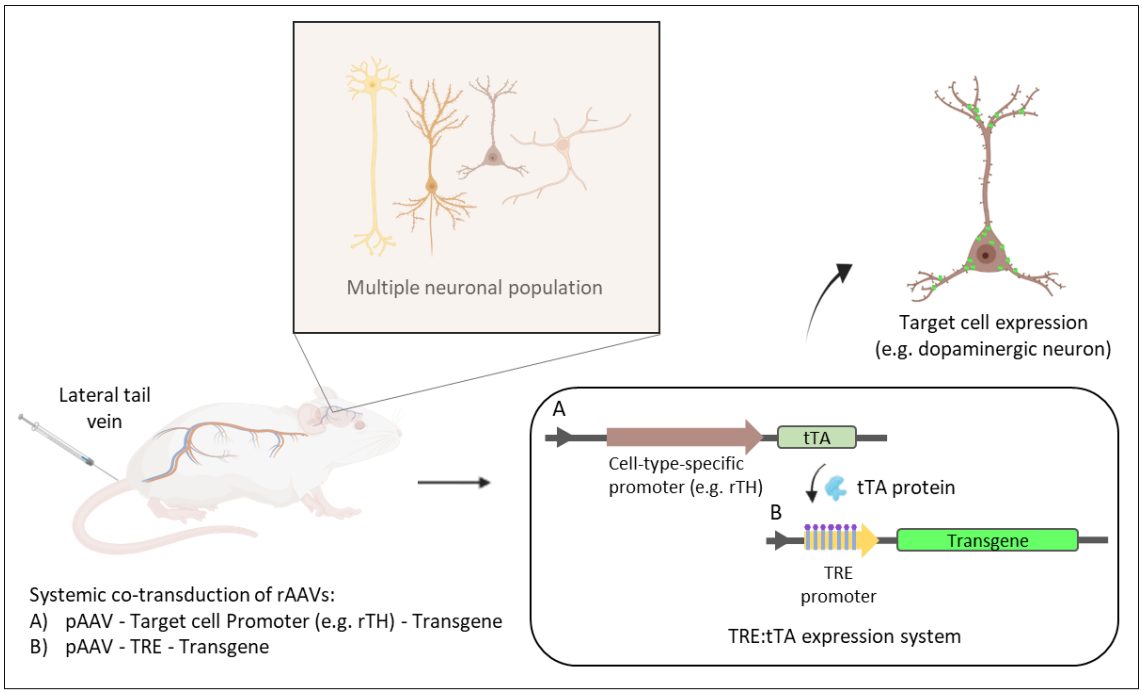

Figure 8. Representative of tetracycline-inducible expression system. Systemic delivery of rAAVs and expression of the gene of interest in a specific subpopulation of neurons by exploiting the cell promoter specificity (Image created by S. Abyari by Biorender).

1.10.3 Adeno-associated virus serotypes

AAV serotype is defined as "capsid variants or a group of capsids that have distinct neutralization properties" (Deverman et al., 2018). Currently, more than 12 strains of AAV are recognized based on phylogenic analysis (Korneyenkov & Zamyatnin, 2021) (Table 4). These serotypes show disparate tropism features as a result of differences in the amino acid contents of the capsid, capsid surface domains, and target-cell surface receptors (Fajardo-Serrano et al., 2021; Grimm et al., 2006). Origins of different serotypes vary, such that AAV serotypes (1/3/4/7/8/10) were derived from non-human primates, and serotypes (2/5/6/9) were discovered from humans (Korneyenkov & Zamyatnin, 2021). AAV serotype 2 has been the most extensively used and studied serotype since the

establishment of the first rAAV in 1982 by (Samulski et al., 1982). AAV2 provides long-term stable expression, and broad range cell transduction, and is reported to induce no immunogenicity. However, its broad tropism set a drawback for the expression of the transgene targeting specific regions of the brain (Wu et al., 2006). The preferred tropism for the CNS infection, are AAV serotypes (1/2/4/5/7/8/9/AAVrh10) most of which are able to transduce both neurons and astrocytes (Zhang et al., 2011). Among these serotypes, AAV9 and AAVrh10, represent the strongest CNS tropism spreading widely through axons either anterogradely (from the soma to the axon tip) or retrogradely (from the axon tip to soma) (D. Liu et al., 2021); this facilitates synaptic transmission across different subpopulations of neurons (Castle et al., 2014; Hordeaux et al., 2015). Comparing the efficiency of AAVrh10 isolated from rhesus monkeys (Gao et al., 2002) and AAV9, the former is reported to provide a higher expression efficiency when administrated intravenously to the spinal cord, CNS, and peripheral nervous systems of neonatal mice (Tanguy et al., 2015).

Table 4. Characteristics of different AAV serotypes (Adopted from Saraiva et al., 2016).

Serotype	Origin	Natural tissue tropism
AAV1	Non-human primate	Muscle, CNS, heart, liver, lungs
AAV2	human	Heart, CNS, liver, lungs, retina
AAV3	Non-human primate	Liver
AAV4	Non-human primate	Retina, lungs, kidney
AAV5	Human	Retina, CNS, liver
AAV6	Human	Heart, liver, muscle, retina
AAV7	Non-human primate	Liver
AAV8	Non-human primate	Muscle, heart, CNS, liver
AAV9	Human	Heart, CNS, liver
AAV10	Non-human primate	Muscle, myoblast tissue
AAV11	Non-human primate	Muscle, myoblast tissue
AAV12	Non-human primate	Salivary glands, muscle

One of the first big choices for AAV-based administration, is which capsid serotype to use depending on, a) the type of desired transgene delivery (e.g. broad tropism, cell-type-specific tropism, or retrograde transport) and b) routes of vector administration for the model organisms (Castle et al., 2016; J. Wang & Zhang, 2021). Regardless of its natural serotype, AAV can be modified to acquire distinct capsid variation with altered characteristics that bear beneficial features of different serotypes (Kwon & Schaffer, 2008). One strategy is to create mosaic AAVs using a mixture of VP subunits of different AAV serotype capsids (Choi et al., 2005). Alternative AAV serotypes can mitigate problems due to preexisting neutralizing antibodies formed as a result of an immune response during prior treatment with AAVs (Wu et al., 2006). Moreover, owing to the higher efficiency of AAV, the vector load into the target cells is reduced (Wu et al., 2006). For example, the mosaic AAV2/1 vector was created using capsid elements of both serotypes (Rabinowitz et al., 2004). Another approach is to utilize random or targeted mutagenesis to induce nucleotide alteration changes across the capsids (Maheshri et al., 2006). This approach exploits a random DNA-shuffling system, *in vitro* or *in vivo,* and generate a library of cpasids (Gray et al., 2010). Scientists used this method to transform AAV2's heparan sulfate binding to galactose binding by replacing 10 residues of AAV9 capsid, resulting in the development of AAV9 that can target liver cells (Adachi et al., 2014; Bedbrook et al., 2018).

After creating a diverse library of capsids using the methods described above, it is important to screen and select certain capsids capable of performing the desired function. The transduction characteristics for small-scale collections of capsids can be evaluated by systemic or direct injection. This technique, however, is insufficient for selecting cell-type-specific capsids in large-scale libraries. One recently developed method to mitigate this problem is the Cre recombination-based AAV targeted evolution (CREATE). In this method, PCR is used to build the capsid library, which is then injected into mice with Cre expression in a specified cell population. Cre can flip the polyadenylation sequence of rAAVs in CRE+ cells. Subsequently, PCR is used to identify and recover the rAAV serotypes that successfully transduced the target cells, based on the cre-recombined sequence (Deverman et al., 2016). Using this method, Deverman et al., 2016 and Chan et al., 2017 developed novel capsid serotypes AAV-PHP.B and enhanced AAV-PHP.eb respectively, that can cross BBB and efficiently transduce neurons and astrocytes in mice. AAV-PHP.eB provides more efficient transduction of CNS compared to other generated serotypes of date. One study compared the efficiency of PHP.eB with the naturally

occurring AAV9 serotype and found that when the need for circumventing BBB is eliminated by direct injection of AAVs into CNS, both variants performed similarly. This proves that what improves the AAV-PHP.eB transduction efficiency, is its capacity to cross the BBB (Mathiesen et al., 2020).

1.11 Study aims

Several dysregulated molecular and cellular pathways have been suggested as potential contributors to the onset of PD. Nevertheless, the role and significance of many other key target molecules that trigger PD in the early stages still need to be validated. Hopefully, this understanding will pave the way for diagnosis of the disease at the primary stages and the development of disease-modifying drugs for PD.

An earlier study from the Coffey research group on rotenone rat models of PD and cultured dopaminergic neurons treated with rotenone revealed phosphorylation disruption in three different proteins downstream of LRRK2 kinase activities. These proteins are potentially implicated in the pathogenesis of PD and are all involved in the regulation of CME in neuronal cells. The impacts of mentioned protein phosphorylation change on CME and their contribution to different PD-related neuropathogenic events and neurodegeneration needed to be evaluated. To achieve this, genes that encode phospho-mutants of those proteins were generated using site-directed mutagenesis-based PCR, resulting in phospho-deficient and phosphomimetic proteins. Phospho-deficient proteins imitate the constant deactivated form of proteins, whereas phosphomimetic proteins are constantly in the activated state. However, in order to be functionally tested in neuronal cells or animal models, mutant genes first needed to be delivered to the target dopaminergic neurons; which led to the aims of this Master's thesis project:

1- To generate AAV vector tools enabling us to systematically transmit our genes of interest in a proper and sensitive manner to the cultured target neuronal cells. This includes the generation of AAVs for mutated genes of all three target proteins.

2- To optimize the best functioning titer of AAVs and the AAVs' ratio used in the binary tetracyclin-inducible expression system. These optimizations yield the most integration of AAVs into the target cells; thus, the most effective transduction of cultured midbrain neurons. This provides a better resolution of our target genes when they will be functionally tested *in vitro* in neuronal cultured cells, and for future validation in mouse models and cultured patients fibroblasts.

2 Materials and Methods

2.1 Study design

This study was designed to generate high-titer rAAVs that can be used as vector tools to transduce cultured rat midbrain neurons *in vitro* and systematically administrate them *in vivo* in the follow-up experiments. The rAAVs contained different cargoes of three genes, each encoding for distinct proteins. All three target genes were generated in previous work as wild type, phosphomimetic mutants, and phospho-deficient mutants (Table 5). Phospho mimetic and phospho-deficient mutants are the constant ON and OFF states of proteins respectively which were generated by altering specific Serin residue of natural protein into Aspartate (ON) or Alanine (OFF). Depending on the AAV capacity and the transgene length, each target was fused with either hemagglutinin (HA) tag or a green fluorescent protein (GFP). The target genes were designed according to the tetracycline-inducible binary expression system.

Table 5. List of the plasmids with transgenes used for viral preparation.

Plasmids	Transgene function
pAAV-TRE-HA-T1-WT	Wild type protein
pAAV-TRE-HA-T1-Asp	Phospho-mimetic mutant
pAAV-TRE-HA-T1-Ala	Phospho-deficient mutant
pAAV-TRE-HA-T1-KD	Kinase-dead
pAAV-TRE-HA-T2-WT	Wild type protein
pAAV-TRE-HA-T2-Asp	Phospho-mimetic mutant
pAAV-TRE-HA-T2-Ala	Phospho-deficient mutant
pAAV-TRE-GFP-T3-WT	Wild type protein
pAAV-TRE-GFP-T3-xAsp	Phospho-mimetic mutant
pAAV-TRE-GFP-T3-yAsp	Phospho-mimetic mutant
pAAV-rTH-tTA	AAV genome that expresses tTA from the rat TH promoter (Addgene #133268)

T1: Target one, T2: Target two, T3: Target three, WT: Wild type protein, KD: Kinase-dead, x, y: Different mutant positions, GFP: Green fluorescent protein, HA: Hemagglutinin, rTH: rat tyrosine hydroxylase, tTA: tetracyclin-transactivator

The generated rAAVs were then transduced in culture midbrain neurons for optimizing their labeling titer and ratio, followed by immunofluorescent immunostaining visualization. The efficient rAAVs will be used *in vivo* in the rotenone rat model of PD for further evaluation of the disease mechanisms.

2.2 Ethical statement

The Sprague Dawley rats were provided by Central Animal Laboratory, University of Turku. All experiments were authorized by the National Animal Experiment Board (Eläinkoelautakunta ELLA) and conducted in accordance with the University of Turku and Åbo Akademi University's institutional guidelines and in agreement with Finnish law (497/2013 Act on the Protection of Animals Used for Scientific or Educational Purposes), and European legislation (Directive 2010/63/EU).

2.3 Antibodies

A list of all the primary and secondary antibodies used in this study is shown in Table 6.

Table 6. List of the antibodies used in this study

Antibody	Source/Type	Dilution	Application	Supplier
TH	Sheep/Polyclonal	1:500	ICC, 1°	Invitrogen, Waltham, USA
HA	Rabbit/Polyclonal	1:200	ICC, 1°	Invitrogen, Waltham, USA
Alexa Fluor® 568	Goat anti-rabbit	1:500	IF, 2°	Invitrogen, Waltham, USA
Alexa Fluor® 488	Donkey anti-sheep	1:500	IF, 2°	Invitrogen, Waltham, USA

1° - Primary antibody; 2° - Secondary antibody; IF – Immunofluorescence staining; ICC – Immunocytochemistry staining.

2.4 Cell transformation with pUCmini-iCAP-PHP and pHelper

Bacterial stabs of pAdDeltaF6 (phelper) and pUCmini-iCAP-PHP plasmids (Addgene, #112867 and #103005, respectively) were purchased (Addgene, Watertown, USA), and the prepared plasmids were stored as DNA mini-preps previously in our lab. The pUCmini-iCAP-PHP was generated by Chan et al., 2017, and consisted of AAV2 Rep-AAV-PHP.eB Cap, ampicillin resistance cassette, and a tTA-TRE amplification system (Figure 9). The pAdDeltaF6 plasmid was generated by Wilson JM (unpublished data),

which contained genes encoding E4, E2a, and VA and an ampicillin resistance cassette (Figure 10).

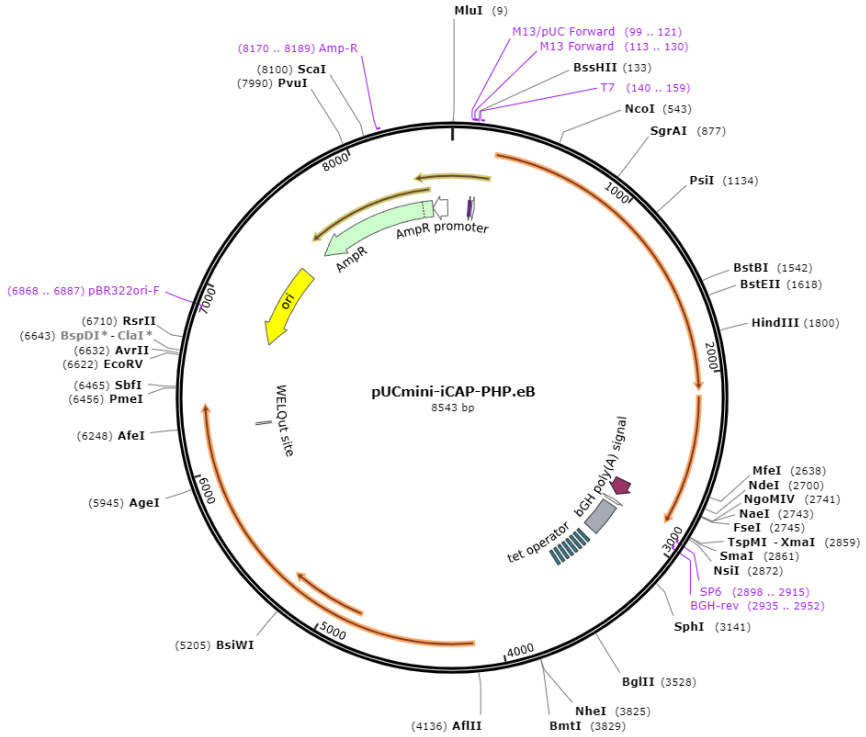

Figure 9. Vector map of pUCmini-iCAP-PHP.eB (Addgene).

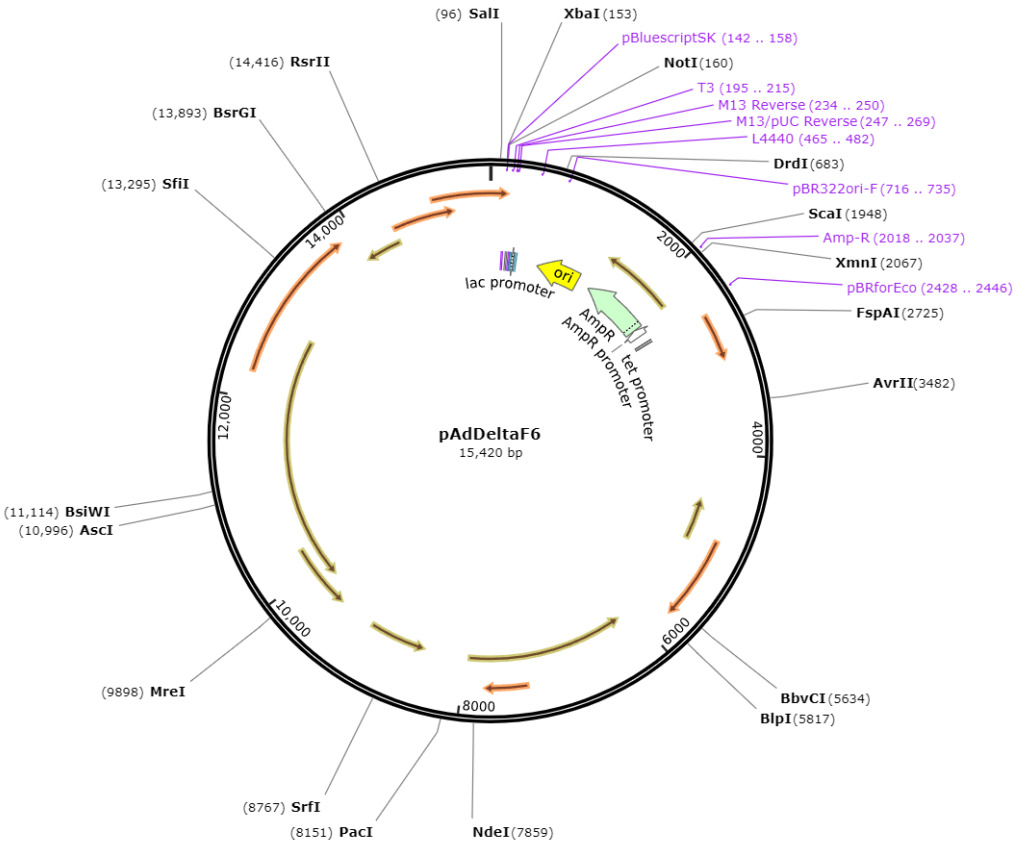

Figure 10. Vector map of pAdDeltaF6 (Addgene).

The heat-shock method was used to transform the pUCmini-iCAP-PHP and pHelper DNAs in NEB Stable and DH5α strains of competent *E. coli* (Invitrogen), respectively. in two prechilled polypropylene tubes. The bacteria-DNA mix was incubated for 10 minutes on ice, heath-shocked for 45 seconds at 42°C, and again incubated on ice for 2 minutes. Ice-cold SOB++ media (containing 10 mM NaCl (Sigma-Aldrich), 10 mM $MgSO_4$ (Sigma-Aldrich), 10 mM $MgCl_2$ (Sigma-Aldrich), 2.5 mM KCl (Sigma-Aldrich), 20 mM glucose (Sigma-Aldrich), 0.5% yeast extract (Biokar Diagnostics, Allonne, France), 2% tryptone (Sigma-Aldrich)) was added by 10x volume of previously added bacteria. Next, the transformation mix was placed on a shaker incubator at 220 rpm for 1 hour at 37 °C (Brunswick, Illinois, USA). The bacteria were spread on 1% agar plates (bacto agar (VWR, Pennsylvania, USA) prepared in LB medium (Turku Bioscience, Turku, Finland) with the addition of 50 µg/mL ampicillin (Sigma-Aldrich)) and incubated overnight at 37 °C. Two colonies from each plate were cultured in LB/ampicillin medium overnight at 37 °C on a shaker incubator (Brunswick). Larger cultures of each colony were propagated in 1 L of LB and 50 µg/mL ampicillin for pHelper and 2 L of LB and 50 µg/mL ampicillin for pUCmini-iCAP-PHP.eB. Next, they were grown overnight on a shaker incubator at 220 rpm and pelleted in an Avanti® J-26XP centrifuge (Beckman Coulter, California, USA) at 6000 x g for 15 minutes at 4 °C. Bacterial pellets were used for plasmid extraction using the maxi plasmid DNA purification kit (Macherey-Nagel, Düren, Germany). The extracted plasmid for pHelper and pUCmini-iCAP-PHP.eB DNAs were verified in a restriction digestion reaction with HindIII (Thermo Fisher) and BamHI (Thermo Fisher), respectively. The restriction enzymes for pHelper and pUCmini-iCAP-PHP.eB were HindIII (Thermo Fisher) and BamHI (Thermo Fisher) respectively. The digestion reaction was performed using the FastDigest green buffer (10X) buffer (Thermo Fisher), incubated for 20 minutes at 37 °C on a heating block (Eppendorf, Hamburg, Germany). Restriction digest products were run on 1% agarose in gel-electrophoresis, with GeneRuller 1 kb ladder (Thermo Fisher), and the gel was visualized in ChemiDoc MP imager (Bio-Rad, California, USA) with ethidium bromide (Sigma-Aldrich).

2.5 Maintenance of HEK 293FT cell line

The HEK 293FT cells were maintained over the period of AAV production. The cells were passaged at 75%-90% confluency in 175 cm^2 cell culture flasks (Greiner bio-one). Before each round of replating, the confluency and state of the cells was checked using the CK40 inverted phase-contrast microscope (Olympus, Tokyo, Japan). To start, the used culture medium was discarded and cells were gently rinsed two times with 5 ml of

versene (phosphate buffer saline (PBS) (Biowest) and 0.2% EDTA (Sigma-Aldrich)). Cells were detached from the flask surface with 10 ml of 25% trypsin (Sigma-Aldrich) in versene and incubated for 5 minutes at 37 °C. Next, the dispersed cells were collected into a 50 ml conical tube, and the remaining cells in the flask were added to the collection tube by rinsing them out with versene two more times. Cells were centrifuged in a 5804 centrifuge machine (Eppendorf, Hamburg, Germany) at 100 RCF for 5 minutes at RT. After centrifugation, the supernatant was removed and the cell pellet was resuspended gently 10-15 times with 1 ml of complete Dulbecco's Modified Eagle Medium (DMEM) (450 ml DMEM (Thermo Fisher), 10% fetal bovine serum (FBS), 5 ml of 200 mM L-Glutamine (100X) (Biowest), 2.5 ml of Penicillin-streptomycin (100X) (Biowest), 5 ml of 10 mM MEM Non-Essential Amino Acids (100X) (Thermo Fisher Scientific), 5 ml of Sodium Pyruvate 100 mM (100X) (Thermo Fisher Scientific)). According to the required confluency, between 100 to 200 µl of the suspension was pipetted to the 40 ml of 1% 50 mg/ml active geneticin (Thermo Fisher) in complete DMEM, mixed gently, and then plated back into the flask. The cells were grown in the incubator at 37 ºC with 5% CO_2.

2.6 AAV vector production

Generation of AAV vectors for each target DNA lasted 7 days according to Challis et al., 2019.

On day 0, the number of dishes required per viral prep were determined using the 'Transfection calculator' of the supplementary Table 2 from Challis et al., 2019. According to the number of dishes, 150 mm plates (Greiner bio-one) were seeded with HEK 293FT cells while replating them in cell culture flasks. The total cell counts required for each 150 mm dish was $7x10^6$ that measured by 100 µl of 90% dilutions of resuspended cell plates. Counting was performed manually on 0,1 mm counting chambers (Marienfeld, Harsewinkel, Germany)

On day 1, triple transient transfection of HEK 293FT cells with Polyethylenimine (PEI) (Thermo Fisher) was performed on 80-90% confluent cell plates from day 0. First, the PEI and Dulbecco's phosphate-buffered saline (DPBS) (Thermo Fisher) master mix was generated by thawing PEI at 37 °C, and then vortexed. The required volumes of PEI and DPBS for 5 x 15 mm dishes were calculated according to the 'Transfection calculator' from Challis et al., 2019, and then mixed in a 50 ml falcon tube. Second, the 'Transfection calculator' was used to calculate volumes of DPBS and DNA for each viral prep. According to this protocol, the ratio of 1:4:2 was used for pAAV: pUCmini-iCAP-PHP:

pHelper plasmid in 40 µg of total plasmid DNA. The list of the previously made transgenes is shown in Table 5. The concentration of each plasmid was measured on the NanoDrop™ 2000/2000c spectrophotometers (Thermo Fisher Scientific) before making the master mix. To prepare the transfection solution, the required volume of PEI+DPBS master mix was added dropwise with a 1 ml pipette to the DNA+DPBS solution while gently mixing them. The tube was then capped and vortexed for 10 seconds. The mixture was incubated at RT for 2-10 minutes. Finally, 2 ml of the transfection solution was added to each 15 mm dish (containing 20 ml of 80-90% confluent cell culture) dropwise and scattered; after swirling, the dishes were placed in the Heracell™ 150i CO_2 incubator (Thermo Fisher, Massachusetts, USA), at 37 °C with 5% CO_2.

On day 2, at 24 hours post-transfection, the media of each dish were changed with a fresh prewarmed complete DMEM by aspirating the old media in 10% bleach and without touching the dish surface and incubated for 48 hours at 37 °C with 5% CO_2. It should be noted that from day 2, all the procedures were performed with sterile equipment and in a biosafety cabinet of the Genome Editing Core (Turku Bioscience, Turku, Finland). After each use, all the AAV contaminated equipment and surfaces were disinfected with the easydes (Kiilto).

On day 3, the 40% (wt/vol) polyethylene glycol (PEG) (Sigma-Aldrich) stock solution was prepared for day six. 146.1 g of NaCl (Sigma-Aldrich) was mixed in 500 ml of Milli-Q water (MQW) on a hotplate magnetic stirrer (Variomag, Florida, USA) in a 1-liter sterile bottle. When completely dissolved, 400 g of PEG (Sigma-Aldrich) was added and heated at 68 °C overnight until it dissolved into an extremely viscous solution. Next, MQW was added to the solution for a total of 1 L and then filter sterilized with a pre-wet Nalgene™ Rapid-Flow™ Disposable filter unit (Thermo Fisher). The PEG stock was stored at 4 °C.

On day 4, the 72 hours post-transfected cell culture media of each dish was harvested with a 25 ml serological pipette while tilting the dishes, followed by replacing the media with 20 ml of fresh prewarmed DMEM and placing in the incubator. The harvested media was stored in a sterile bottle at 4 °C.

On day 5, the dishes were kept in the incubator.

On day 6, at 120 hours post-transfection, the media of all dishes were harvested again with a 25 ml serological pipette and the cells were gently scraped with a cell scraper at a

30° angle from each dish. This procedure was performed for each dish at a time and both the media and the cells were added to the harvested media from day 4. For 5 x 15 mm dishes, the expected harvest media from days four and six was around 200 ml. Harvested cells and the media were pooled and centrifuged at 2000 x g for 15 minutes at RT 5804 R centrifuge machine (Eppendorf, Hamburg, Germany) in 50 ml falcon tubes. Next, the supernatants were transferred to a sterile 500 ml bottle while the falcon tubes with cell pellets were kept on ice.

Supernatants were filtered through 0.45 µm PES filters (Sartorius) and after that 50 ml of PEG solution were added to 200 ml of filtered supernatant. Then the PEG was mixed with a magnetic stirrer for 1 hour at 4 °C and the mix was kept overnight at 4 °C for full precipitation of viruses. Meanwhile, the cell pellets were frozen using the dry ice-ethanol bath for 5 minutes and kept at -80 for the next day.

On day 7, 20 ml of lysis buffer was prepared containing 16 ml of 1x PBS, 4 ml of 1M NaCl/PBS, 20 µl of 1M MgCl2, and 2 µl of 10% Pluronic™ F-68 (Thermo Fisher Scientific). The supernatant from day six was divided into 4 x 50 ml falcon tubes and centrifuged (Eppendorf) at 2820 x g for 15 minutes at 4 °C. The supernatant was discarded and the small virus pellets were resuspended with 5 ml of lysis buffer and transferred into a 50 ml conical tube, then kept on ice.

The cell pellets from day 6 were thawed and resuspended with 5 ml of lysis buffer. After that, three rounds of the freeze-thaw cycle were performed by placing the pellets into the dry ice-ethanol bath for 5 minutes and then rapidly into a water bath set at 37 °C. Next, the suspension was centrifuged at 3220 x g for 15 minutes at 4 °C to pellet cell debris followed by transferring the clear lysate (~ 5 ml) to the 50 ml tube containing the resuspended virus. Residual DNA carried over the packaging process was degraded with 2 µl of benzonase (Sigma-Aldrich) followed by 45 minutes of incubation at 37 °C. The clarified supernatant was obtained from 10 minutes of centrifugation (Eppendorf) at 4 °C which was transferred to a new tube for the purification process.

2.7 AAV purification and concentration

After generating viral suspensions, to achieve high titer AAVs, purification and concentration steps were followed by the "AAV Purification by Iodixanol Gradient Ultracentrifugation" protocol provided by Addgene.

First, reagents for the purification step were prepared beforehand.

1 M NaCl/ PBS-MK buffer was prepared by dissolving 26.3 mg $MgCL_2 \cdot 6H2O$ (VWR International), 14.91 mg of KCl (VWR International), and 5.84 g NaCl (Sigma-Aldrich) in 1x PBS to the final volume of 100 ml; filter-sterilized with 0.22 µm filters.
1x PBS-MK buffer was prepared by dissolving 14.91 mg of KCl and 26.3 mg of $MgCL_2 \cdot 6H2O$ in 1x PBS to a total volume of 100 ml; filter-sterilized with 0.22 µm filters.
Iodixanol gradient solutions at different densities were prepared (Table 7) as a medium to purify the AAVs.

Table 7. List of iodixanol gradients prepared.

Gradients	Reagents	Total volume
15% iodixanol	4.5 ml 60% iodixanol, 13.5 ml 1 M NaCl/PBS-MK buffer	20 ml
25% iodixanol	5 ml 60% iodixanol + 7 ml 1x PBS-MK buffer + 30 µl phenol red (Sigma-Aldrich)	~ 12 ml
40% iodixanol	6.7 ml 60% iodixanol + 3.3 ml 1x PBS-MK buffer	10 ml
60% iodixanol	10 ml 60% iodixanol + 45 µl phenol red	~ 10 ml

Each solution was overlayed into a Quick-seal tube (Beckman Coulter) using an 18 g needle with a 10 ml syringe while avoid making air bubbles inside the tube. The tube was first filled with 5 ml of 60% iodixanol, followed by 5 ml of 40% iodixanol, 6 ml of 25% iodixanol, 8 ml of 15% iodixanol, and 5 ml of clarified supernatant. The tube was then filled to the top with 1x PBS. After, the Quickseal tube was sealed with a tube sealer (Wahl Clipper). Two Quickseal tubes were prepared for 10 ml of the clarified virus. Next, the tubes were carefully moved for ultracentrifugation in Beckman Optima L-90K Ultracentrifuge (Beckman Coulter, California, USA) at 350,000x g in T70i rotor (Beckman Coulter, California, USA) for 90 minutes at 10 °C. After centrifugation finished, the fractions were collected as follows: the Quickseal tube was punctured by 20g needle at 60-40% interface with the needle bevel facing the 40% gradient, meanwhile, the upper part of the tube was also punctured to allow air pressure flow, and up to 5 ml of 40 % solution was collected into a 50 ml tube.

The purified AAVs then proceeded to the concentration step. The buffer exchange stock for concentration was prepared as given in Table 8.

Table 8. Lists of buffers prepared for AAV concentration.

Buffer	Reagent
A. **0.1% Pluronic-F68**	49.5 ml PBS + 500 ul 10% Pluronic-F68
B. **0.01% Pluronic-F68**	45 ml PBS + 5 ml of A (0.1% Pluronic-F68)
C. **0.001% Pluronic-F68 + NaCl**	45 ml PBS + 5 ml of B (0.01% Pluronic-F68) + 200 mM NaCl
Formulation buffer (FB)	0.001% Pluronic-F68: 45 ml PBS + 5 ml of B (0.01% Pluronic-F68)

To start, the filter membrane of Amicon® Ultra-15 Centrifugal tubes (Sigma-Aldrich) was covered with 15 ml of buffer A and incubated for 10 minutes at RT. Next, buffer A was discarded and 15 ml of buffer B was added followed by spinning at 3000 RPM for 5 minutes at 4 °C. This step was repeated again by discarding the flow-through and adding buffer C followed by centrifugation (Eppendorf) at 3000 RPM for 5 minutes at 4 °C. Then the flow-through was discarded and a small amount of viral sample (500-1000 ml) was mixed with 1-2 ml of FB and proceeded for 8 minutes of centrifugation (Eppendorf) at 3500 RPM and 4 °C. Afterward, the flow-through was discarded. The final steps consisted of repeated rounds (~20) of FB exchange while adding a little bit of sample (0.5-1 ml) at each round and centrifuging (Eppendorf) at 3500 rpm for 4 minutes at 4 °C. It should be noted that since iodixanol was not removed easily, more FB was added at each round, and to prevent the iodixanol from settling down, the buffer and sample were mixed thoroughly on top of the filter membrane. Eventually, when the concentrated volume reached less than 300 µl, it was collected into 0.5 ml microtubes (Sarstedt), frozen in liquid nitrogen, and kept at -80 °C.

2.8 Quantitative real-time polymerase chain reaction

The concentration of the generated and purified rAAVs was determined with titration in a quantitative real-time polymerase chain reaction (qPCR). Prior to qPCR reactions, rAAV viruses were treated with DNase I (Thermo Fisher) to eliminate any traces of contaminating plasmid DNA possibly carried over from the production and purification process. DNase I treatment was done with 5 µL of stock virus and 10x DNase buffer (Thermo Fisher) in 50 µL reaction mix, gently mixed, and incubated in a heat block at 37 ºC for 30 minutes. The reaction was stopped on ice. Standards used were pAAV-hSyn-

EGFP #50465-AAV1 (Addgene) and pAAV-mDlx-GFP-Fishell-1 #83900-AAV1 (Addgene). All generated rAAV of unknown titer (samples), two standards, and negative controls (no template control (ntc)) were done in duplicates. The starting 1:10 dilutions of samples and standards after the DNase I treatment was used for preparing further dilution series. Amplifying primers (biomers.net, GmbH, Ulm, Germany) were the forward ITR primer, 5'-GGAACCCCTAGTGATGGAGTT-3', and the reverse ITR primer, 5'-CGGCCTCAGTGAGCGA-3'.

The two standards were prepared in series of six standard dilutions in duplicates, at 10^9, 10^8, 10^7, 10^6, 10^5, and 10^4 viral genomes (vg) in 5 µL. MQW was used as the ntc. The samples were prepared in series of six dilutions, with dilution factors 200, 1000, 5000, 25000, 125000, and 625000 times. For one reaction, 5 µl of each dilution of standard, sample, or ntc, was used in 20 µL reactions, with 10 µL of PowerTrack SYBR Green Master Mix (Thermo Fisher), 10 µM of each primer, and MQW. The qPCR reaction mixes were added to the Applied Biosystems™ MicroAmp™ EnduraPlate™ optical 96-well clear barcoded plate (Thermo Fisher) with 4titude® seal (Azenta Life Sciences, Wotton, United Kingdom). The amplification reactions were performed in the QuantStudio™ 12K Flex Real-Time PCR System (Thermo Fisher). The qPCR conditions were optimized according to the size of the target sequence for amplification and the enzyme, where the initial denaturation step was set to 3 minutes at 98 °C, followed by 40 cycles for amplification, and with the final melt curve analysis. Each amplification cycle consisted of 15 seconds of denaturation at 98 °C, 30 seconds of annealing at 58 °C, and 1-minute of extension at 72 °C.

The amplification results and the melt curve analysis were analyzed using the instrument's QuantStudio 12 K Flex software (Thermo Fisher). The physical titer of sample viruses was determined as a number of vg per ml. It was calculated based on the standard curve and the sample dilution factor.

2.9 Midbrain cell culture

Newborn rats (Central Animal Laboratory, University of Turku) were used at postnatal 0 to culture primary midbrain neurons. Rats were decapitated and brains removed. Midbrain tissue was isolated by dissection and dissociation in DM/KyMg^{++} medium (contained 81.8 mM Na_2SO_4 (Sigma-Aldrich), 30 mM K_2SO_4 (Sigma-Aldrich), 5.8 mM $MgCl_2$ (Sigma-Aldrich), 0.001% phenol-red (Sigma-Aldrich), 0.25 mM Hepes pH 7.4 (Calbiochem, San Diego, USA), 1 mM D-glucose (Sigma-Aldrich)) enriched with 1 µM

kynurenic acid (Sigma-Aldrich). The dissected midbrain was rinsed with 2 ml of cold dissection media three times followed by two times digestion with 10 U/mL prewarmed papain solution (Worthington Biochemical, Lakewood, US) in DM/KyMg for 15 minutes at 37 °C. The leftover papain was discarded by washing the tissues with DM/KyMg, following 5 minutes of double treatment with trypsin inhibitor (Sigma-Aldrich) in 10 mg/mL DM/KyMg at 37 °C. The Neurobasal A growth medium (supplemented with 2% B27 (Gibco Life Technologies), 2 mM L-glutamine (Sigma-Aldrich), 50 µg/mL streptomycin (Sigma-Aldrich), and 50 U/mL penicillin (Sigma-Aldrich)) was used three times to wash the midbrain tissues. Neuronal cells were dissociated two times with 15 strokes in growth media, followed by 10 minutes of centrifugation at 100 g in Eppendorf® Centrifuge 5804R (Sigma-Aldrich). Midbrain neurons were resuspended in 1 ml of the enriched growth medium and seeded on 13 mm diameter acid wash-treated glass coverslips (Marienfeld) in 24-well plates (Greiner bio-one), at a density of 800 000 cells/well, and incubated at 37°C with 5% CO_2.

2.10 *In vitro* viral transduction

Different rAAV viruses were used (according to the experiment) for the transduction of cultured midbrain neurons in 24-well plates. Cells in all experiments were transduced at the day *in vitro* (DIV) 2 by first removing 300 µl of medium from each well to a sterile Eppendorf tube, followed by adding the required rAAVs volume, depending on the AAV stock titer. Next, the remaining 700 µl of medium (conditioned media) from each well was collected in a sterile falcon tube and immediately replaced with 300 µl medium containing the virus treatment in the same well. The conditioned medium was stored at 37°C, and the infected cells were incubated for 4 hours and/or overnight at 37°C. Afterward, the rAAV-containing medium was removed from each well and 700 µl of conditioned media was added back, and cells were placed in the incubator at 37 ºC with 5% CO2. The cells were monitored every day and fixed with 4% paraformaldehyde (PFA) (Sigma-Aldrich) at DIV 7 (post-transduction day 5).

2.10.1 Titer optimization

To determine the efficient functioning (labeling) titer, the midbrain neurons were co-transduced with the rAAV-TRE-GFP-T3-WT and rAAV-TH-tTA as described above in the rAAV titers described in Table 9. The transduction was performed both for 4 hours and overnight infection incubation, to test which worked better. The co-transduction was done with a 1:1 ratio of TRE:tTA viruses.

Table 9. Different labeling titers used in this experiment.

Virus treatments	Labeling titers per well according to stock titer
• **rAAV-PHP.eB -TRE-GFP-T3-WT (effector vector)** • **rAAV-TH-tTA (inducer vector)** **The TRE:tTA ratio in this experiment was 1:1.**	2.5×10^{11} vg/ml
	1.0×10^{11} vg/ml
	5.0×10^{10} vg/ml
	2.5×10^{10} vg/ml
	1.0×10^{10} vg/ml

2.10.2 Optimization of the co-transduction ratio of TRE:tTA viruses

The ratio of TRE and tTA elements was optimized by co-transduction of midbrain neurons with rAAV-PHP.eB -TRE-GFP-T3-WT and rAAV-TH-tTA as described above (2.10). Cells were transduced for overnight infection incubation with the middle range labeling titer $5x10^{10}$ vg/ml. The ratios of 1:4, 1:2, 1:1.5, 1:1, 1:0.5 and 1:0.2 for TRE:tTA rAAVs was used.

2.10.3 Target 1 and 2 transduction

The pAAV-TRE-HA-T1-WT and pAAV-TRE-HA-T2-WT were each co-transduced with pAAV-TH-tTA according to the general transduction protocol. Transduction was performed with the highest labeling titer ($2.5x10^{11}$ vg/ml), overnight infection incubation, and 1:1 ratio of TRE:tTA according to the results of two previous transduction.

2.11 Immunofluorescence staining

All transduced midbrain neuronal cultures were fixed at DIV 7 (7 days post-transfection) by first washing them in cold PBS (Biowest), fixing with 400 µl 4% PFA (for 11 mm coverslips in 24-well plates) at RT for 20 minutes, followed by washing three times with 1 ml PBS. The coverslips with fixed transduced midbrain neurons were then transferred to the parafilm platform, washed with 1x PBS for 10 minutes, and permeabilized 3 times for 15 minutes with 4% TBS-T (tris-buffered saline (TBS) with 0.4% Triton X-100) (Sigma-Aldrich). The multicolor staining was performed by sequential staining of the corresponding transduced neurons with one antigen after the other. As a result, the staining of fixed samples was performed by sequentially repeating the staining process for the two antigens of interest (tyrosine hydroxylase (TH) and hemagglutinin (HA)). It

was assured that all primary and corresponding secondary antibodies were employed from distinct species and did not cross-react. The coverslips were blocked with blocking buffer (1x PBS, 10% horse serum, 0.3% Triton X-100) for 1 hour at RT on a shaker to avoid non-specific background. Blocking buffer for immunostaining against TH was prepared with primary sheep anti-TH antibody at 1:500 in TBS-T and 1% of horse serum. Blocking buffer for immunostaining HA tag was prepared with primary rabbit anti-HA antibody at 1:200 in 1x PBS with 1% BSA, and 0.3% Triton X-100. Next, the coverslips were incubated overnight at 4 °C in a humidified chamber, protected from light. The next day, coverslips were washed three times with TBS-T and incubated with corresponding secondary antibodies (donkey anti-sheep 488 (1:500) and goat anti-rabbit 568 (1:500)). Following that, coverslips were washed three times with PBS, and the cell nuclei were stained with Hoechst-33342 (1:3000) in PBS for 30 minutes at RT. Finally, coverslips were washed three times with PBS and mounted inverted onto Mowiol mounting medium (Sigma-Aldrich) on 1 mm VWR® Microscope slides (VWR International, Radnor, USA). One-step staining was performed for target 3, and two-step staining was performed for targets 1 and 2.

2.12 Widefield imaging

Widefield fluorescence microscopy was performed on fixed immunofluorescence immunostained rat midbrain neurons. Imaging was conducted using the Nikon Eclipse Ti2-E widefield inverted microscope (Nikon, Tokyo, Japan) and the NIS Elements AR 5.11.01 64-bit software (Nikon) in the Cell Imaging and Cytometry (CIC) Core (Turku Bioscience, Turku, Finland). The 6.5 µm pixel size images were obtained using the Hamamatsu sCMOS Orca Flash 4.0 v3 camera. The two objectives, 10x Nikon CFI Plan-Fluor and 20x Nikon CFI S Plan Fluor ELWD, were used for imaging. Three-channel imaging was performed using the following emission filters on samples treated with rAAV containing targets 1 and 2: the TRITC 595/40nm filter (for TH), DAPI sPx 435/26nm (for Hoescht-33342), and YFP 540/21nm (for HA tag). Three-channel imaging was performed using the following emission filters on samples treated with rAAV containing target 3: the TRITC 595/40nm filter (for TH), DAPI sPx 435/26nm (for Hoescht-33342), and GFP sPx 515/30nm (for GFP) emission filters. Hamamatsu sCMOS Orca emission filter was used for light transmission. Images were 16bit and with pixel dimensions of 2048 x 2048. Images were processed using Fiji software (Schindelin et al., 2012).

3 Results

3.1 Cell transformation with pHelper and pUCmini-iCAP-PHP.eB

A large amount of pHelper and pUCmini-iCAP-PHP plasmids were required for the triple transient transfection of HEK 293ft cells. Therefore, the first step was to amplify these two genetic constructs from the stock. Each plasmid was successfully transferred into different competent *E .coli* strains, and the amplified DNAs were purified using the maxi prep kit after overnight incubation of cultured *E. coli*. The restriction enzyme digestion reaction was performed to evaluate a successful amplification of the purified plasmids using HindIII enzyme for pHelper and BamHI enzymes for pUCmini-iCAP-PHP. The reaction was expected to yield five bands (5.6, 3, 2.9,2.4, and 1.5 kb) for the former and two bands (5.2, and 3.4 kb) for the latter. Figure 11 represents the successful amplification of each plasmid in comparison to the original control stocks.

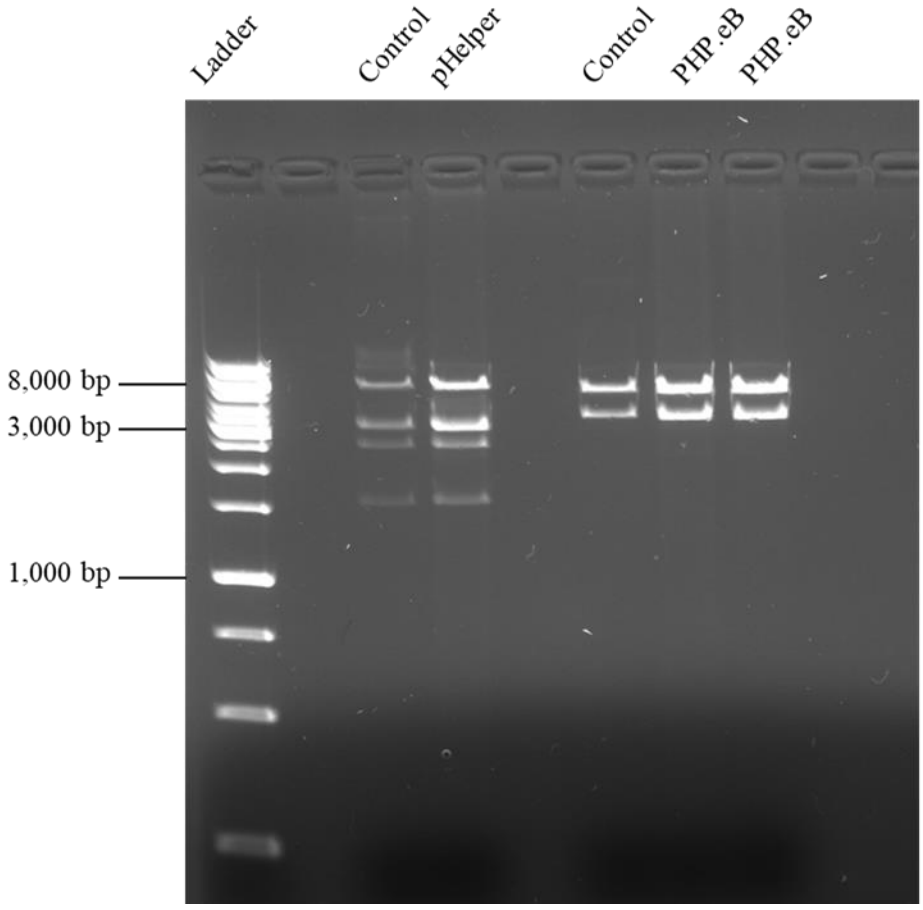

Figure 11. Example of restriction enzyme digestion test, on 1% agarose gel. Results show a successful amplification of two pHelper and pUCmini-iCAP-PHP.eB plasmids when compared to control samples. The expected bands for pHelper plasmid after the restriction digestion with Hind III were at 5.6, 3, 2.9, 2.4, and 1.5 kb. The expected bands for pUCmini-iCAP-PHP.eB after the restriction digestion with BamHI were at 5.2 and 3.4 kb.

3.2 Generation, purification, and stock titer of rAAV viruses

The first aim of this project was to generate three sets of rAAVs bearing the genes encoding various phosphomutant and wild-type proteins. The 11 rAAVs listed below (Table 10) were generated using the pUCmini-iCAP-PHP.eB plasmid which was developed by Chan et al., 2017, pAdDeltaF6 helper plasmid, and the previously made transgenes in the Coffey lab, or ordered from Addgene (plasmid #133268).

The physical (stock) viral titers were determined in the real-time qPCR reaction with forward and reverse ITR sequence amplifying primers. The qPCR instrument's software QuantStudio 12 K Flex (Thermo Fisher) was used to quantify the viral genomes and generate the melt curve. The physical titer of sample viruses was determined as a number of vg per 1 ml (vg/ml). It was calculated based on the standard curve generated with six dilution series of two standard viruses, and the sample dilution factor. The software calculated the number of genome copies in 5 µL of diluted sample. To get the vg/ml concentrations, this value was recalculated to 1 ml and multiplied by the dilution factor of the selected sample dilution. The final rAAV concentrations in vg/ml are presented in Table 10.

Table 10. List of generated rAAVs and corresponding titer.

rAAVs constructs	Stock Titer
1) rAAV- PHP.eB-TRE-HA-T1-WT	3.00 x 10^{13} vg/ml
2) rAAV- PHP.eB-TRE-HA-T1-PM	4.88 x 10^{13} vg/ml
3) rAAV- PHP.eB-TRE-HA-T1-PD	2.30 x 10^{13} vg/ml
4) rAAV- PHP.eB-TRE-HA-T1-KD	5.58 x 10^{13} vg/ml
5) rAAV- PHP.eB-TRE-HA-T2-WT	2.10 x 10^{13} vg/ml
6) rAAV- PHP.eB-TRE-HA-T2-PM	1.11 x 10^{13} vg/ml
7) rAAV- PHP.eB-TRE-HA-T2-PD	1.16 x 10^{13} vg/ml
8) rAAV-PHP.eB -TRE-GFP-T3-WT	0.26 x 10^{13} vg/ml
9) rAAV- PHP.eB-TRE-GFP-T3-xPM	0.61 x 10^{13} vg/ml
10) rAAV- PHP.eB-TRE-GFP-T3-yPM	0.45 x 10^{13} vg/ml

11) rAAV-PHP.eB-TH-tTA	1.56 x 10^{13} vg/ml

T1: Target one, T2: Target two, T3: Target three, WT: Wild type protein, KD: Kinase-dead, x, y: Different mutant positions, GFP: Green fluorescent protein, HA: Hemagglutinin, TH: Tyrosine hydroxylase, tTA: Tetracyclin-transactivator

3.3 Functional titer optimization

This study utilized the tetracyclin-inducible binary expression system, enabling targeted delivery of the transgene specifically to dopaminergic neurons, in this case. However, efficient transduction requires the highest integration of the viral construct into the target cells, which is determined by the labeling titer. To achieve an efficient labeling titer, two different variables must be optimized. Those variables are a) the concentration of infectious viral particles that transduce the cells (i.e. functionally) and b) the different time periods that the cells are exposed to viruses (infection incubation time).

To optimize these variables, rat primary midbrain neuronal cultures at DIV 2 were co-transduced using the rAAV-PHP.eB-TRE-GFP-T3-WT and the rAAV-PHP.eB-TH-tTA vectors in a 1:1 ratio. The former contained the green fluorescent protein gene and the transgene, while the other contained the dopaminergic cell-type-specific tyrosine hydroxylase (TH) promoter which allows expression of tTA, only when integrated into DA producing neurons (Figure 8). After co-transduction, cultured neurons either had 4 hours or overnight infection incubation. At DIV 7, cells were fixed and immunostained for TH as the gold standard marker for dopaminergic neurons (B. White & G. Thomas, 2012). TH immunostaining was visualized by Alexa Fluor® 488 secondary antibody reporter that allows distinguishing dopaminergic neurons from the background cells which were visualized with nuclei staining with Hoechst-33342.

Widefield microscopy was used to image stained samples. Cells expressing green fluorescent protein tags were identified as successfully transduced neurons. The efficient labeling titer was determined to be the concentration of rAVVs that transduced the greatest number of target cells. Successful transduction was expected to be demonstrated as colocalization of TH immunostained cells and green fluorescent emitting cells.

Results from 4 hours of infection incubation are shown in Figure 12. The dopaminergic cells are shown in red and the transduced cells expressing the target protein tagged with GFP are represented in green. The highest labeling titer ($2.5x10^{11}$ viral genome (vg)/ml) transduced a higher number of cells when comparing the different rAAV concentrations. As the concentration decreased, lower numbers of cells were transduced and no cells were transduced at concentrations of less than $5x10^{10}$ vg/ml during a 4-hour incubation period.

Figure 12C shows a 10X magnification to provide a wider view of the transduced cells while the other samples were imaged in 20X magnification.

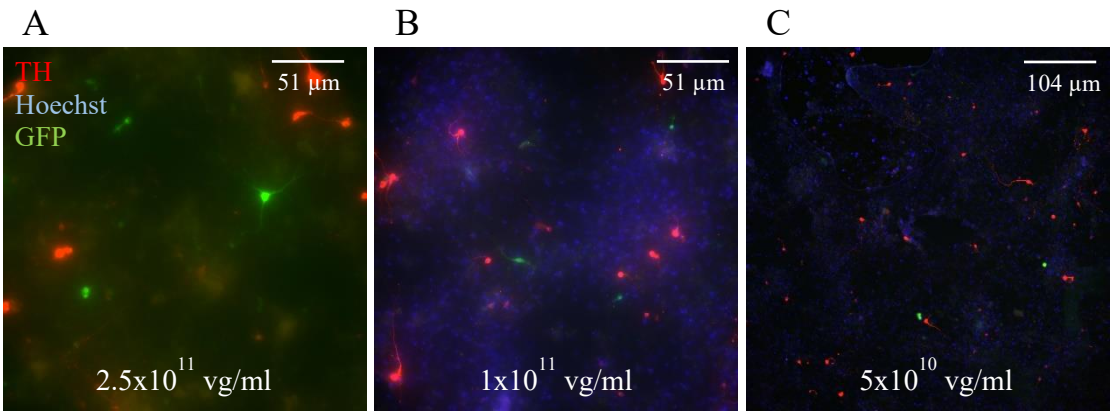

Figure 12. Results from labeling titer optimization using different viral concentrations in the range of the LOWEST to HIGHEST vg/ml after 4 hours of infection incubation. Representative widefield images of immunostained TH-expressing dopaminergic neurons (shown in red), visualized with Alexa Fluor® 488, target protein 3 fused with GFP (shown in green), and cell nuclei (shown in blue) stained with Hoechst. Scale bars 51 µm and 104 µm. (A) represents the highest transduction of dopaminergic cells in comparison to (B) and (C).

In comparison to 4 hours of infection incubation, the results from overnight incubation (Figure 13) of midbrain neurons with AAVs had higher efficiency transduction of dopaminergic cells, as the number of cells expressing GFP was higher. Obviously, when less viral concentration was used, less viral integration into cells occurred. As a result, the $2.5x10^{11}$ vg/ml and overnight infection incubation provided the most efficient labeling titer for cell transduction. In addition, based on the results, the $5x10^{10}$ vg/ml in overnight incubation was considered to provide the middle range transduction efficiency and chosen as the reference titer for further optimizations

Although for target three, colocalization was not observed thoroughly except in one or two cases (Figures 12 and 13), the transduction is believed to be successful.

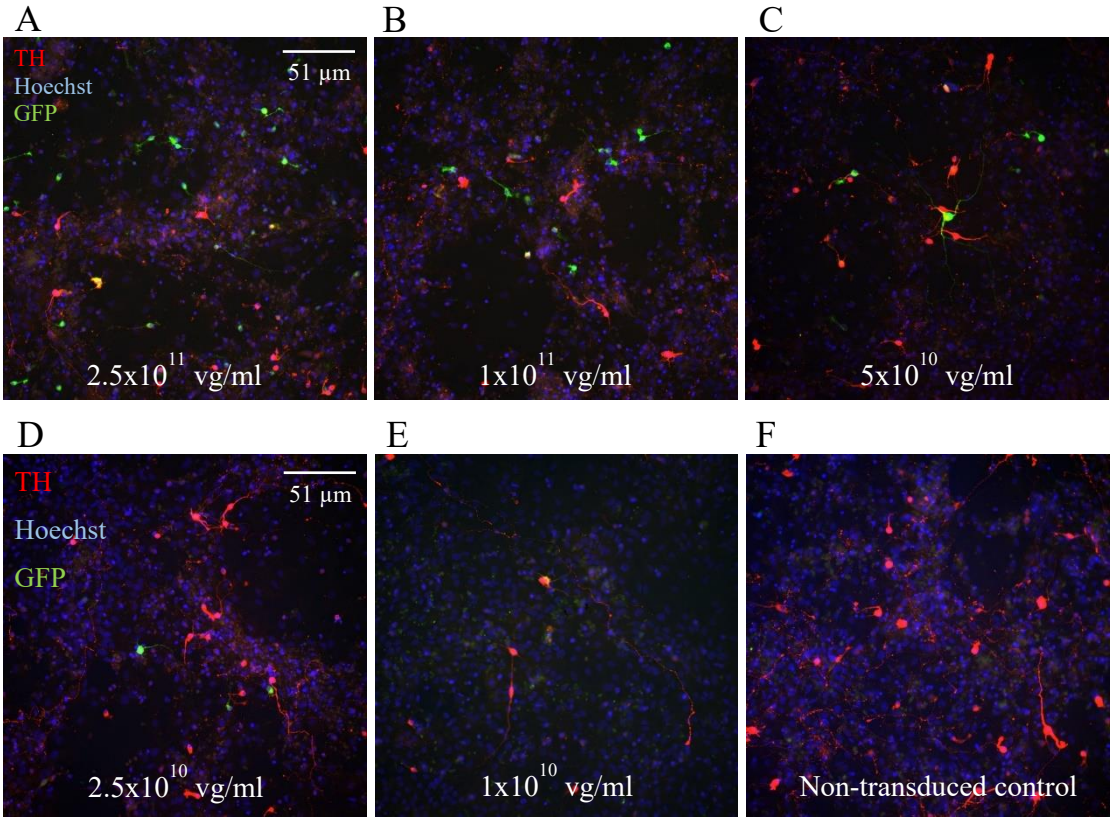

Figure 13. Representative widefield images for labeling titer optimization using different viral concentrations ranging from LOWEST to HIGHEST after overnight infection incubation. Dopaminergic neurons (shown in red) visualized with Alexa Fluor® 488, target protein 3 fused with GFP (shown in green), and cell nuclei (shown in blue) stained with Hoechst-33342. Scale bar 51 µm. (A) represents the highest transduction of dopaminergic cells in comparison to (E) with the lowest efficient labeling titer. Colocalization was shown in yellow which only occurred in (A) and (E). Non-transduced control is shown in (F).

3.4 The TRE:tTA ratio optimization

In order to obtain more efficient transduction, the rational amounts between the tTA protein and TRE promoter for each experiment needed to be optimized. To achieve this, different ratios of tTA were assessed with regard to TRE. This experiment was performed using the rAAV-PHP.eB-TRE-GFP-T3-WT and the rAAV-PHP.eB-TH-tTA vectors in overnight infection incubation and with the middle range labeling titer ($5x10^{10}$ vg/ml). Different ratios used in this experiment for TRE:tTA are 1:4, 1:2, 1:1.5, 1:1, 1:0.5, 1:0.2. Dopaminergic neurons that were immunostained for TH are shown in red and cells in green were transduced and expressed the GFP tag, background cells are stained in blue with Hoechst (Figure 14). Interestingly, the highest amount of tTA to TRE did not trigger more transduction but rather suppressed it (A). However, the 1:2, 1:1.5, and 1:1 TRE:tTA

ratios (B, C, and D respectively) represented relatively the same transduction pattern in different samples. The lowest transduction efficiency was related to 1:0.5 ratio (E), and below that no transduction occurred.

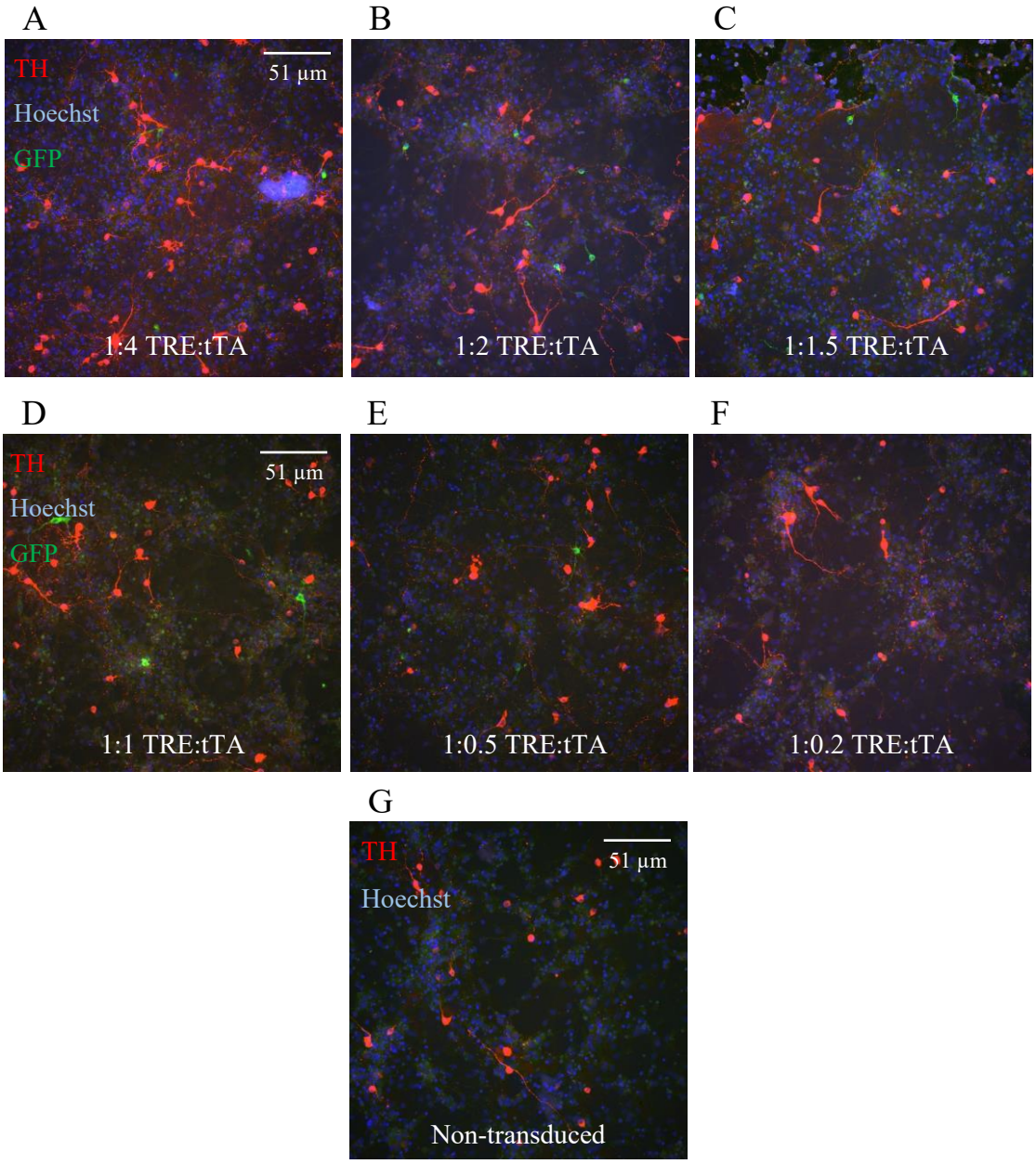

Figure 14. Representative widefield images for TRE:tTA ratio optimization using different concentrations (vg/ml) of rAAV-PHP.eB-TH-tTA vector. Dopaminergic neurons (shown in red) visualized with Alexa Fluor® 488, target protein 3 fused with GFP (shown in green), and cell nuclei (shown in blue) stained with Hoechst-33342. Scale bar 51 µm. (A) represents the highest concentration of tTA to TRE. In (B), (C), and (D), the TRE:tTA ratio was shown to be optimized as more numbers of cells were transduced. Non-transduced control is shown in (G).

3.5 Testing HA tag for targets 1 and 2

To assess whether the other two wild-type constructs expressed the transgene in target cells, cultured midbrain neurons transduced at DIV 2 with either rAAV- PHP.eB-TRE-HA-T1-WT or rAAV- PHP.eB-TRE-HA-T2-WT in addition to co-transduction of rAAV-PHP.eB-TH-tTA in 1:1 ratio. The most efficient labeling titer ($2.5x10^{11}$ vg/ml) was used in this experiment. Cells were fixed on DIV 7 and immunostained for TH and HA tag. The general antibody epitope HA tag was visualized by Alexa Fluor® 568 secondary antibody reporter demonstrating the cells with the integrated virus. The background cells were distinguished by Hoechst staining.

The stained samples were imaged using widefield microscopy. Successfully transduced neurons were expected to produce colocalized signals of TH and HA immunostaining. In this experiment, TH immunostained cells were represented by pseudocolor green, and cells expressing the tagged target proteins were shown in red.

Results of this experiment show a successful integration of WT constructs in the target cells, as almost all of the transduced cells were also expressed TH which is shown by the colocalization of TH and HA signals in yellow (Figure 15). Target 1 transduced more cells as compared to target 2.

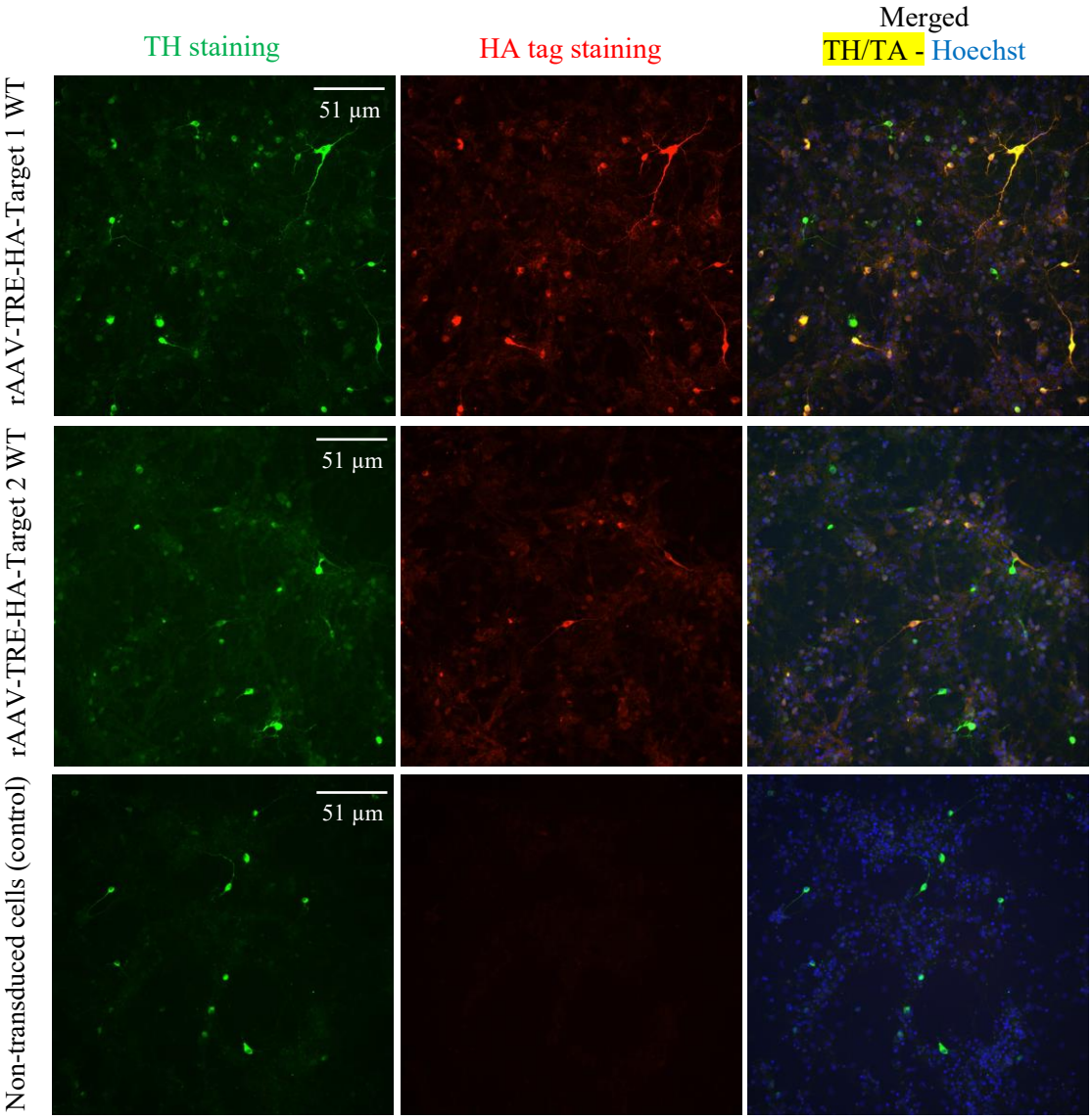

Figure 15. Representative widefield images of midbrain neurons transduced with target proteins 1 and 2 using the most efficient labeling titer ($2.5x10^{11}$ vg/ml) and TRE:tTA ratio of 1:1. Dopaminergic neurons (shown in pseudocolor green) visualized with Alexa Fluor® 488 secondary antibody, target proteins 1 and 2 (shown in red) visualized with Alexa Fluor® 568 secondary antibody, and background cells nuclei (shown in blue) stained with Hoechst. Scale bar 51 µm. Merged images of both targets show successful transduction (shown in yellow). Non-transduced control showed no expressed HA tag among dopaminergic and background neurons.

4 Discussion

PD is a complicated and multifaceted disease affecting an increasing number of people. The underlying pathophysiology of PD comprises various cellular and molecular pathways and cannot be characterized as a single process due to its heterogeneity. Many of those implicated mechanisms and interactions have yet to be thoroughly defined. As a result, current therapies and medications are mainly focused on slowing down the course of the disease. Furthermore, these treatments might ease the PD symptoms with varying degrees of efficiency depending on the etiology of the disease. This highlights the importance of targeting the baseline components that contribute to the pathological mechanisms of PD in order to develop novel drugs for therapy. Even though the majority of PD cases are idiopathic with various and/or unknown causes, understanding how genetic factors may influence the disease progression can provide insights into the shared biological pathways between familial and idiopathic cases, which in turn allows the development of disease-modifying medicines for both groups. One such pathway is that of the LRRK2 kinase and the molecular processes it regulates. Mutations in LRRK2, particularly the G2019S mutation, account for the highest number of familial PD cases, but it is also the most commonly identified genetic factor in idiopathic PD. Therefore understanding the downstream effects of its pathways on PD models, *in vitro* and *in vivo*, can pave the way for validating promising target molecules for novel drug development. These effects can be studied by introducing mutant proteins that are implicated in disease pathogenesis. However, before this can be done, it is required to develop tools for delivering these mutants into the target cells with a particular interest in viral vector tools with high transduction efficiency. This defines the aim of this Master's thesis.

4.1 Generation of rAAV constructs

Among several viral-mediated gene transfer methods, the AAV vector system is a highly versatile and attractive candidate which is used for CNS studies (Saraiva et al., 2016). An ideal AAV vector should provide no off-target effect, minimal immunogenicity, steady expression for long-term gene delivery, and scalable vector synthesis (Grieger & Samulski, 2012; Saraiva et al., 2016). Thus, as the first goal of this project, AAVs were generated to transfer 11 target genes *in vitro* and *in vivo* for follow-up studies of PD mechanism. A successful gene delivery requires a balanced combination between the appropriate AAV capsid and the cargo (Fajardo-Serrano et al., 2021). The capsid serotype is critical since it determines the AAV biodistribution as well as its cell or tissue tropism

specificity (Bedbrook et al., 2018). For this project, it was important to selectively target the dopaminergic neurons as they are the most impacted contributors to PD development. In addition, when it comes to *in vivo* experiments, the hurdles of BBB should be overcome with enhanced engineered capsids when rAAVs are systematically administrated. As a result, the recently developed AAV-PHP.eB capsid variant by Chan et al., 2017 with increased BBB bypassing ability was used in this study. This capsid variant is reported as one of the most efficient AAV vectors for CNS gene delivery (Dayton et al., 2018; Mathiesen et al., 2020).

After capsid characteristics, another major factor in successful transduction is the rAAVs' cargo. Extra levels of transduction specificity and efficiency can be obtained by including cell type-specific components in the transgene cassette. For this project, the TH promoter, as the most well-studied promoter for the dopaminergic system, was used. This promoter has been shown to induce high-level and durable gene expression in *in vivo* studies (Rolland et al., 2016, 2017). The TH promoter encodes for TH protein which is a rate-limiting enzyme in the pathway of producing DA from tyrosine and is exclusively expressed in dopaminergic neurons (Daubner et al., 2011). Therefore, the TH protein is used as a marker for dopaminergic neurons.

Most conventional viral vectors are employed to constitutively express the transgene of interest, with the researchers having little or no control over the duration or levels of expression. Such unregulated expression might have unforeseen consequences, such as cell death. To overcome this problem, the two-component expression system was applied when designing the transgene for this project. One component consisted of a TH promoter upstream of the tTA gene, and the other component consisted of TRE promoter upstream of the variable transgenes. The successful transduction in this system occurs when two components co-exist in target dopaminergic cells of the midbrain, where the TH promoter expresses tTA and tTA activates the TRE promoter leading to the expression of the gene of interest (Figure 8). To trace the transduction efficiency and expression of transgenes, the GFP reporter or hemagglutinin epitope tag was fused to the cargo while considering the rAAVs packaging capacity.

The relatively limited packaging capacity (~4.7 kb) of AAVs narrows down the choices of different components and brings constraints for bigger inserts. In 2008, (Allocca et al., 2008) incorporated a genome of 8.9 kb into a mosaic rAAV2/5 vector to overcome the limiting cargo capacity of AAV and interestingly reported successful transduction and

expression of this large insert in mice. The follow-up studies though determined that even when bigger vector genomes are packed, the genome's physical size still remains about 4.7 kb (Dong et al., 2010; Wu et al., 2010). Different studies conducted to describe this phenomenon suggested that the oversized AAV genome is fragmented upon packaging and those partial fragments complement each other and recombine inside the transduced cells. It is less likely that larger DNA fragments are efficiently packaged in the AAV capsids (Hirsch et al., 2010). Efforts to circumvent the AAVs' small packaging capacity have led to the development of a few strategies. One strategy is to split the large transgene into two or three separate rAAV vectors, followed by co-transduction. After transduction, the rAAV genome concatemerize and recombine the separate genes into a full-length gene. There are currently three different splitting strategies that were successfully used in large transgene delivery (Akil, 2020).

Considering all the above criteria a total of 11 different transgenes were generated in this thesis project. The transgenes were encapsulated by the PHP.eB capsid inside the HEK 293FT cells with helper plasmids following the Challis et al. Protocol described in 2019. The PEI infection strategy was employed in this protocol which provides high viral yields and is a less expensive method compared to commonly used calcium phosphate or lipofectamine reagents. The estimated viral yields (stock titer) for this method were reported to be $\geq 1 \times 10^{13}$ vg/ml which might differ from transgene to transgene or prep to prep. According to the qPCR results, the titer of generated rAAVs in this project ranged from 0.26×10^{13} to 5.58×10^{13} vg/ml following the expected production efficiency.

When comparing different physical titers of each target group, relatively similar titers are associated in each group with target proteins 1, 2, and 3 having the most to least titers, respectively. This difference might be due to the gene size of different targets. Our target genes' lengths were around 3 to 3.2 kb and despite the efforts to fit the size of the transgenes, they were still exceeding the AAVs' standard vector capacity, together with other genome elements. During the rAAV generation, the same amounts of HEK cells were seeded and further used for rAAV preps; it is possible that the slightly lower titer which was achieved for target 3 (Table 10) resulted from the bigger transgene size. In addition, using the GFP for target 3 might be another influencing factor, as the GFP is a fusion protein while the HA tag which is used for the other two targets is just a 9 amino acid epitope.

4.2 Important considerations and criteria when generating AAVs

Generation of high titer rAAV is an expensive, resource- and time-intensive process. Therefore, each step of the production must be handled carefully, and there are a number of critical steps throughout the AAV production and purification protocol. When preparing the DNA-PEI master mix, the transfection solution should appear slightly cloudy, otherwise, the DNA-PEI complex has not formed. One crucial step that needs to be cautiously done is providing the density gradient flow, as they can easily mix. Also when filling the gradient and sealing the tube, caution should be taken to not leave an air bubble, as this might lead to tube collapse in the ultracentrifuge and contaminate the instrument and laboratory environment. When puncturing the tube to extract the DNA, too much force might create two holes in the Quick-seal tube and mix the gradients. In addition, the needle should be placed in the 40-60% interface carefully; as the 40-25% interface includes a layer of proteinaceous substances and contaminants including empty capsids.

4.3 Transduction efficiency and optimization of labeling titer

Stock titers measured by qPCR do not often provide any indication of the number of infectious particles but rather a maximum value of the number of viral particles. The functioning titer of a viral stock, on the other hand, can vary depending on the preparation, vector system, insert, and the transduction target and can also be affected by freezing and thawing the viral solution after each use (Lock et al., 2010). The titer used for labeling is dependent on the concentration of viral particles that can transduce the cells. This is typically quantified by cell transduction assays (François et al., 2018). Higher transduction efficiency is dependent on several factors such as rAAV tropism, physical titer, infection incubation time, and promoter strength.

The produced rAAV constructs were functionally tested on cultured midbrain neurons to see with what efficiency they express the transgenes. The experiments were performed by 1:1 co-transduction of the rAAV bearing the target 3 transgene and the tTA inducer vector. In order to optimize the most efficient labeling titer for the follow-up experiments, a series of expected efficiency from the stock titer of the rAAVs were transduced into cultured midbrain neurons with different infection incubation times. The transduced cells were immunostained for TH for imaging and further analysis. The results demonstrated the highest labeling titer as being the most efficient labeling titer in both 4 hours and overnight infection incubation.

When comparing infection times, the overnight incubation provided a higher transduction efficiency. The rAAVs transduction pathway includes cellular uptake, which occurs by several endocytic pathways, with CME suggested as the most important route (Berry & Asokan, 2017). In one study, transduction of AAV2 was unsuccessful with the presence of mutant dynamin proteins (Duan et al., 1999). Following cellular uptake, only 30% of rAAVs will successfully express the transgene (Xiao et al., 2012). After entry to the cell, rAAVs traffic to the nuclei in the early endosomes with the help of Rab protein families and through the endomembrane system (Berry & Asokan, 2017). The rAAVs then must enter the nucleus, which is reported to be the most rate-limiting step of cell transduction (Bartlett et al., 2000). The whole process of viral transduction to the nucleus entry depends on several varieties, such as capsid type or the cell type which is being infected. Based on these mechanisms and how durable they are, the overnight infection incubation resulted in higher integration of viral particles into cell nuclei and expressed form.

However, hardly any colocalizations of the TH and rAAV expressing cells were observed contrary to what was expected. This might be because of the GFP-tag fusion protein that folded improperly which is causing problems or suppressing the expression of TH protein by seizing the cellular translational mechanisms. In one study published in 2017, Rolland et al. generated rAAVs expressing the mCherry fluorescent protein under the control of the TH promoter, to evaluate its sensitivity for transduction in dopaminergic neurons. The immunofluorescent staining results for colocalization of mCherry and TH protein confirmed the TH promoter's ability to successfully express the transgene in the substantia nigra region of mice. However, they reported that not all the mCherry expressing profiles were TH-positive, and conversely, not all the dopaminergic neurons expressed mCherry (Rolland et al., 2017), like what was observed in our study. Surprisingly, they found that the percent of the mCherry-expressing cells that are also positive for TH protein consisted of only 20% of mCherry-labeled cells. Two explanations were raised for this; one was the limitations of TH immunostaining, such as the limitation of reagents penetration or fixation which hardly could include 80% false-positive results. The other was that the transgenic expression suppressed the TH phenotype in DA neurons because it had a competitive advantage for crucial transcriptional factors for its expression over the endogenous TH promoter (Rolland et al., 2017). This might be the case for our transgene with GFP tagged.

4.4 Optimization of the co-transduction ratio of TRE:tTA viruses

As we exploit the tetracyclin-inducable co-transduction system in this study, it was important to observe whether a change in the ratio of viruses can affect the efficiency of the expression. The 1:1 ratio for *in vitro* studies mediates the effective expression of the transgene, whereas effective expression for *in vivo* experiments requires a 1:4 ratio of TRE:tTA vectors (B. Liu et al., 2008). Nevertheless, while some studies revealed that a 1: 1 TRE/tTA ratio provided excellent induction with little to no background expression, others discovered that greater or lower ratios were better (Lee et al., 2005; Smith-Arica et al., 2000). Multiple variables could play a role in these disparate results, such as the employed promoter for tTA, the target cell line, and the accuracy of the detection approach for transgenes' expression levels (Liu et al., 2008). Therefore, it is recommended that the optimal setting for each experiment be determined separately (Liu et al., 2008). To assess the effects of TRE:tTA ratio changes in this study, cultured midbrain neurons were treated with different ratios of inducer vector (tTA expressing rAAV) (Table 9). The middle range labeling titer (5.0×10^{10} vg/ml) for this experiment was chosen to be assessed because if the most efficient labeling titer was used, it might overlap with the effects of different ratios. Intrestingly, the 1:4 ratio not only failed to boost the transduction efficiency but also decreased it to some extent. Although a two-component vector approach facilitates efficient transgene targeting and expression, the need for dual vectors raises the total viral load required for successful transgene expression which might induce toxicity and inflammatory response (Lee et al., 2005). Thus, the increased number of total viral particles in 1:4 ratio might be the reason for the suppression of efficient expression. On the contrary, the transgene expression using the 1:2 to 1:1 ratios followed a similar pattern, showing the optimal transduction and expression of the transgene and confirming the suggested optimal ratio for *in vitro* experiments (Liu et al., 2008). As expected, below the 1:1 ratio, the efficiency of expression decreased.

4.5 Validation of rAAVs with target proteins 1 and 2

To evaluate the functionality of target proteins 1 and 2, rAAVs with transgenes encoding wild-type proteins of these targets were transduced in cultured midbrain neurons. The transduction setting was applied based on the optimized results of the two previous experiments. The highest efficiency labeling titer (2.5×10^{13} vg/ml) of rAAVs was used with a co-transduction rate of 1:1 for TRE:tTA. Immunofluorescence staining was

performed for the TH protein and HA tag. The results showed efficient expression of the transgene for both of these targets. Contrary to what was observed for target 3, no suppression of TH occurred and expression of all the HA-labelled cells were positive for TH phenotype, indicating that the cell type specificity of targetting cells was 100%. This might be due to the use of the HA-tag, as it should not compete with the endogenous TH promoter for expression. When comparing targets 1 and 2, target 1 showed a high efficiency of transduction so it was expressed in a greater proportion of dopaminergic neurons.

4.6 Future prospect

The optimization result of this project was based on the signaling proteins fused in the transgene. Observing the signals from tags does not tell that the transgene protein is intact. So, one additional check to be done before using the vectors is to test how much of the protein is in full length using western blotting. After confirming that the target proteins are intact, the effects of phospho-variant proteins on nerve cells physiology will be evaluated by measuring compromised functions in crucial cellular pathways that occur in PD. For instance, their impact on CME will be evaluated in animal models of PD using endocytosis assays. In addition, because rAAVs of different phospho-mutants carry reverse mutations (phosphomimetic and phosphodeficient), they allow for a double functionality experiment. For instance, we can examine if one of the mutants disturbs cellular processes; does the other mutation reverse this effect or rescue it?

5 Conclusion

In this project, a total of 11 rAAV constructs were generated and the effects of the wild-type constructs were evaluated and optimized in different assays. The findings of this study reveal that our insert transgenes are efficiently and specifically expressed in the target neurons. Nevertheless, when employing the AAV vector system, several considerations should be made in advance. One relates to the cargo transgene elements and tag used for visualization. As it was shown, the use of different tags, influenced the efficiency of transgene expression. This suggests that a thorough understanding of the target cell transcriptional and translational system before designing the rAAV cargo would help to opt for the best-suited elements, although the rAAV capsid capacity might impose limitations. In addition, choosing the most appropriate capsid for the rAAV is important to achieve specificity for the cell type of interest. In conclusion, the whole process of generating rAAVs and assessing their functionality depends on several different factors starting from designing the transgene and rAAV compartments, to the expression approach and transduction setting. To yield the most efficient final results, one must consider optimizing every step of the process from the beginning to the end.

References

Aasly, J. O. (2020). Long-Term Outcomes of Genetic Parkinson's Disease. *Journal of Movement Disorders*, *13*(2), 81–96. https://doi.org/10.14802/jmd.19080

Abdollahi, M., Ranjbar, A., Shadnia, S., Nikfar, S., & Rezaie, A. (2004). *Pesticides and oxidative stress: a review RA*. http://www.MedSciMonit.com/pub/vol_10/no_6/4163.pdfwww.MEDSCIMONIT.com

Adachi, K., Enoki, T., Kawano, Y., Veraz, M., & Nakai, H. (2014). Drawing a high-resolution functional map of adeno-associated virus capsid by massively parallel sequencing. *Nature Communications 2014 5:1*, *5*(1), 1–14. https://doi.org/10.1038/ncomms4075

Agha-Mohammadi, S., O'Malley, M., Etemad, A., Wang, Z., Xiao, X., & Lotze, M. T. (2004). Second-generation tetracycline-regulatable promoter: Repositioned tet operator elements optimize transactivator synergy while shorter minimal promoter offers tight basal leakiness. *Journal of Gene Medicine*, *6*(7), 817–828. https://doi.org/10.1002/jgm.566

Akil, O. (2020). Dual and triple AAV delivery of large therapeutic gene sequences into the inner ear. *Hearing Research*, *394*, 107912. https://doi.org/10.1016/J.HEARES.2020.107912

Albanese, F., Domenicale, C., Volta, M., & Morari, M. (2022). Modeling Parkinson's disease in LRRK2 mice: Focus on synaptic dysfunction and the autophagylysosomal pathway. In *Biochemical Society Transactions* (Vol. 50, Issue 1, pp. 621–632). Portland Press Ltd. https://doi.org/10.1042/BST20211288

AlDakheel, A., Kalia, L. v., & Lang, A. E. (2014). Pathogenesis-Targeted, Disease-Modifying Therapies in Parkinson Disease. *Neurotherapeutics*, *11*(1), 6–23. https://doi.org/10.1007/s13311-013-0218-1

Allocca, M., Doria, M., Petrillo, M., Colella, P., Garcia-Hoyos, M., Gibbs, D., Kim, S. R., Maguire, A., Rex, T. S., di Vicino, U., Cutillo, L., Sparrow, J. R., Williams, D. S., Bennett, J., & Auricchio, A. (2008). Serotype-dependent packaging of large genes in adeno-associated viral vectors results in effective gene delivery in mice. *The Journal of Clinical Investigation*, *118*(5), 1955–1964. https://doi.org/10.1172/JCI34316

Antonina Kouli, Kelli M. Torsney, & Wei-Li Kuan. (2018). *Parkinson's Disease Pathogenesis and Clinical Aspects*.

Arranz, A. M., Delbroek, L., van Kolen, K., Guimarães, M. R., Mandemakers, W., Daneels, G., Matta, S., Calafate, S., Shaban, H., Baatsen, P., de Bock, P. J., Gevaert, K., Berghe, P. vanden, Verstreken, P., de Strooper, B., & Moechars, D. (2015). LRRK2 functions in synaptic vesicle endocytosis through a kinase-dependent mechanism. *Journal of Cell Science*, *128*(3), 541–552. https://doi.org/10.1242/JCS.158196

Atchison, R. W., Casto, B. C., & Hammon, W. M. (1965). *Adenovirus-Associated Defective Virus Particles*. https://doi.org/10.1126/science.149.3685.754

B. White, R., & G. Thomas, M. (2012). Moving beyond tyrosine hydroxylase to define dopaminergic neurons for use in cell replacement therapies for Parkinson's disease. *CNS & Neurological Disorders Drug Targets*, *11*(4), 340–349. https://doi.org/10.2174/187152712800792758

Barker, L. A., Dowdall, M. J., & Whittaker, V. P. (1972). Choline metabolism in the cerebral cortex of guinea pigs. Stable-bound acetylcholine. *Biochemical Journal*, *130*(4), 1063–1075. https://doi.org/10.1042/BJ1301063

Bartlett, J. S., Wilcher, R., & Samulski, R. J. (2000). Infectious Entry Pathway of Adeno-Associated Virus and Adeno-Associated Virus Vectors. *Journal of Virology*, *74*(6), 2777. https://doi.org/10.1128/JVI.74.6.2777-2785.2000

Becerra, S. P., Koczot, F., Fabisch, P., & Rose, J. A. (1988). Synthesis of Adeno-Associated Virus Structural Proteins Requires Both Alternative mRNA Splicing and Alternative Initiations from a Single Transcript. In *JOURNAL OF VIROLOGY*.

Bedbrook, C. N., Deverman, B. E., & Gradinaru, V. (2018). *Viral Strategies for Targeting the Central and Peripheral Nervous Systems*. https://doi.org/10.1146/annurev-neuro-080317

Berardelli, A., Rothwell, J. C., Thompson, P. D., Hallett, M., & Berardelli, A. (2001). Pathophysiology of bradykinesia in Parkinson's disease. In *Brain* (Vol. 124).

Berardelli, A., Wenning, G. K., Antonini, A., Berg, D., Bloem, B. R., Bonifati, V., Brooks, D., Burn, D. J., Colosimo, C., Fanciulli, A., Ferreira, J., Gasser, T., Grandas, F., Kanovsky, P., Kostic, V., Kulisevsky, J., Oertel, W., Poewe, W., Reese, J. P., … Vidailhet, M. (2013). EFNS/MDS-ES recommendations for the diagnosis of Parkinson's disease. *European Journal of Neurology*, *20*(1), 16–34. https://doi.org/10.1111/ene.12022

Berger, Z., Smith, K. A., & Lavoie, M. J. (2010). Membrane localization of LRRK2 is associated with increased formation of the highly active lrrk2 dimer and changes in

its phosphorylation. *Biochemistry*, *49*(26), 5511–5523. https://doi.org/10.1021/bi100157u

Berns, Kenneth. I., & Linden, R. M. (1995). *The cryptic life style of adeno-associated virus*. https://doi.org/10.1002/bies.950170310

Berry, G. E., & Asokan, A. (2017). Cellular transduction mechanisms of adeno-associated viral vectors. *Current Opinion in Virology*, *21*, 54. https://doi.org/10.1016/J.COVIRO.2016.08.001

Bessis, N., GarciaCozar, F. J., & Boissier, M. C. (2004). Immune responses to gene therapy vectors: Influence on vector function and effector mechanisms. In *Gene Therapy* (Vol. 11, pp. S10–S17). https://doi.org/10.1038/sj.gt.3302364

Betarbet, R., Sherer, T. B., MacKenzie, G., Garcia-Osuna, M., Panov, A. v., & Greenamyre, J. T. (2000). Chronic systemic pesticide exposure reproduces features of Parkinson's disease. *Nature Neuroscience*, *3*(12), 1301–1306. https://doi.org/10.1038/81834

Bhatia, K. P., Bain, P., Bajaj, N., Elble, R. J., Hallett, M., Louis, E. D., Raethjen, J., Stamelou, M., Testa, C. M., & Deuschl, G. (2018). Consensus Statement on the classification of tremors. from the task force on tremor of the International Parkinson and Movement Disorder Society. *Movement Disorders*, *33*(1), 75–87. https://doi.org/10.1002/mds.27121

Biskup, S., Moore, D. J., Celsi, F., Higashi, S., West, A. B., Andrabi, S. A., Kurkinen, K., Yu, S. W., Savitt, J. M., Waldvogel, H. J., Faull, R. L. M., Emson, P. C., Torp, R., Ottersen, O. P., Dawson, T. M., & Dawson, V. L. (2006). Localization of LRRK2 to membranous and vesicular structures in mammalian brain. *Annals of Neurology*, *60*(5), 557–569. https://doi.org/10.1002/ana.21019

Blauwendraat, C., Heilbron, K., Vallerga, C. L., Bandres-Ciga, S., von Coelln, R., Pihlstrøm, L., Simón-Sánchez, J., Schulte, C., Sharma, M., Krohn, L., Siitonen, A., Iwaki, H., Leonard, H., Noyce, A. J., Tan, M., Gibbs, J. R., Hernandez, D. G., Scholz, S. W., Jankovic, J., … Singleton, A. B. (2019). Parkinson's disease age at onset genome-wide association study: Defining heritability, genetic loci, and α-synuclein mechanisms. *Movement Disorders*, *34*(6), 866–875. https://doi.org/10.1002/mds.27659

Bloem, B. R., Okun, M. S., & Klein, C. (2021). Parkinson's disease. In *The Lancet* (Vol. 397, Issue 10291, pp. 2284–2303). Elsevier B.V. https://doi.org/10.1016/S0140-6736(21)00218-X

Bordia, T., McGregor, M., Papke, R. L., Decker, M. W., Michael McIntosh, J., & Quik, M. (2015). The α7 nicotinic receptor agonist ABT-107 protects against nigrostriatal damage in rats with unilateral 6-hydroxydopamine lesions. *Experimental Neurology*, *263*, 277–284. https://doi.org/10.1016/j.expneurol.2014.09.015

Bower, J. J., Song, L., Bastola, P., & Hirsch, M. L. (2021). Harnessing the natural biology of Adeno-associated virus to enhance the efficacy of cancer gene therapy. In *Viruses* (Vol. 13, Issue 7). MDPI. https://doi.org/10.3390/v13071205

Burchell, V. S., Nelson, D. E., Sanchez-Martinez, A., Delgado-Camprubi, M., Ivatt, R. M., Pogson, J. H., Randle, S. J., Wray, S., Lewis, P. A., Houlden, H., Abramov, A. Y., Hardy, J., Wood, N. W., Whitworth, A. J., Laman, H., & Plun-Favreau, H. (2013). The Parkinson's disease–linked proteins Fbxo7 and Parkin interact to mediate mitophagy. *Nature Neuroscience 2013 16:9*, *16*(9), 1257–1265. https://doi.org/10.1038/nn.3489

Burger, C., Gorbatyuk, O. S., Velardo, M. J., Peden, C. S., Williams, P., Zolotukhin, S., Reier, P. J., Mandel, R. J., & Muzyczka, N. (2004). Recombinant AAV viral vectors pseudotyped with viral capsids from serotypes 1, 2, and 5 display differential efficiency and cell tropism after delivery to different regions of the central nervous system. *Molecular Therapy*, *10*(2), 302–317. https://doi.org/10.1016/j.ymthe.2004.05.024

Burré, J., Sharma, M., & Südhof, T. C. (2014). α-Synuclein assembles into higher-order multimers upon membrane binding to promote SNARE complex formation. *Proceedings of the National Academy of Sciences*, *111*(40). https://doi.org/10.1073/pnas.1416598111

Cartelli, D., Casagrande, F., Busceti, C. L., Bucci, D., Molinaro, G., Traficante, A., Passarella, D., Giavini, E., Pezzoli, G., Battaglia, G., & Cappelletti, G. (2013). Microtubule Alterations Occur Early in Experimental Parkinsonism and The Microtubule Stabilizer Epothilone D Is Neuroprotective. *Scientific Reports*, *3*(1), 1837. https://doi.org/10.1038/srep01837

Castle, M. J., Perlson, E., Holzbaur, E. L. F., & Wolfe, J. H. (2014). Long-distance axonal transport of AAV9 is driven by dynein and kinesin-2 and is trafficked in a highly motile Rab7-positive compartment. *Molecular Therapy*, *22*(3), 554–566. https://doi.org/10.1038/mt.2013.237

Castle, M. J., Turunen, H. T., Vandenberghe, L. H., & Wolfe, J. H. (2016). Controlling AAV Tropism in the Nervous System with Natural and Engineered Capsids.

Methods in Molecular Biology (Clifton, N.J.), *1382*, 133. https://doi.org/10.1007/978-1-4939-3271-9_10

Cearley, C. N., & Wolfe, J. H. (2007). A single injection of an adeno-associated virus vector into nuclei with divergent connections results in widespread vector distribution in the brain and global correction of a neurogenetic disease. *The Journal of Neuroscience : The Official Journal of the Society for Neuroscience*, *27*(37), 9928–9940. https://doi.org/10.1523/JNEUROSCI.2185-07.2007

Ceccarelli, B., Hurlbut, W. P., & Mauro, A. (1973). TURNOVER OF TRANSMITTER AND SYNAPTIC VESICLES AT THE FROG NEUROMUSCULAR JUNCTION. *Journal of Cell Biology*, *57*(2), 499–524. https://doi.org/10.1083/JCB.57.2.499

Challis, R. C., Ravindra Kumar, S., Chan, K. Y., Challis, C., Beadle, K., Jang, M. J., Kim, H. M., Rajendran, P. S., Tompkins, J. D., Shivkumar, K., Deverman, B. E., & Gradinaru, V. (2019). Systemic AAV vectors for widespread and targeted gene delivery in rodents. *Nature Protocols*, *14*(2), 379–414. https://doi.org/10.1038/s41596-018-0097-3

Chan, K. Y., Jang, M. J., Yoo, B. B., Greenbaum, A., Ravi, N., Wu, W. L., Sánchez-Guardado, L., Lois, C., Mazmanian, S. K., Deverman, B. E., & Gradinaru, V. (2017). Engineered AAVs for efficient noninvasive gene delivery to the central and peripheral nervous systems. *Nature Neuroscience*, *20*(8), 1172–1179. https://doi.org/10.1038/nn.4593

Chandler, R. J., Sands, M. S., & Venditti, C. P. (2017). Recombinant Adeno-Associated Viral Integration and Genotoxicity: Insights from Animal Models. *Human Gene Therapy*, *28*(4), 314–322. https://doi.org/10.1089/hum.2017.009

Chaudhuri, K. R., Healy, D. G., & Schapira, A. H. (2006). Non-motor symptoms of Parkinson's disease: diagnosis and management. *The Lancet Neurology*, *5*(3), 235–245. https://doi.org/10.1016/S1474-4422(06)70373-8

Choi, V. W., McCarty, D. M., & Samulski, R. J. (2005). AAV Hybrid Serotypes: Improved Vectors for Gene Delivery. *Current Gene Therapy*, *5*(3), 299. https://doi.org/10.2174/1566523054064968

Choong, C.-J., & Mochizuki, H. (2022). Neuropathology of α-synuclein in Parkinson's disease. *Neuropathology*, *42*(2), 93–103. https://doi.org/10.1111/NEUP.12812

Choudhury, S. R., Harris, A. F., Cabral, D. J., Keeler, A. M., Sapp, E., Ferreira, J. S., Gray-Edwards, H. L., Johnson, J. A., Johnson, A. K., Su, Q., Stoica, L., DiFiglia, M., Aronin, N., Martin, D. R., Gao, G., & Sena-Esteves, M. (2016). Widespread

Central Nervous System Gene Transfer and Silencing After Systemic Delivery of Novel AAV-AS Vector. *Molecular Therapy : The Journal of the American Society of Gene Therapy*, *24*(4), 726–735. https://doi.org/10.1038/MT.2015.231

Cookson, M. R. (2010). The role of leucine-rich repeat kinase 2 (LRRK2) in Parkinson's disease. In *Nature Reviews Neuroscience* (Vol. 11, Issue 12, pp. 791–797). https://doi.org/10.1038/nrn2935

Daneman, R., & Prat, A. (2015). The blood–brain barrier. *Cold Spring Harbor Perspectives in Biology*, *7*(1). https://doi.org/10.1101/cshperspect.a020412

Daniëls, V., Vancraenenbroeck, R., Law, B. M. H., Greggio, E., Lobbestael, E., Gao, F., de Maeyer, M., Cookson, M. R., Harvey, K., Baekelandt, V., & Taymans, J. M. (2011). Insight into the mode of action of the LRRK2 Y1699C pathogenic mutant. *Journal of Neurochemistry*, *116*(2), 304–315. https://doi.org/10.1111/j.1471-4159.2010.07105.x

Daubner, S. C., Le, T., & Wang, S. (2011). Tyrosine Hydroxylase and Regulation of Dopamine Synthesis. *Archives of Biochemistry and Biophysics*, *508*(1), 1. https://doi.org/10.1016/J.ABB.2010.12.017

Day, J. O., & Mullin, S. (2021). The Genetics of Parkinson's Disease and Implications for Clinical Practice. *Genes*, *12*(7), 1006. https://doi.org/10.3390/genes12071006

Dayton, R. D., Grames, M. S., & Klein, R. L. (2018). More expansive gene transfer to the rat CNS: AAV PHP.EB vector dose–response and comparison to AAV PHP.B. *Gene Therapy 2018 25:5*, *25*(5), 392–400. https://doi.org/10.1038/s41434-018-0028-5

Deng, H., Wang, P., & Jankovic, J. (2018). The genetics of Parkinson disease. *Ageing Research Reviews*, *42*, 72–85. https://doi.org/10.1016/j.arr.2017.12.007

Deverman, B. E., Pravdo, P. L., Simpson, B. P., Kumar, S. R., Chan, K. Y., Banerjee, A., Wu, W. L., Yang, B., Huber, N., Pasca, S. P., & Gradinaru, V. (2016). Cre-dependent selection yields AAV variants for widespread gene transfer to the adult brain. *Nature Biotechnology*, *34*(2), 204–209. https://doi.org/10.1038/nbt.3440

Deverman, B. E., Ravina, B. M., Bankiewicz, K. S., Paul, S. M., & Sah, D. W. Y. (2018). Gene therapy for neurological disorders: Progress and prospects. In *Nature Reviews Drug Discovery* (Vol. 17, Issue 9, pp. 641–659). Nature Publishing Group. https://doi.org/10.1038/nrd.2018.110

Dickson, D. W. (2017). Neuropathology of Parkinson disease. *Parkinsonism & Related Disorders*, *46*, S30–S33. https://doi.org/10.1016/j.parkreldis.2017.07.033

Dimidschstein, J., Chen, Q., Tremblay, R., Rogers, S. L., Saldi, G. A., Guo, L., Xu, Q., Liu, R., Lu, C., Chu, J., Grimley, J. S., Krostag, A. R., Kaykas, A., Avery, M. C., Rashid, M. S., Baek, M., Jacob, A. L., Smith, G. B., Wilson, D. E., … Fishell, G. (2016). A viral strategy for targeting and manipulating interneurons across vertebrate species. *Nature Neuroscience*, *19*(12), 1743–1749. https://doi.org/10.1038/nn.4430

Dong, B., Nakai, H., & Xiao, W. (2010). Characterization of genome integrity for oversized recombinant AAV vector. *Molecular Therapy : The Journal of the American Society of Gene Therapy*, *18*(1), 87–92. https://doi.org/10.1038/MT.2009.258

Dorsey, E. R., Sherer, T., Okun, M. S., & Bloemd, B. R. (2018). The emerging evidence of the Parkinson pandemic. In *Journal of Parkinson's Disease* (Vol. 8, Issue s1, pp. S3–S8). IOS Press. https://doi.org/10.3233/JPD-181474

Duan, D., Li, Q., Kao, A. W., Yue, Y., Pessin, J. E., & Engelhardt, J. F. (1999). Dynamin is required for recombinant adeno-associated virus type 2 infection. *Journal of Virology*, *73*(12), 10371–10376. https://doi.org/10.1128/JVI.73.12.10371-10376.1999

DUFFY, P. E., & TENNYSON, V. M. (1965). PHASE AND ELECTRON MICROSCOPIC OBSERVATIONS OF LEWY BODIES AND MELANIN GRANULES IN THE SUBSTANTIA NIGRA AND LOCUS CAERULEUS IN PARKINSON'S DISEASE. *Journal of Neuropathology and Experimental Neurology*, *24*(3), 398–414. https://doi.org/10.1097/00005072-196507000-00003

Duque, S., Joussemet, B., Riviere, C., Marais, T., Dubreil, L., Douar, A. M., Fyfe, J., Moullier, P., Colle, M. A., & Barkats, M. (2009). Intravenous administration of self-complementary AAV9 enables transgene delivery to adult motor neurons. *Molecular Therapy*, *17*(7), 1187–1196. https://doi.org/10.1038/mt.2009.71

Earley, L. F., Powers, J. M., Adachi, K., Baumgart, J. T., Meyer, N. L., Xie, Q., Chapman, M. S., & Nakai, H. (2017). Adeno-associated Virus (AAV) Assembly-Activating Protein Is Not an Essential Requirement for Capsid Assembly of AAV Serotypes 4, 5, and 11. *Journal of Virology*, *91*(3). https://doi.org/10.1128/jvi.01980-16

Edvardson, S., Cinnamon, Y., Ta-Shma, A., Shaag, A., Yim, Y. I., Zenvirt, S., Jalas, C., Lesage, S., Brice, A., Taraboulos, A., Kaestner, K. H., Greene, L. E., & Elpeleg, O. (2012). A deleterious mutation in DNAJC6 encoding the neuronal-specific

clathrin-uncoating co-chaperone auxilin, is associated with juvenile parkinsonism. *PloS One*, *7*(5). https://doi.org/10.1371/JOURNAL.PONE.0036458

Erb, M. L., & Moore, D. J. (2020). LRRK2 and the Endolysosomal System in Parkinson's Disease. In *Journal of Parkinson's Disease* (Vol. 10, Issue 4, pp. 1271–1291). IOS Press BV. https://doi.org/10.3233/JPD-202138

Esteves, A. R., Swerdlow, R. H., & Cardoso, S. M. (2014). LRRK2, a puzzling protein: Insights into Parkinson's disease pathogenesis. In *Experimental Neurology* (Vol. 261, pp. 206–216). Academic Press Inc. https://doi.org/10.1016/j.expneurol.2014.05.025

Fajardo-Serrano, A., Rico, A. J., Roda, E., Honrubia, A., Arrieta, S., Ariznabarreta, G., Chocarro, J., Lorenzo-Ramos, E., Pejenaute, A., Vázquez, A., & Lanciego, J. L. (2021). Adeno-associated viral vectors as versatile tools for parkinson's research, both for disease modeling purposes and for therapeutic uses. In *International Journal of Molecular Sciences* (Vol. 22, Issue 12). MDPI. https://doi.org/10.3390/ijms22126389

Feigin, V. L., Krishnamurthi, R. v., Theadom, A. M., Abajobir, A. A., Mishra, S. R., Ahmed, M. B., Abate, K. H., Mengistie, M. A., Wakayo, T., Abd-Allah, F., Abdulle, A. M., Abera, S. F., Mohammed, K. E., Abyu, G. Y., Asgedom, S. W., Atey, T. M., Betsu, B. D., Mezgebe, H. B., Tuem, K. B., … Zaki, M. E. (2017). Global, regional, and national burden of neurological disorders during 1990–2015: a systematic analysis for the Global Burden of Disease Study 2015. *The Lancet Neurology*, *16*(11), 877–897. https://doi.org/10.1016/S1474-4422(17)30299-5

François, A., Bouzelha, M., Lecomte, E., Broucque, F., Penaud-Budloo, M., Adjali, O., Moullier, P., Blouin, V., & Ayuso, E. (2018). Accurate Titration of Infectious AAV Particles Requires Measurement of Biologically Active Vector Genomes and Suitable Controls. *Molecular Therapy. Methods & Clinical Development*, *10*, 223. https://doi.org/10.1016/J.OMTM.2018.07.004

Freire, C., & Koifman, S. (2012). Pesticide exposure and Parkinson's disease: Epidemiological evidence of association. In *NeuroToxicology* (Vol. 33, Issue 5, pp. 947–971). https://doi.org/10.1016/j.neuro.2012.05.011

Gallia, G. L., & Khalili, K. (1998). *Evaluation of an autoregulatory tetracycline regulated system*. http://www.stockton-press.co.uk/onc

Gallo, K. A., & Johnson, G. L. (2002). Mixed-lineage kinase control of JNK and p38 MAPK pathways. In *Nature Reviews Molecular Cell Biology* (Vol. 3, Issue 9, pp. 663–672). https://doi.org/10.1038/nrm906

Gan-Or, Z., Dion, P. A., & Rouleau, G. A. (2015). Genetic perspective on the role of the autophagy-lysosome pathway in Parkinson disease. *Https://Doi.Org/10.1080/15548627.2015.1067364*, *11*(9), 1443–1457. https://doi.org/10.1080/15548627.2015.1067364

Gao, G.-P., Alvira, M. R., Wang, L., Calcedo, R., Johnston, J., & Wilson, J. M. (2002). *Novel adeno-associated viruses from rhesus monkeys as vectors for human gene therapy*. www.pnas.orgcgidoi10.1073pnas.182412299

Gibb WR, & Lees AJ. (1991). Anatomy, pigmentation, ventral and dorsal subpopulations of the substantia nigra, and differential cell death in Parkinson's disease. *J Neurol Neurosurg Psychiatry*, *54.5*. https://doi.org/10.1136/jnnp.54.5.388

Gil-Farina, I., & Schmidt, M. (2016). Interaction of vectors and parental viruses with the host genome. In *Current Opinion in Virology* (Vol. 21, pp. 35–40). Elsevier B.V. https://doi.org/10.1016/j.coviro.2016.07.004

Girouard, H., & Munter, L. M. (2018). The many faces of vascular cognitive impairment. *Journal of Neurochemistry*, *144*(5), 509–512. https://doi.org/10.1111/JNC.14287

Goertsen, D., Flytzanis, N. C., Goeden, N., Chuapoco, M. R., Cummins, A., Chen, Y., Fan, Y., Zhang, Q., Sharma, J., Duan, Y., Wang, L., Feng, G., Chen, Y., Ip, N. Y., Pickel, J., & Gradinaru, V. (2021). AAV capsid variants with brain-wide transgene expression and decreased liver targeting after intravenous delivery in mouse and marmoset. *Nature Neuroscience 2021 25:1*, *25*(1), 106–115. https://doi.org/10.1038/s41593-021-00969-4

Goetz, C. G., Tilley, B. C., Shaftman, S. R., Stebbins, G. T., Fahn, S., Martinez-Martin, P., Poewe, W., Sampaio, C., Stern, M. B., Dodel, R., Dubois, B., Holloway, R., Jankovic, J., Kulisevsky, J., Lang, A. E., Lees, A., Leurgans, S., LeWitt, P. A., Nyenhuis, D., … Zweig, R. M. (2008). Movement Disorder Society-Sponsored Revision of the Unified Parkinson's Disease Rating Scale (MDS-UPDRS): Scale presentation and clinimetric testing results. *Movement Disorders*, *23*(15), 2129–2170. https://doi.org/10.1002/mds.22340

Gray, S. J., Blake, B. L., Criswell, H. E., Nicolson, S. C., Samulski, R. J., & McCown, T. J. (2010). Directed evolution of a novel adeno-associated virus (AAV) vector that crosses the seizure-compromised blood-brain barrier (BBB). *Molecular Therapy : The Journal of the American Society of Gene Therapy*, *18*(3), 570–578. https://doi.org/10.1038/MT.2009.292

Greenland, J. C., & Barker, R. A. (2018). The Differential Diagnosis of Parkinson's Disease. In *Parkinson's Disease: Pathogenesis and Clinical Aspects* (pp. 109–128). Codon Publications. https://doi.org/10.15586/codonpublications.parkinsonsdisease.2018.ch6

Grieger, J. C., & Samulski, R. J. (2012). Adeno-associated virus vectorology, manufacturing, and clinical applications. *Methods in Enzymology*, *507*, 229–254. https://doi.org/10.1016/B978-0-12-386509-0.00012-0

Grimm, D., Pandey, K., Nakai, H., Storm, T. A., & Kay, M. A. (2006). Liver Transduction with Recombinant Adeno-Associated Virus Is Primarily Restricted by Capsid Serotype Not Vector Genotype. *Journal of Virology*, *80*(1), 426–439. https://doi.org/10.1128/jvi.80.1.426-439.2006

Haery, L., Deverman, B. E., Matho, K. S., Cetin, A., Woodard, K., Cepko, C., Guerin, K. I., Rego, M. A., Ersing, I., Bachle, S. M., Kamens, J., & Fan, M. (2019). Adeno-Associated Virus Technologies and Methods for Targeted Neuronal Manipulation. In *Frontiers in Neuroanatomy* (Vol. 13). Frontiers Media S.A. https://doi.org/10.3389/fnana.2019.00093

Harding, T. C., Geddes, B. J., Murphy, D., Knight, D., & Uney, J. B. (1998). Switching transgene expression in the brain using an adenoviral tetracycline-regulatable system. *Nature Biotechnology*, *16*(6), 553–555. https://doi.org/10.1038/NBT0698-553

Hattori, N., & Mizuno, Y. (2015). Mitochondrial Dysfunction in Parkinson's Disease. *Experimental Neurobiology*, *24*(2), 406–411. https://doi.org/10.5607/EN.2015.24.2.103

Hendricks, R. M., & Khasawneh, M. T. (2021). An Investigation into the Use and Meaning of Parkinson's Disease Clinical Scale Scores. *Parkinson's Disease*, *2021*. https://doi.org/10.1155/2021/1765220

Hernán, M. A., Takkouche, B., Caamaño-Isorna, F., & Gestal-Otero, J. J. (2002). A meta-analysis of coffee drinking, cigarette smoking, and the risk of Parkinson's disease. *Annals of Neurology*, *52*(3), 276–284. https://doi.org/10.1002/ana.10277

Heuser, J. E., & Reese, T. S. (1973). EVIDENCE FOR RECYCLING OF SYNAPTIC VESICLE MEMBRANE DURING TRANSMITTER RELEASE AT THE FROG NEUROMUSCULAR JUNCTION. *Journal of Cell Biology*, *57*(2), 315–344. https://doi.org/10.1083/JCB.57.2.315

Higashi, S., Moore, D. J., Colebrooke, R. E., Biskup, S., Dawson, V. L., Arai, H., Dawson, T. M., & Emson, P. C. (2007). Expression and localization of Parkinson's

disease-associated leucine-rich repeat kinase 2 in the mouse brain. *Journal of Neurochemistry*, *100*(2), 368–381. https://doi.org/10.1111/j.1471-4159.2006.04246.x

Hirsch, M. L., Agbandje-Mckenna, M., & Samulski, R. J. (2010). Little Vector, Big Gene Transduction: Fragmented Genome Reassembly of Adeno-associated Virus. *Molecular Therapy*, *18*(1), 6. https://doi.org/10.1038/MT.2009.280

Hong, C. T., Chan, L., & Bai, C.-H. (2020). The Effect of Caffeine on the Risk and Progression of Parkinson's Disease: A Meta-Analysis. *Nutrients*, *12*(6), 1860. https://doi.org/10.3390/nu12061860

Hordeaux, J., Dubreil, L., Deniaud, J., Iacobelli, F., Moreau, S., Ledevin, M., le Guiner, C., Blouin, V., le Duff, J., Mendes-Madeira, A., Rolling, F., Cherel, Y., Moullier, P., & Colle, M. A. (2015). Efficient central nervous system AAVrh10-mediated intrathecal gene transfer in adult and neonate rats. *Gene Therapy*, *22*(4), 316–324. https://doi.org/10.1038/gt.2014.121

Howden, S. E., Voullaire, L., & Vadolas, J. (2008). The transient expression of mRNA coding for Rep protein from AAV facilitates targeted plasmid integration. *Journal of Gene Medicine*, *10*(1), 42–50. https://doi.org/10.1002/jgm.1118

Iwai, A., Masliah, E., Yoshimoto, M., Ge, N., Flanagan, L., Rohan de Silva, H. A., Kittel, A., & Saitoh, T. (1995). The precursor protein of non-Aβ component of Alzheimer's disease amyloid is a presynaptic protein of the central nervous system. *Neuron*, *14*(2), 467–475. https://doi.org/10.1016/0896-6273(95)90302-X

Jankovic, J. (2008). Parkinson's disease: Clinical features and diagnosis. In *Journal of Neurology, Neurosurgery and Psychiatry* (Vol. 79, Issue 4, pp. 368–376). BMJ Publishing Group. https://doi.org/10.1136/jnnp.2007.131045

Jost, W. H. (2010). Gastrointestinal dysfunction in Parkinson's Disease. *Journal of the Neurological Sciences*, *289*(1–2), 69–73. https://doi.org/10.1016/j.jns.2009.08.020

Kaksonen, M., & Roux, A. (2018). Mechanisms of clathrin-mediated endocytosis. In *Nature Reviews Molecular Cell Biology* (Vol. 19, Issue 5, pp. 313–326). Nature Publishing Group. https://doi.org/10.1038/nrm.2017.132

Kalia, L. v., Brotchie, J. M., & Fox, S. H. (2013). Novel nondopaminergic targets for motor features of Parkinson's disease: Review of recent trials. *Movement Disorders*, *28*(2), 131–144. https://doi.org/10.1002/mds.25273

Kalia, L. v., & Lang, A. E. (2015). Parkinson's disease. In *The Lancet* (Vol. 386, Issue 9996, pp. 896–912). Lancet Publishing Group. https://doi.org/10.1016/S0140-6736(14)61393-3

Kanazawa, T., Uchihara, T., Takahashi, A., Nakamura, A., Orimo, S., & Mizusawa, H. (2008). Three-Layered Structure Shared Between Lewy Bodies and Lewy Neurites—Three-Dimensional Reconstruction of Triple-Labeled Sections. *Brain Pathology*, *18*(3), 415–422. https://doi.org/10.1111/j.1750-3639.2008.00140.x

Kelly, K., Wang, S., Boddu, R., Liu, Z., Moukha-Chafiq, O., Augelli-Szafran, C., & West, A. B. (2018). The G2019S mutation in LRRK2 imparts resiliency to kinase inhibition. *Experimental Neurology*, *309*, 1–13. https://doi.org/10.1016/j.expneurol.2018.07.012

Kolahdouzan, M., & Hamadeh, M. J. (2017). The neuroprotective effects of caffeine in neurodegenerative diseases. *CNS Neuroscience & Therapeutics*, *23*(4), 272–290. https://doi.org/10.1111/cns.12684

Korneyenkov, M. A., & Zamyatnin, A. A. (2021). Next step in gene delivery: Modern approaches and further perspectives of aav tropism modification. *Pharmaceutics*, *13*(5). https://doi.org/10.3390/pharmaceutics13050750

Kotterman, M. A., Chalberg, T. W., & Schaffer, D. v. (2015). Viral Vectors for Gene Therapy: Translational and Clinical Outlook. In *Annual Review of Biomedical Engineering* (Vol. 17, pp. 63–89). Annual Reviews Inc. https://doi.org/10.1146/annurev-bioeng-071813-104938

Kouli, A., Torsney, K. M., & Kuan, W.-L. (2018). Parkinson's Disease: Etiology, Neuropathology, and Pathogenesis. In *Parkinson's Disease: Pathogenesis and Clinical Aspects* (pp. 3–26). Codon Publications. https://doi.org/10.15586/codonpublications.parkinsonsdisease.2018.ch1

Kügler, S., Kilic, E., & Bähr, M. (2003). Human synapsin 1 gene promoter confers highly neuron-specific long-term transgene expression from an adenoviral vector in the adult rat brain depending on the transduced area. In *Gene Therapy* (Vol. 10, Issue 4, pp. 337–347). https://doi.org/10.1038/sj.gt.3301905

Kwon, I., & Schaffer, D. v. (2008). Designer gene delivery vectors: Molecular engineering and evolution of adeno-associated viral vectors for enhanced gene transfer. In *Pharmaceutical Research* (Vol. 25, Issue 3, pp. 489–499). https://doi.org/10.1007/s11095-007-9431-0

Lashuel, H. A., Petre, B. M., Wall, J., Simon, M., Nowak, R. J., Walz, T., & Lansbury, P. T. (2002). α-Synuclein, Especially the Parkinson's Disease-associated Mutants, Forms Pore-like Annular and Tubular Protofibrils. *Journal of Molecular Biology*, *322*(5), 1089–1102. https://doi.org/10.1016/S0022-2836(02)00735-0

Lee, Y. B., Cosgrave, A. S., Glover, C. P. J., Bienemann, A., Heywood, D., Hobson, R. J., & Uney, J. B. (2005). Increased utility in the CNS of a powerful neuron-specific tetracycline-regulatable adenoviral system developed using a post-transcriptional enhancer. *The Journal of Gene Medicine*, *7*(5), 576–583. https://doi.org/10.1002/JGM.694

Lees, A. J., Hardy, J., & Revesz, T. (2009). Parkinson's disease. In *The Lancet* (Vol. 373, Issue 9680, pp. 2055–2066). Elsevier B.V. https://doi.org/10.1016/S0140-6736(09)60492-X

Lehtonen, Š., Sonninen, T. M., Wojciechowski, S., Goldsteins, G., & Koistinaho, J. (2019). Dysfunction of cellular proteostasis in Parkinson's disease. *Frontiers in Neuroscience*, *13*(MAY), 457. https://doi.org/10.3389/FNINS.2019.00457/BIBTEX

Lenka, A., & Jankovic, J. (2021). Tremor Syndromes: An Updated Review. In *Frontiers in Neurology* (Vol. 12). Frontiers Media S.A. https://doi.org/10.3389/fneur.2021.684835

Li, X., Tan, Y. C., Poulose, S., Olanow, C. W., Huang, X. Y., & Yue, Z. (2007). Leucine-rich repeat kinase 2 (LRRK2)/PARK8 possesses GTPase activity that is altered in familial Parkinson's disease R1441C/G mutants. *Journal of Neurochemistry*, *103*(1), 238–247. https://doi.org/10.1111/j.1471-4159.2007.04743.x

Li, Y., Liu, L., Ji, W., Peng, H., Zhao, R., & Zhang, X. (2020). Strategies and materials of "SMART" non-viral vectors: Overcoming the barriers for brain gene therapy. In *Nano Today* (Vol. 35). Elsevier B.V. https://doi.org/10.1016/j.nantod.2020.101006

Lindersson, E., Beedholm, R., Højrup, P., Moos, T., Gai, W. P., Hendil, K. B., & Jensen, P. H. (2004). Proteasomal Inhibition by α-Synuclein Filaments and Oligomers *. *Journal of Biological Chemistry*, *279*(13), 12924–12934. https://doi.org/10.1074/JBC.M306390200

Liu, B., Wang, S., Brenner, M., Paton, J. F. R., & Kasparov, S. (2008). Enhancement of cell-specific transgene expression from a Tet-Off regulatory system using a transcriptional amplification strategy in the rat brain. *The Journal of Gene Medicine*, *10*(5), 583. https://doi.org/10.1002/JGM.1178

Liu, D., Zhu, M., Zhang, Y., & Diao, Y. (2021). Crossing the blood-brain barrier with AAV vectors. *Metabolic Brain Disease*, 45–52. https://doi.org/10.1007/s11011-020-00630-2/Published

Lock, M., McGorray, S., Auricchio, A., Ayuso, E., Beecham, E. J., Blouin-Tavel, V., Bosch, F., Bose, M., Byrne, B. J., Caton, T., Chiorini, J. A., Chtarto, A., Clark, K. R., Conlon, T., Darmon, C., Doria, M., Douar, A., Flotte, T. R., Francis, J. D., … Snyder, R. O. (2010). Characterization of a recombinant adeno-associated virus type 2 Reference Standard Material. *Human Gene Therapy*, *21*(10), 1273–1285. https://doi.org/10.1089/HUM.2009.223

Lorenzen, N., Nielsen, S. B., Buell, A. K., Kaspersen, J. D., Arosio, P., Vad, B. S., Paslawski, W., Christiansen, G., Valnickova-Hansen, Z., Andreasen, M., Enghild, J. J., Pedersen, J. S., Dobson, C. M., Knowles, T. P. J., & Otzen, D. E. (2014). The role of stable α-synuclein oligomers in the molecular events underlying amyloid formation. *Journal of the American Chemical Society*, *136*(10), 3859–3868. https://doi.org/10.1021/JA411577T

MacLeod, D. A., Rhinn, H., Kuwahara, T., Zolin, A., di Paolo, G., MacCabe, B. D., Marder, K. S., Honig, L. S., Clark, L. N., Small, S. A., & Abeliovich, A. (2013). RAB7L1 Interacts with LRRK2 to Modify Intraneuronal Protein Sorting and Parkinson's Disease Risk. *Neuron*, *77*(3), 425–439. https://doi.org/10.1016/j.neuron.2012.11.033

Maheshri, N., Koerber, J. T., Kaspar, B. K., & Schaffer, D. v. (2006). Directed evolution of adeno-associated virus yields enhanced gene delivery vectors. *Nature Biotechnology*, *24*(2), 198–204. https://doi.org/10.1038/NBT1182

Mallet, Delgado, Chazalon, Miguelez, & Baufreton. (2019). Cellular and Synaptic Dysfunctions in Parkinson's Disease: Stepping out of the Striatum. *Cells*, *8*(9), 1005. https://doi.org/10.3390/cells8091005

Marks Jr, W. J., Ostrem, J. L., A Starr, N. P., Larson, P. S., Verhagen, L., Kordower, J. H., Marks Jr, W. J., Bartus, R. T., Siff ert, J., Davis, C. S., Lozano, A., Boulis, N., Vitek, J., Stacy, M., Turner, D., Verhagen, L., Bakay, R., Watts, R., Guthrie, B., … Warren Olanow, C. (2010). Gene delivery of AAV2-neurturin for Parkinson's disease: a double-blind, randomised, controlled trial. *Articles Lancet Neurol*, *9*, 1164–1172. https://doi.org/10.1016/S1474

Marks, W. J., Ostrem, J. L., Verhagen, L., Starr, P. A., Larson, P. S., Bakay, R. A. E., Taylor, R., Cahn-Weiner, D. A., Stoessl, J., Olanow, W., & Bartus, R. T. (2008). *Safety and tolerability of intraputaminal delivery of CERE-120 (adeno-associated virus serotype 2-neurturin) to patients with idiopathic Parkinson's disease: an open-label, phase I trial*. *7*. https://doi.org/10.1016/S1474

Mata, I. F., Wedemeyer, W. J., Farrer, M. J., Taylor, J. P., & Gallo, K. A. (2006). LRRK2 in Parkinson's disease: protein domains and functional insights. In *Trends in Neurosciences* (Vol. 29, Issue 5, pp. 286–293). https://doi.org/10.1016/j.tins.2006.03.006

Mathiesen, S. N., Lock, J. L., Schoderboeck, L., Abraham, W. C., & Hughes, S. M. (2020). CNS Transduction Benefits of AAV-PHP.eB over AAV9 Are Dependent on Administration Route and Mouse Strain. *Molecular Therapy - Methods & Clinical Development*, *19*, 447–458. https://doi.org/10.1016/J.OMTM.2020.10.011

McCarty, D. M., Young, S. M., & Samulski, R. J. (2004). Integration of adeno-associated virus (AAV) and recombinant AAV vectors. In *Annual Review of Genetics* (Vol. 38, pp. 819–845). https://doi.org/10.1146/annurev.genet.37.110801.143717

McNaught, K. S. P., Belizaire, R., Jenner, P., Olanow, C. W., & Isacson, O. (2002). Selective loss of 20S proteasome α-subunits in the substantia nigra pars compacta in Parkinson's disease. *Neuroscience Letters*, *326*(3), 155–158. https://doi.org/10.1016/S0304-3940(02)00296-3

Miyazaki, J.-I., Takaki, S., Araki, K., Tashiroe, F., Tominaga, A., Takatsu, K., & Yamamura=, K.-I. (1989). Expression vector system based on the chicken /?-actin promoter directs efficient production of interleukin-5 (Recombinant DNA; DNA transfection; transient expression; DNA replication; promoter activity; &galacto-sidase assay; SV40 T antigen; splicing). In *Gene* (Vol. 79).

Nguyen, M., & Krainc, D. (2018). LRRK2 phosphorylation of auxilin mediates synaptic defects in dopaminergic neurons from patients with Parkinson's disease. *Proceedings of the National Academy of Sciences of the United States of America*, *115*(21), 5576–5581. https://doi.org/10.1073/pnas.1717590115

Nichols, R. J., Dzamko, N., Morrice, N. A., Campbell, D. G., Deak, M., Ordureau, A., Macartney, T., Tong, Y., Shen, J., Prescott, A. R., & Alessi, D. R. (2010). 14-3-3 Binding to LRRK2 is disrupted by multiple Parkinson's disease-associated mutations and regulates cytoplasmic localization. *Biochemical Journal*, *430*(3), 393–404. https://doi.org/10.1042/BJ20100483

Noyce, A. J., Bestwick, J. P., Silveira-Moriyama, L., Hawkes, C. H., Giovannoni, G., Lees, A. J., & Schrag, A. (2012). Meta-analysis of early nonmotor features and risk factors for Parkinson disease. *Annals of Neurology*, *72*(6), 893–901. https://doi.org/10.1002/ana.23687

O'Connor, D. M., & Boulis, N. M. (2015). Gene therapy for neurodegenerative diseases. In *Trends in Molecular Medicine* (Vol. 21, Issue 8, pp. 504–512). Elsevier Ltd. https://doi.org/10.1016/j.molmed.2015.06.001

Oh, M. S., Hong, S. J., Huh, Y., & Kim, K. S. (2009). Expression of transgenes in midbrain dopamine neurons using the tyrosine hydroxylase promoter. *Gene Therapy*, *16*(3), 437–440. https://doi.org/10.1038/gt.2008.148

Ou, Z., Pan, J., Tang, S., Duan, D., Yu, D., Nong, H., & Wang, Z. (2021). Global Trends in the Incidence, Prevalence, and Years Lived With Disability of Parkinson's Disease in 204 Countries/Territories From 1990 to 2019. *Frontiers in Public Health*, *9*, 1994. https://doi.org/10.3389/FPUBH.2021.776847/BIBTEX

Ow, Y. L. P., Green, D. R., Hao, Z., & Mak, T. W. (2008). Cytochrome c: functions beyond respiration. *Nature Reviews Molecular Cell Biology 2008 9:7*, *9*(7), 532–542. https://doi.org/10.1038/nrm2434

Pickart, C. M. (2003). Mechanisms Underlying Ubiquitination. *Http://Dx.Doi.Org/10.1146/Annurev.Biochem.70.1.503*, *70*, 503–533. https://doi.org/10.1146/ANNUREV.BIOCHEM.70.1.503

Pieri, L., Madiona, K., Bousset, L., & Melki, R. (2012). Fibrillar α-synuclein and huntingtin exon 1 assemblies are toxic to the cells. *Biophysical Journal*, *102*(12), 2894–2905. https://doi.org/10.1016/J.BPJ.2012.04.050

Postuma, R. B., Berg, D., Stern, M., Poewe, W., Olanow, C. W., Oertel, W., Obeso, J., Marek, K., Litvan, I., Lang, A. E., Halliday, G., Goetz, C. G., Gasser, T., Dubois, B., Chan, P., Bloem, B. R., Adler, C. H., & Deuschl, G. (2015). MDS clinical diagnostic criteria for Parkinson's disease. In *Movement Disorders* (Vol. 30, Issue 12, pp. 1591–1601). John Wiley and Sons Inc. https://doi.org/10.1002/mds.26424

Postuma, R. B., Lang, A. E., Munhoz, R. P., Charland, K., Pelletier, A., Moscovich, M., Filla, L., Zanatta, D., Rios Romenets, S., Altman, R., Chuang, R., & Shah, B. (2012). Caffeine for treatment of Parkinson disease: A randomized controlled trial. *Neurology*, *79*(7), 651–658. https://doi.org/10.1212/WNL.0b013e318263570d

Poulopoulos, M., Cortes, E., Vonsattel, J. P. G., Fahn, S., Waters, C., Cote, L. J., Moskowitz, C., Honig, L. S., Clark, L. N., Marder, K. S., & Alcalay, R. N. (2012). Clinical and pathological characteristics of LRRK2 G2019S patients with PD. *Journal of Molecular Neuroscience*, *47*(1), 139–143. https://doi.org/10.1007/s12031-011-9696-y

Rabinowitz, J. E., Bowles, D. E., Faust, S. M., Ledford, J. G., Cunningham, S. E., & Samulski, R. J. (2004). Cross-Dressing the Virion: the Transcapsidation of Adeno-

Associated Virus Serotypes Functionally Defines Subgroups. *Journal of Virology*, *78*(9), 4421–4432. https://doi.org/10.1128/JVI.78.9.4421-4432.2004/ASSET/DFB85E08-CCD4-4FD4-92B2-03BABA7EBF45/ASSETS/GRAPHIC/ZJV0090419500008.JPEG

Rayaprolu, V., Kruse, S., Kant, R., Venkatakrishnan, B., Movahed, N., Brooke, D., Lins, B., Bennett, A., Potter, T., McKenna, R., Agbandje-McKenna, M., & Bothner, B. (2013). Comparative Analysis of Adeno-Associated Virus Capsid Stability and Dynamics. *Journal of Virology*, *87*(24), 13150–13160. https://doi.org/10.1128/jvi.01415-13

Rinalduzzi, S., Trompetto, C., Marinelli, L., Alibardi, A., Missori, P., Fattapposta, F., Pierelli, F., & Currà, A. (2015). Balance dysfunction in Parkinson's disease. In *BioMed Research International* (Vol. 2015). Hindawi Limited. https://doi.org/10.1155/2015/434683

Rodova, M., Jayini, R., Singasani, R., Chipps, E., & Islam, M. R. (2013). CMV promoter is repressed by p53 and activated by JNK pathway. *Plasmid*, *69*(3), 223–230. https://doi.org/10.1016/j.plasmid.2013.01.004

Rolland, A. S., Kareva, T., Kholodilov, N., & Burke, R. E. (2017). A quantitative evaluation of a 2.5-kb rat tyrosine hydroxylase promoter to target expression in ventral mesencephalic dopamine neurons in vivo. *Neuroscience*, *346*, 126–134. https://doi.org/10.1016/J.NEUROSCIENCE.2017.01.014

Rolland, A. S., Kareva, T., Yarygina, O., Kholodilov, N., & Burke, R. E. (2016). Expression mediated by three partial sequences of the human tyrosine hydroxylase promoter in vivo. *Molecular Therapy - Methods & Clinical Development*, *3*, 16062. https://doi.org/10.1038/MTM.2016.62

Samulski, R. J., Berns, K. I., Tan, M., & Muzyczka, N. (1982). Cloning of adeno-associated virus into pBR322: Rescue of intact virus from the recombinant plasmid in human cells (latent viruses/excision/cruciforms/palindromes). In *Proc. Natt Acad. Sci. USA* (Vol. 79). https://www.pnas.org

Saraiva, J., Nobre, R. J., & Pereira de Almeida, L. (2016). Gene therapy for the CNS using AAVs: The impact of systemic delivery by AAV9. In *Journal of Controlled Release* (Vol. 241, pp. 94–109). Elsevier B.V. https://doi.org/10.1016/j.jconrel.2016.09.011

Schechter, M., & Sharon, R. (2021). An Emerging Role for Phosphoinositides in the Pathophysiology of Parkinson's Disease. *Journal of Parkinson's Disease*, *11*(4), 1725. https://doi.org/10.3233/JPD-212684

Schindelin, J., Arganda-Carreras, I., Frise, E., Kaynig, V., Longair, M., Pietzsch, T., Preibisch, S., Rueden, C., Saalfeld, S., Schmid, B., Tinevez, J. Y., White, D. J., Hartenstein, V., Eliceiri, K., Tomancak, P., & Cardona, A. (2012). Fiji: an open-source platform for biological-image analysis. *Nature Methods 2012 9:7*, *9*(7), 676–682. https://doi.org/10.1038/nmeth.2019

Shahmoradian, S. H., Lewis, A. J., Genoud, C., Hench, J., Moors, T. E., Navarro, P. P., Castaño-Díez, D., Schweighauser, G., Graff-Meyer, A., Goldie, K. N., Sütterlin, R., Huisman, E., Ingrassia, A., Gier, Y. de, Rozemuller, A. J. M., Wang, J., Paepe, A. de, Erny, J., Staempfli, A., … Lauer, M. E. (2019). Lewy pathology in Parkinson's disease consists of crowded organelles and lipid membranes. *Nature Neuroscience 2019 22:7*, *22*(7), 1099–1109. https://doi.org/10.1038/s41593-019-0423-2

Shin, N., Jeong, H., Kwon, J., Heo, H. Y., Kwon, J. J., Yun, H. J., Kim, C. H., Han, B. S., Tong, Y., Shen, J., Hatano, T., Hattori, N., Kim, K. S., Chang, S., & Seol, W. (2008). LRRK2 regulates synaptic vesicle endocytosis. *Experimental Cell Research*, *314*(10), 2055–2065. https://doi.org/10.1016/j.yexcr.2008.02.015

Smith-Arica, J. R., Morelli, A. E., Larregina, A. T., Smith, J., Lowenstein, P. R., & Castro, M. G. (2000). Cell-Type-Specific and Regulatable Transgenesis in the Adult Brain: Adenovirus-Encoded Combined Transcriptional Targeting and Inducible Transgene Expression. *Molecular Therapy*, *2*(6), 579–587. https://doi.org/10.1006/MTHE.2000.0215

Snyder, B. R., Boulis, N. M., & Federici, T. (2010). Viral vector-mediated gene transfer for CNS disease. In *Expert Opinion on Biological Therapy* (Vol. 10, Issue 3, pp. 381–394). https://doi.org/10.1517/14712590903514074

Steger, M., Diez, F., Dhekne, H. S., Lis, P., Nirujogi, R. S., Karayel, O., Tonelli, F., Martinez, T. N., Lorentzen, E., Pfeffer, S. R., Alessi, D. R., & Mann, M. (2017). *Systematic proteomic analysis of LRRK2-mediated Rab GTPase phosphorylation establishes a connection to ciliogenesis*. https://doi.org/10.7554/eLife.31012.001

Südhof, T. C. (2004). The synaptic vesicle cycle. In *Annual Review of Neuroscience* (Vol. 27, pp. 509–547). https://doi.org/10.1146/annurev.neuro.26.041002.131412

Sveinbjornsdottir, S. (2016). The clinical symptoms of Parkinson's disease. In *Journal of Neurochemistry* (pp. 318–324). Blackwell Publishing Ltd. https://doi.org/10.1111/jnc.13691

Tanguy, Y., Biferi, M. G., Besse, A., Astord, S., Cohen-Tannoudji, M., Marais, T., & Barkats, M. (2015). Systemic AAVrh10 provides higher transgene expression than

AAV9 in the brain and the spinal cord of neonatal mice. *Frontiers in Molecular Neuroscience*, *8*(JULY). https://doi.org/10.3389/fnmol.2015.00036

Ullah, I., Zhao, L., Hai, Y., Fahim, M., Alwayli, D., Wang, X., & Li, H. (2021). "Metal elements and pesticides as risk factors for Parkinson's disease - A review." *Toxicology Reports*, *8*, 607–616. https://doi.org/10.1016/j.toxrep.2021.03.009

Usmani, A., Shavarebi, F., & Hiniker, A. (2021). The Cell Biology of LRRK2 in Parkinson's Disease. *Molecular and Cellular Biology*, *41*(5). https://doi.org/10.1128/mcb.00660-20

Vidyadhara, D. J., Lee, J. E., & Chandra, S. S. (2019). Role of the endolysosomal system in Parkinson's disease. In *Journal of Neurochemistry* (Vol. 150, Issue 5, pp. 487–506). Blackwell Publishing Ltd. https://doi.org/10.1111/jnc.14820

Wakabayashi, K., Tanji, K., Odagiri, S., Miki, Y., Mori, F., & Takahashi, H. (2012). The Lewy Body in Parkinson's Disease and Related Neurodegenerative Disorders. *Molecular Neurobiology 2012 47:2*, *47*(2), 495–508. https://doi.org/10.1007/S12035-012-8280-Y

Wang, J., & Zhang, L. (2021). Retrograde axonal transport property of adeno-associated virus and its possible application in future. *Microbes and Infection*, *23*(8), 104829. https://doi.org/10.1016/J.MICINF.2021.104829

Wang, L., Yin, Z., Wang, Y., Lu, Y., Zhang, D., Srivastava, A., Ling, C., Aslanidi, G. v., & Ling, C. (2015). Productive life cycle of adeno-associated virus serotype 2 in the complete absence of a conventional polyadenylation signal. *The Journal of General Virology*, *96*(Pt 9), 2780. https://doi.org/10.1099/JGV.0.000229

Webb, J. L., Ravikumar, B., Atkins, J., Skepper, J. N., & Rubinsztein, D. C. (2003). α-Synuclein Is Degraded by Both Autophagy and the Proteasome *. *Journal of Biological Chemistry*, *278*(27), 25009–25013. https://doi.org/10.1074/JBC.M300227200

Winner, B., Jappelli, R., Maji, S. K., Desplats, P. A., Boyer, L., Aigner, S., Hetzer, C., Loher, T., Vilar, M., Campioni, S., Tzitzilonis, C., Soragni, A., Jessberger, S., Mira, H., Consiglio, A., Pham, E., Masliah, E., Gage, F. H., & Riek, R. (2011). In vivo demonstration that α-synuclein oligomers are toxic. *Proceedings of the National Academy of Sciences of the United States of America*, *108*(10), 4194–4199. https://doi.org/10.1073/PNAS.1100976108/-/DCSUPPLEMENTAL/PNAS.201100976SI.PDF

Wood, S. J., Wypych, J., Steavenson, S., Louis, J.-C., Citron, M., & Biere, A. L. (1999). α-Synuclein Fibrillogenesis Is Nucleation-dependent. *Journal of Biological Chemistry*, *274*(28), 19509–19512. https://doi.org/10.1074/jbc.274.28.19509

Wrangel, C. von, Schwabe, K., John, N., Krauss, J. K., & Alam, M. (2015). The rotenone-induced rat model of Parkinson's disease: Behavioral and electrophysiological findings. *Behavioural Brain Research*, *279*, 52–61. https://doi.org/10.1016/j.bbr.2014.11.002

Wright, R. (2022). Mitochondrial dysfunction and Parkinson's disease. *Nature Neuroscience 2022 25:1*, *25*(1), 2–2. https://doi.org/10.1038/s41593-021-00989-0

Wu, Z., Asokan, A., & Samulski, R. J. (2006). Adeno-associated Virus Serotypes: Vector Toolkit for Human Gene Therapy. In *Molecular Therapy* (Vol. 14, Issue 3, pp. 316–327). https://doi.org/10.1016/j.ymthe.2006.05.009

Wu, Z., Yang, H., & Colosi, P. (2010). Effect of genome size on AAV vector packaging. *Molecular Therapy : The Journal of the American Society of Gene Therapy*, *18*(1), 80–86. https://doi.org/10.1038/MT.2009.255

Xiao, P. J., Li, C., Neumann, A., & Samulski, R. J. (2012). Quantitative 3D tracing of gene-delivery viral vectors in human cells and animal tissues. *Molecular Therapy : The Journal of the American Society of Gene Therapy*, *20*(2), 317–328. https://doi.org/10.1038/MT.2011.250

Xu, L., Nagai, Y., Kajihara, Y., Ito, G., & Tomita, T. (2021). The regulation of rab gtpases by phosphorylation. In *Biomolecules* (Vol. 11, Issue 9). MDPI. https://doi.org/10.3390/biom11091340

Zahoor, I., Shafi, A., & Haq, E. (2018). Pharmacological Treatment of Parkinson's Disease. In *Parkinson's Disease: Pathogenesis and Clinical Aspects* (pp. 129–144). Codon Publications. https://doi.org/10.15586/codonpublications.parkinsonsdisease.2018.ch7

Zhang, H., Yang, B., Mu, X., Ahmed, S. S., Su, Q., He, R., Wang, H., Mueller, C., Sena-Esteves, M., Brown, R., Xu, Z., & Gao, G. (2011). Several rAAV vectors efficiently cross the blood-brain barrier and transduce neurons and astrocytes in the neonatal mouse central nervous system. *Molecular Therapy*, *19*(8), 1440–1448. https://doi.org/10.1038/mt.2011.98

Zimprich, A., Biskup, S., Leitner, P., Lichtner, P., Farrer, M., Lincoln, S., Kachergus, J., Hulihan, M., Uitti, R. J., Calne, D. B., & Stoessl, A. J. (2004). Mutations in LRRK2 Cause Autosomal-Dominant Parkinsonism with Pleomorphic Pathology families, we have found six disease-segregating muta-tions (five missense and one

putative splice site muta-tion) in a gene encoding a large, multifunctional pro. In *Neuron* (Vol. 44). http://www.neuron.org/cgi/content/full/44/4/